INVESTIGATION OF INTERFACE SHEAR STRESSES ON WHEELCHAIR SEAT CUSHIONS AND THE EFFECTS ON SUBCUTANEOUS BUTTOCK SOFT TISSUES

by

Jonathan S. Akins

B.S., Mechanical Engineering, Oklahoma State University, 2003

Submitted to the Graduate Faculty of

Swanson School of Engineering in partial fulfillment

of the requirements for the degree of

Masters of Science in Bioengineering

University of Pittsburgh

2008

UNIVERSITY OF PITTSBURGH

SWANSON SCHOOL OF ENGINEERING

This thesis was presented

by

Jonathan S. Akins

It was defended on

November 7, 2008

and approved by

Mark Redfern, PhD, Professor, Department of Bioengineering
Professor, Department of Otolaryngology
Professor, Department of Physical Therapy

Patricia Karg, MS, Assistant Professor, Department of Rehabilitation Science and Technology

David M. Brienza, PhD, Professor, Department of Rehabilitation Science and Technology
Associate Professor, Department of Bioengineering
Associate Professor, McGowan Institute for Regenerative Medicine
Thesis Advisor

INVESTIGATION OF INTERFACE SHEAR STRESSES ON WHEELCHAIR SEAT CUSHIONS AND THE EFFECTS ON SUBCUTANEOUS BUTTOCK SOFT TISSUES

Jonathan S. Akins, MS

University of Pittsburgh, 2008

Pressure ulcer incidence rates have remained constant [1] even though wheelchair seat cushion technologies have advanced. Shear stress is recognized as a risk factor for pressure ulcer development [2] and is a focus of many shear reduction technologies incorporated into cushions; however, shear reduction has not been quantified in the literature. This study evaluated 21 commercial wheelchair seat cushions using a methodology developed to quantify interface shear stress and calculate overall and local horizontal stiffness values. For statistical analyses, the cushions were grouped by Healthcare Common Procedure Coding System (HCPCS) codes. The general use cushion category (E2601) resulted in significantly greater interface shear stresses ($p \leq .001$) than all other categories and the adjustable skin protection cushion category (K0734) resulted in significantly less interface shear stress ($p \leq .001$) than all other categories. Additionally, this study provided evidence that the current horizontal stiffness test methodology (ISO 16840-2) [3] provides sufficient information to characterize wheelchair seat cushions, but does not directly quantify interface shear stress.

Results from the evaluation of commercial wheelchair seat cushions provided evidence of materials and technologies that may reduce the risk of pressure ulcers. Based on these results, three prototype cushions were conceptualized and prototyped into a closed-loop control system. The closed-loop control system monitored interface stress amplitude to actively modulate

cushion properties. None of the prototypes effectively reduced interface shear stress using the methodology developed for cushion testing.

Subcutaneous buttock soft tissues were investigated using a finite element model. Researchers have previously used finite element models [4-13]; however, this study improved upon image collection methodology and validation techniques. MR images of one subject were collected in three seated postures and were used to create 3-D models of the buttock. A non-linear 3-D finite element model was developed with anatomical geometries using hyperelastic and viscoelastic constitutive models. Interface pressure, interface shear stress, and soft tissue displacements were used to validate the model. A parametric analysis resulted in a partially validated model that provided subcutaneous stresses and strains for the upright seated posture. The validated model will be used in future studies to evaluate the SCI population and to evaluate commercial and prototype wheelchair seat cushions.

TABLE OF CONTENTS

LIST OF TABLES

LIST OF FIGURES

PREFACE

First, I would like to thank my wife Nancy for pushing me to apply to graduate school and for her tireless support and understanding throughout this process. I would like to thank my thesis advisor, Dr. David Brienza, and my thesis committee, Ms. Patricia Karg and Dr. Mark Redfern, for their knowledge, feedback and continued guidance. I would like to thank BC Deemer and Sandeep Urankar for their technical guidance, Erik Porach for his assistance with testing, Dr. Richard Debski for use of his facilities, and my RST South Side colleagues (Rich, Mike T, Yi-Ting, Sue, Ana, Mike L, Debby, Cheryl, Joe, Linda S, Linda V, Jong Bae, Ashli, Mary Beth) for their friendship, support and feedback for the last two years. Last I would like to thank the National Institute on Disability and Rehabilitation Research (NIDRR), Rehabilitation Engineering Research Center (RERC) on Spinal Cord Injury and The Technology Collaborative (TTC) for their financial support.

1.0 INTRODUCTION

1.1 OVERVIEW

In the United States, annual pressure ulcer treatment costs have risen from $1.34 billion in 1992 [14] to approximately $17.2 billion in 2003 [15], with nearly 90% billed to Medicare or Medicaid. In 2003, approximately 455,000 hospital stays were due principally to pressure ulcers and 167,000 hospital stays were patients with paralysis and/or SCI [15]. The average hospital charge per stay was $37,800 resulting in $6.3 billion in treatment costs for the SCI population. With constant incidence rates of approximately 7.6% from 1999 to 2004 [1] research into pressure ulcer prevention is essential.

Wheelchair seat cushions are designed to reduce extrinsic risk factors known to increase the risk of pressure ulcers. These extrinsic risk factors are pressure, shear, heat, and humidity [2]. Cushion manufacturers routinely incorporate shear reduction technologies into cushion designs, but without shear quantification, designers are left without a valid means to evaluate products. For example, two-way stretch cushion cover materials and segmented cube foam cushion construction are two methods of shear reduction. While both designs promote shear reduction, practitioners are left without a basis for shear related clinical decision making. Large shear magnitudes occlude blood flow [16] and negligible shear magnitudes could result in the users sliding out of the wheelchair.

1.2 OBJECTIVE

The purpose of this study was to quantify interface shear stresses of the commercial wheelchair seat cushions, develop a prototype wheelchair seat cushion, and model subcutaneous buttock tissues stresses and strains. Mechanical testing of cushions in each Healthcare Common Procedure Coding System (HCPCS) category was performed to determine shear characteristics of commercial wheelchair seat cushions. Results of the cushion testing were used to conceptualize and prototype three cushion design elements. Subcutaneous stresses and strains were investigated using a validated non-linear 3-D finite element model developed with anatomical geometries using hyperelastic and viscoelastic constitutive models.

Specific Aim 1 – Develop a test methodology to determine shear characteristics of commercial wheelchair seat cushions

Specific Aim 2 – Develop and evaluate a prototype shear reducing cushion design element

Specific Aim 3 – Develop and validate a non-linear 3-D FE model of the buttock using subject specific geometry

Shear force reduction has the potential to reduce the incidence of pressure ulcers in the spinal cord injury (SCI), elderly, and other high risk populations. The validated FE model of this study will establish the methodology to evaluate high risk populations and prototype wheelchair seat cushions. Results from high risk populations will provide design specifications to assist cushion designers in reducing shear stresses in buttock soft tissue.

2.0 BACKGROUND

Shear related pressure ulcer research, wheelchair seat cushion technology, shear related wheelchair seat cushion evaluation techniques, and methods of quantifying subcutaneous tissue stresses and strains are reviewed to provide a knowledge base for the research conducted in this study.

2.1 LITERATURE REVIEW OF SHEAR RELATED PRESSURE ULCER RESEEARCH

Pressure and shear created between wheelchair seat cushions and users are identified as extrinsic risk factors known to increase the risk of pressure ulcers [2]. A review of shear related pressure ulcer literature was performed using the Ovid MEDLINE database and Google Scholar search engine. The combinations of keywords used were: shear and pressure ulcer; shear and decubitus ulcer; and shear and wheelchair cushion. The relevant literature is detailed in human and animal studies.

2.1.1 Human Studies

Reichel [17] first expressed the importance of shearing forces in the SCI population. Without the sensation of discomfort, patients do not feel pain and do not have the ability to reposition themselves. Raising the head of the patient's bed adds the weight of the torso to the sacral area causing the superficial fascia to slide with respect to the anchored deep fascia. This sliding compromises the sacral tissue vasculature and can result in tissue necrosis, a common pathological finding in pressure ulcers.

Bennett et al. [16] measured local pressure, shear, and blood flow in the first shear related human experiment. Local measurement is extremely important because the buttock does not apply a uniform load to the cushion. Peak pressures occur at the sacrum and ischial tuberosities (IT), which coincide with the locations of many pressure ulcers. Bennett et al. [16] pioneered local force measurement, but was only able to record data on a flat, rigid surface. Two pressure sensors measured normal force and helped to minimize shear effects during initial loading by minimizing the pressure gradient. A photoplethysmograph between the two pressure sensors measured cutaneous blood flow and an adjacent shear sensor measured shear stress. The shear sensor was designed with known limitations, but quantified interface parameters. Four subjects pressed their palms against the stationary transducer and obtained arteriole occlusion in low and high shear modes [16]. Occlusion occurred between 100-120 mmHg in low shear (~1.2 kPa) and between 60-80 mmHg in high shear (~7.6 kPa). Bennett et al. concluded that shear force reduced the pressure necessary for arteriole occlusion in the human palm by approximately 50%. Occlusion of arterioles leads to tissue ischemia and eventual tissue necrosis [18]. Bennett et al. [19] next collected data from a wheelchair with a flat, rigid seat instrumented with the transducer 2-3 cm lateral to the IT. Fourteen geriatric and nine control subjects positioned themselves in a

self-selected posture. Baseline and tipped measurements were recorded with the wheelchair horizontal and rotated 20° backwards, respectively. The backwards rotation increased cutaneous blood flow and reduced pressure and shear stress in the geriatric group (Figure 1). Baseline variability in pressure was greater in the geriatric group, but the mean pressure was similar to the control group. The control group experienced an increase in cutaneous blood flow and little changes in pressure and shear stress (Figure 1).

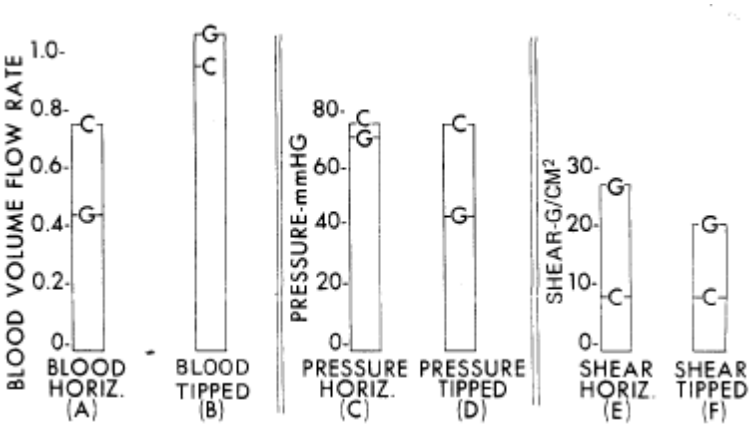

Figure 1: Cutaneous blood flow, pressure and shear stress measurements of geriatric (G) and control (C) subjects resulting from 20° backward rotation [19]

Bennett et al. [20] later used the same methodology to collect data from three groups: 1) nine control subjects; 2) 14 geriatric subjects; and 3) 16 subjects with paraplegia. Median pressure was similar for all groups as found previously. Shear stresses in the geriatric and paraplegia groups were approximately three times greater than the control group and cutaneous blood flow rates were approximately three times less than the control group. Many limitations were discussed; however, data collected from subject groups evaluated in identical environments

provided useful information. The local measurements were conservative because the transducer was 2-3 cm lateral to the IT versus inferior to the IT.

Goossens et al. focused on local shear stress measurement in multiple experiments [21-23]. Skin oxygen tension was monitored while applying pressure and shear to the sacrum of 10 healthy young subjects [23]. Application of shear stress (3.1 kPa) reduced the cut-off pressure, defined as skin oxygen tension less than 1.3 kPa, from 87 to 65 mmHg. Goossens et al. concluded that the addition of a shear stress reduces the normal force required to occlude cutaneous blood flow. Goossens et al. [22] later developed and validated a small deformable shear sensor that measured local shear stress. The shear sensor was composed of two electrodes separated by a layer of silicon rubber that provided a linear relationship between electrode displacement and capacitance. Four capacitors were used to measure shear in two directions and made up a contact area of 4.05 cm^2. Shear stress measurements were recorded on an instrumented seat, the seat of a foldable wheelchair and a hospital mattress. The instrumented seat measured global shear stress using a force plate and was orientated in two positions: 1) 10° forward tilt and 2) 10° backward tilt. Global shear stress is defined as the total horizontal force applied to the surface. Local shear stress was measured with an array of 32 shear force sensors, summed and compared to the global shear stress. The forward tilt resulted in equal global and local measurements, but the backward tilt did not. Shear stress measurements were recorded on the seat of a foldable wheelchair in four configurations: 1) seat angle of 0º with no cushion; 2) seat angle of 8º with no cushion; 3) seat at 0º with a gel cushion; and 4) seat at 8º with a gel cushion. The gel cushion significantly reduced medial-lateral shear at both seat angles. Local shear stress measurements were recorded at the sacrum of 10 healthy subjects on a hospital mattress. Trunk angle was 45º and the seat angle was varied from 0º to 20º in 5º increments. No

significant difference in shear stress measurements were found for the different seat angles. Sacral measurements resulted in greater anterior-posterior shear stresses on the hospital bed and IT measurements resulted in greater medial-lateral shear stresses on the wheelchair. Goossens et al. [21] also measured interface shear stresses on a foam cushion, a gel cushion, and a LiquiCell cushion with results ranging between 4.1 – 6.8 kPa.

2.1.2 Animal Studies

Rose et al. [24] demonstrated that pigs are preferred as an animal model for skin research because the deep fascia and reticular layer of the dermis are more intimately connected than the loosely draped skin of dogs and rodents. Pigs were chosen by the two authors who have conducted animal studies.

Dinsdale [25] used a mechanical pressure system to apply pressure or pressure-and-friction to pigs. Various load magnitudes were applied to 10 white female pigs eight days after percutaneous transaction at the junction of the thoracic and lumbar vertebrae. Pressure was applied to one posterior superior iliac spine (PSIS) and pressure-and-friction was applied to the contralateral PSIS for three hours. The pressure-and-friction function applied six 2.54 cm excursions every 15 minutes. Each pressure site was observed for seven days and characterized as normal, partial or full-thickness lesion. Partial and full-thickness lesions appeared within 24 hours after load application. The results suggested that friction increased skin ulceration at pressures less than 500 mmHg, but no difference in the frequency of ulceration was found at pressures greater than 500 mmHg. Peak pressures found at the cushion interface are approximately 200 mmHg; therefore, Dinsdale concluded that friction increases frequency of ulceration. The second experiment was performed on eight normal white female pigs. Various

loads were applied to the PSIS over two five-day periods using the repeated load protocol. The repeated load protocol applied three 1.5-hour periods of pressure with a one-hour rest period in between each load application. Pressure or pressure-and-friction was randomly applied to one PSIS and the other applied to the contralateral PSIS after the initial five-day period. Pressure sites were characterized as normal, partial or full-thickness lesion seven days after application of the final load. Partial lesions occurred at 45 mmHg when pressure-and-friction was applied, however, 290 mmHg was required to produce ulcers using pressure alone. The third experiment was performed on 14 normal white female pigs using a constant pressure of 159 mmHg. Pressure-and-friction was randomly applied to one PSIS using the repeated load protocol. The contralateral PSIS received only pressure the following day. The pressure sites were blinded against loading protocol and characterized as normal, partial or full-thickness lesion 24 hours after load application. Friction significantly increased the production of pressure ulcers.

Goldstein and Sanders [26] developed a pig model to investigate whether tissue breakdown occurred earlier with increased shear stress. A load applicator applied various combinations of normal and cyclic shear forces using a 7mm x 8mm loading pad. Nonadherent (abundant subdermal soft tissue) and adherent (minimal subdermal soft tissue) sites were loaded and monitored with a computer. Forces were applied in 10-minute intervals up to 40 minutes total. Skin was inspected after each 10-minute interval and loading was stopped if breakdown was apparent. Loaded sites were assessed and skin breakdown rated using the recommendations of the National Pressure Ulcer Advisory Panel (NPUAP). The combination of compressive and shear loads are illustrated in Figure 2. The loading pad applied loads using an area of 56 mm^2 and can be used to calculate the applied pressure and shear stress in mmHg and kPa, respectively. The range of applied pressure was 268–2009 mmHg and applied shear stress was

18–89 kPa. Goldstein's values are well above typical interface pressure (100–200 mmHg) and interface shear stress (1–10 kPa) measurements. Skin breakdown included stage I ulcers, stage II ulcers, and reactive hyperemia. Stage I and II ulcers were observed for 10 days and never progressed to stage III or IV. As shear stress increased, tissue breakdown occurred earlier and tissue injury was more severe.

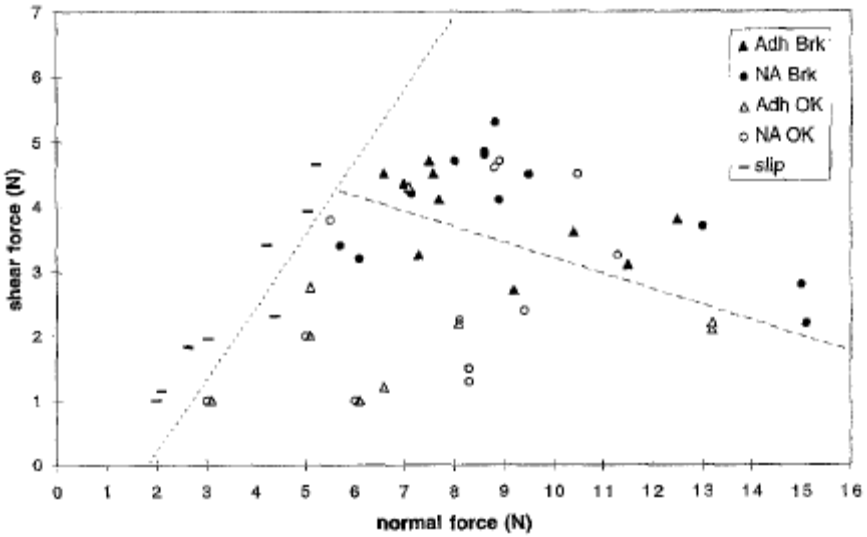

Figure 2: Results of applied force combinations from Goldstein [26]. Adh, adherent; NA, nonadherent; Brk, breakdown

2.2 WHEELCHAIR SEAT CUSHION TECHNOLOGY

The purpose of a wheelchair seat cushion is to provide comfort and aid against pressure ulcer development [27]. Comfort and protection are achieved by deceasing pressure and shear stress through variations in support surface characteristics. Pressure and shear stress are defined as the force per unit area exerted perpendicular and parallel to the plane of interest, respectively [28]. Support surface characteristics include pressure distribution, shear stress, temperature control

and moisture control [29]. Pressure distribution is described by immersion, envelopment and pressure gradient [29]. Immersion is defined as the depth of penetration into a support surface [28], envelopment is defined as the ability of a support surface to conform around irregularities in the body [28], and pressure gradient is defined as pressure change over a distance [29]. Temperature and moisture control are interrelated as increased temperature causes sweating and the increased moisture may lead to maceration [30].

Manufacturers produce a variety of cushion components to meet the needs of wheelchair users. Cushion components include elastic foam, viscoelastic foam, gel, air filled, viscous fluid floatation, honeycomb, powered alternating pressure and combinations thereof [28, 29]. Elastic foam is defined as a porous polymer that conforms in proportion to the applied weight [28] and returns to its original shape. Immersion and envelopment are set by a balance of stiffness and thickness [29]. For example, a soft foam envelops better, but bottoming out may occur if the cushion is too thin. Generic and custom contours are incorporated into foam designs to increase immersion [29].

Viscoelastic foam is defined as a porous polymer that conforms in proportion to applied weight, but at slower rates than elastic foam [28]. Viscoelastic foam is a time and temperature sensitive material [29, 31]. Greater loading rates result in greater resistance and increased temperatures near body temperatures result in foam with less stiffness. Viscoelastic foams do not perform well in cold ambient temperatures or when users wear insulating clothing [29]. Elastic and viscoelastic foams degrade and decrease in stiffness over time.

Gel is defined as a semisolid system which can exhibit elastic or viscoelastic properties [28], but has a greater heat transfer rate than foams [29]. Viscoelastic foams tend to increase skin temperature whereas gels maintain or decrease skin temperature [29].

Air is defined as a low density fluid with minimal resistance to flow [28]. Air filled cushions allow the buttock to immerse without tissue deformation [32]. Air filled designs include single bladders, segmented independent cells and several independent air cells contained within cushion compartments. A single bladder is designed to provide excellent immersion and envelopment. Independent air cells are designed to contour to the buttock by twisting and bending to increase contact area and decrease pressures [32]. Independent air cells can be interconnected to allow air exchange which equalizes reaction forces in an attempt to minimize pressure at bony prominences [32]. The slick surfaces and independent movement of cells attempt to reduce friction and shear stress [32]. Stability is the primary disadvantage of air filled cushions.

Viscous fluid is defined as a fluid with relatively high resistance to flow [28] and viscous fluid floatation requires containment of the viscous fluid. Applied pressure promotes immersion without resistance because the viscous fluid is incompressible. Viscous fluids generally have good thermal properties [31].

Honeycomb is not defined by the NPUAP, but the structure provides several methods of protection. Flex and collapsing of the honeycomb structure walls are designed to absorb compressive and shear stresses [33]. The absorption of compressive stresses attempts to distribute pressure and increase contact area, and the absorption of shear stresses attempts to reduce the reaction force against the skin [33]. Perforations in the honeycomb structure are designed to allow air circulation and moisture evaporation to help maintain tissue integrity and ambient body temperature [33].

Powered alternating pressure cushions are defined as a cushion requiring external energy that provides pressure redistribution via cyclic loading and unloading [28]. Parameter adjustments include pressure, inflation/deflation cycle times and postural support.

Combination cushions are not defined by the NPUAP but are a typical cushion design. For example, manufacturers use air cells or viscous fluid floatation at the IT to reduce mechanical loads and combine layers of elastic and viscoelastic foam to comprise the cushion base for increased stability.

The HCPCS Code Set is one of the standard codes used to ensure that insurance claims are processed in an orderly and consistent manner [34]. Level II HCPCS were established for submitting claims for durable medical equipment, prosthetic, orthotics, and supplies when used outside a physician's office [34]. HCPCS categories for wheelchair seat cushions are:

- General Use Seat Cushion (E2601 & E2602)
- Adjustable Skin Protection Seat Cushion (K0734 & K0735)
- Nonadjustable Skin Protection Seat Cushion (E2603 & E2604)
- Positioning Seat Cushion (E2605 & E2606)
- Adjustable Combination Skin Protection and Positioning Seat Cushion (K0736 & K0737)
- Nonadjustable Combination Skin Protection and Positioning Seat Cushion (E2607 & E2608)
- Custom Fabricated Seat Cushion (E2609)

The two codes listed for each category define cushion width less than 22 inches and cushion width of 22 inches or greater. Cushion categories separate technologies that are specific

to types of wheelchair users. For example, Medicare covers the cost of a General Use Seat Cushion when the patient has a wheelchair that meets certain Medicare coverage criteria [35]. If the patient does not have a covered wheelchair, then the cushion is denied coverage as not medically necessary [35]. Patients with a pressure ulcer, a history of pressure ulcers, limited or no sensation, or those unable to perform a functional weight shift qualify for an Adjustable or Nonadjustable Skin Protection Seat Cushion [35]. Patients with postural asymmetries qualify for a Positioning Seat Cushion. Adjustable and nonadjustable Combination Skin Protection and Positioning Seat Cushion are for patients who qualify for both Skin Protection and Positioning Seat Cushions [35]. Custom Fabricated Seat Cushions are for patients whose licensed clinician identifies a need not met by 'off-the-shelf' cushions [35].

2.3 SHEAR RELATED WHEELCHAIR SEAT CUSHION EVALUATION

Evaluation techniques provide performance characteristics and should demonstrate the ability to differentiate between products. Previous studies that characterized shear as related to wheelchair seat cushions and the inherent limitations are discussed.

Gilsdorf et al. [36] evaluated ROHO and Jay cushions on a modified powered reclining wheelchair. A force plate replaced the standard wheelchair seat and measured normal and global shear forces in various wheelchair back positions. Five subjects sat in the wheelchair and the wheelchair back reclined from an initial position (5° from vertical) to 58° from vertical, recording data at 5° increments. No differences in normal or shear forces were found between cushions; however, the author did not perform a statistical analysis and based conclusions solely on visual inspection of the results. Anatomical differences from subject to subject are likely to

skew the results and the author did not provide anatomical measurements or the standard deviation of weight. The methodology used in this study was unable to demonstrate differences between cushions.

Fontaine et al. [37] compared pressure and shear force measurement of three support surfaces (powered mattress, powered mattress overlay, and non-powered mattress overlays). Eleven subjects laid supine on each surface and the head of the bed was raised to 45°. Shear force were measured at the heel in supine and reclined positions. The methodology was able to demonstrate a statistical difference between the non-powered overlay as compared to a powered overlay and powered mattress; however the range of shear force was large. While descriptive data of the subjects was provided, the large range of measured shear forces was most likely due to the anatomical variability across subjects. Additionally, this shear force was measured with an unavailable, proprietary sensor.

Goossens [21] evaluated a foam cushion, gel cushion, and a LiquiCell overlay in three orientations: 5° forward; 5° backward; and horizontal. Twenty subjects sat on each cushion at each orientation and interface shear stress at the right ischial tuberosity was measured. The methodology was able to demonstrate a statistical difference between the LiquiCell overlay as compared to the gel and foam cushions. Similar to the previous studies, the anatomical difference across subjects is likely to skew data and the shear sensor used is not commercially available.

The International Organization for Standardization (ISO) has published ISO 16840-2 to determine the physical and mechanical characteristics of wheelchair seat cushions [3]. The standard was written to differentiate performance characteristics between wheelchair seat cushions; however, the clinical efficacy of the tests has not been validated. Without established clinical efficacy, use of the standard as a tool to rank or score a cushion’s ability to manage a

person’s tissue integrity is not appropriate. In addition to the seven performance tests, an informative Annex describes a lateral and forward stiffness test. Annex C of ISO 16840-2 is entitled “Lateral and Forward Stiffness” and describes a methodology to determine a cushion’s ability to absorb horizontal perturbations. A rigid cushion loading indenter (RCLI) is used to apply a normal load to the cushion and a single horizontal displacement is applied for 60 seconds. The resulting horizontal force represents the stiffness of the cushion and its ability to deform in response to the horizontal perturbation.

In summary, local shear force measurements demonstrated the ability to differentiate between cushions; however, the shear sensors are not commercially available. Additionally, anatomical variability between subjects was included in the measurements. The RCLI used in Annex C of ISO 16840-2 controls for the anatomical differences across subjects and isolates the measured differences to the cushion. However, the methodology used in ISO 16840-2 recorded one force to represent the stiffness characteristics of the cushion. This single data point does not provide ample data to construct a force-displacement curve nor to calculate a stiffness coefficient. Constructing a line using the single force-displacement data point and a (0,0) data point would imply zero interface shear stress upon the normal load, which is incorrect. A preliminary study applied multiple displacements to eight wheelchair seat cushions to calculate stiffness coefficients and demonstrated the ability to differentiate between commercial wheelchair seat cushions. [38]. This methodology was used to collect data in this study.

2.4 SUBCUTANEOUS TISSUE STRESSES AND STAINS

An FE model is a tool capable of quantifying the effects of extrinsic risk factors on subcutaneous tissues. Large objects are represented as a mesh of finite shapes. Researchers establish boundary conditions and use a numerical algorithm to solve for the unknown values. Chow and Odell [39], Todd and Thacker [13], and Dabnichki et al. [4] developed the first finite element models of the buttock and found the highest stresses in the soft tissues near the bone. Recently, Brosh and Arcan [40] developed a two-dimensional FE model of the buttock using a simplified IT geometry and homogeneous soft tissue. The highest stresses were found in the soft tissue inferior to the IT.

Ragan et al. [11] developed an axisymmetric 3-D FE model of the buttock using simplified IT geometry and homogenous soft tissue to evaluate the effects of polyurethane cushion thickness during sitting. Interface pressures and subcutaneous compressive stresses decreased as cushion thickness increased and subcutaneous shear stress increased slightly with cushion thickness. The subcutaneous compressive stresses were consistently greater than interface pressures and the maximum compressive stress was found just inferior to the surface of the IT. A no-slip constraint was used at the user-cushion interface.

Oomens et al. [10] developed an axisymmetric non-linear 3-D FE model of the buttock using simplified IT geometry and non-homogeneous soft tissue (muscle, fat and skin tissues). The thickness of the tissue layers was estimated using MR image data. Fat material properties were not available in the literature, but adjustments to the fat material properties resulted in minimal changes in the maximum shear strains of muscle near the IT. The maximum von-Mises stress was found in the muscle layer near the IT. Friction at the user-cushion interface decreased compressive stresses and shear strains in the muscle near the IT as compared to a frictionless condition.

Gefen et al. [5] developed a non-linear 3-D FE model using a cross-section near the sacrum from the “Visible Human” (male) digital database and non-homogenous soft tissues. Backrest angles of 70° and 80° were studied and greater peak compressive stresses were found in the muscle tissue at a backrest angle of 80°. Maximum strains were not reported by backrest angle.

Linder-Ganz et al. [7, 8] developed a non-linear 3-D FE model of the buttock using subject-specific geometry obtained from MR images and non-homogeneous soft tissue. The soft tissues included muscle tissue and a fat/skin combined tissue. MR images were collected in two seated postures: 1) non-weight-bearing and 2) weight-bearing. The non-weight-bearing seated posture was obtained with the subjects seated on a rubber tire and the weight-bearing seated posture was obtained with the subject seated on a foam cushion. Ischial tuberosity displacement was used as the displacement boundary conditions and the subcutaneous stress and strain distributions calculated. The maximum stresses and strains were found in the gluteal muscles near the bone interface. A comparison of healthy patients and patients with paraplegia resulted in internal tissues loads that were significantly higher in the patients with paraplegia [8].

Makhsous et al. [9] developed a non-linear 3-D FE model of the buttock and thigh using subject-specific geometry obtained from MR images and non-homogeneous soft tissue. The model included the femur, pelvis, skin, fat, and five muscle groups. MR images were collected in two simulated sitting postures: 1) without sitting pressure and 2) with sitting pressure. The simulated sitting postures were obtained using a custom apparatus of foam and rubber to get 80° hip flexion and 90° knee flexion. The sitting pressure was simulated using an air bladder to apply an upright sitting force to the subject. The air bladder applied an evenly distributed pressure to the buttock and was used in the FE model as initial loading conditions. Pressure distribution of a

seated person is not evenly distributed as peak pressures are typically located under the IT and at the sacrum. Even with atypical loading conditions, the maximum compressive stresses and strains were found in the muscle covering the IT.

Finite element models have become increasingly more complex to capture the anatomical geometry and material properties of soft tissues. Although differences exist in the models, a sound methodology of capturing subject-specific geometry using MR images and performing a FE analysis to identify subcutaneous stresses and strains is established [7-9]. Limitations of the previous studies include image collection and validation techniques. Images collected in the non-loaded condition [7] and loaded condition [9] are not representative of a seated person. In this study, the Upright^{TM} MRI was used to obtain appropriate non-loaded images and displacement boundary conditions were utilized to obtain appropriate loaded conditions. Interface pressures and shear stresses were used to validate the model. This was the first study to use interface shear stresses in addition to interface pressures for model validation. Completion of this work will provide a validated FE model that will be used to evaluate the SCI population and prototype wheelchair seat cushions.

2.5 SUMMARY

The animal and human studies demonstrated that shear force compromises tissue integrity. The animal studies identified that shear forces applied to bony prominences increased the severity of pressure ulcers as compared to pressure alone [25, 26] and the human studies identified that shear forces decreased cutaneous blood flow [16, 19, 20, 23]. The literature has established the importance of reducing shear, yet no previous study had evaluated interface shear stress of

several commercial cushions. This study filled the void in the literature pertaining to interface shear stress of commercial cushions and will aid clinicians when selecting the appropriate cushion to meet the patient's needs. The results of the cushion evaluation can also benefit cushion designers because a technique was established to quantify shear reduction. The cushion materials and technologies identified by the cushion evaluation to reduce shear were used to conceptualize, prototype, and evaluate new cushions designs. A closed-loop control system that was capable of monitoring interface shear stress was the foundation of all designs. In addition to interface measurements, finite element models are able to predict stress and strain distribution of subcutaneous tissues. Models have evolved from simplistic geometric shapes and linear material properties to subject-specific geometry and non-linear material properties. This study addressed the limitations of recent studies which, included image collection methodology, model construction, and validation. Quantification of subcutaneous tissue stresses and strains provides information on the ability of a wheelchair seat cushion to reduce pressure ulcer development. The purpose of this study was to quantify interface shear stresses of the commercial wheelchair seat cushion, develop a prototype wheelchair seat cushion, and model subcutaneous tissues stresses and strains.

3.0 SHEAR CHARACTERISTICS OF WHEELCHAIR SEAT CUSHIONS

Shear-reduction and low-shear are common terms found in marketing literature of wheelchair seat cushion manufactures without published data to support such claims. Literature is available on the interface pressure and pressure redistribution characteristics of commercial cushions [41, 42]; however, no study has evaluated interface shear stress for commercial cushions. This study filled the void in the literature pertaining to interface shear stress of commercial cushions composed of various materials of construction and HCPCS categories.

This study quantified interface pressure and shear stress of commercial wheelchair seat cushions and developed a methodology to calculate overall and local horizontal stiffness of a cushion. Interface pressure was measures in addition to interface shear stress because shear force is a function of normal force and coefficient of friction. Increased normal force applied to the cushion increases the potential shear force. Overall horizontal stiffness is defined as the cushion's ability to resist a tangentially applied force. Local horizontal stiffness is defined as the cushion's ability to locally resist a tangentially applied force. Because many cushions are composed of a combination of materials, a local value of stiffness is important. In a seated posture, tissues inferior to a bony prominence, ischial tuberosities (IT) and sacrum, are at greater risk of pressure ulcer development. Due to this increased risk, many cushion manufactures use a material with lower stiffness to support the bony prominence while a material of high stiffness is

used beneath the thigh. Tissues beneath the thigh are able to tolerate higher loads because no bony prominence is present.

A preliminary trial of eight wheelchair seat cushions resulted in similar interface shear stresses found in the literature and a positive correlation between local horizontal stiffness and interface shear stress [38]. The objectives of this study are:

- Quantify interface shear stress of commercial wheelchair seat cushions
- Determine if a relationship exists between the horizontal stiffness of a cushion and interface shear stress
- Determine if a relationship exists between immersion and interface shear stress

3.1 METHODS

3.1.1 Pressure and Shear Force Sensor

Quantification of interface shear stress requires a thin, deformable sensor to reduce interference. The two commercially available options were the FSA shear force measurement system (Vista Medical Ltd., Canada) and the pressure and shear force sensor (Predia, Molten Corporation, Japan). The pressure and shear force sensor was chosen for this study because preliminary testing of the FSA shear force measurement system resulted in reliability difficulties and multiple sensor failures. The pressure and shear force sensor measures pressure with air displacement and shear force with a strain gauge. The pressure and shear force sensor (sensor) is a made of flexible plastic and has an elliptical shape (Figure 3).

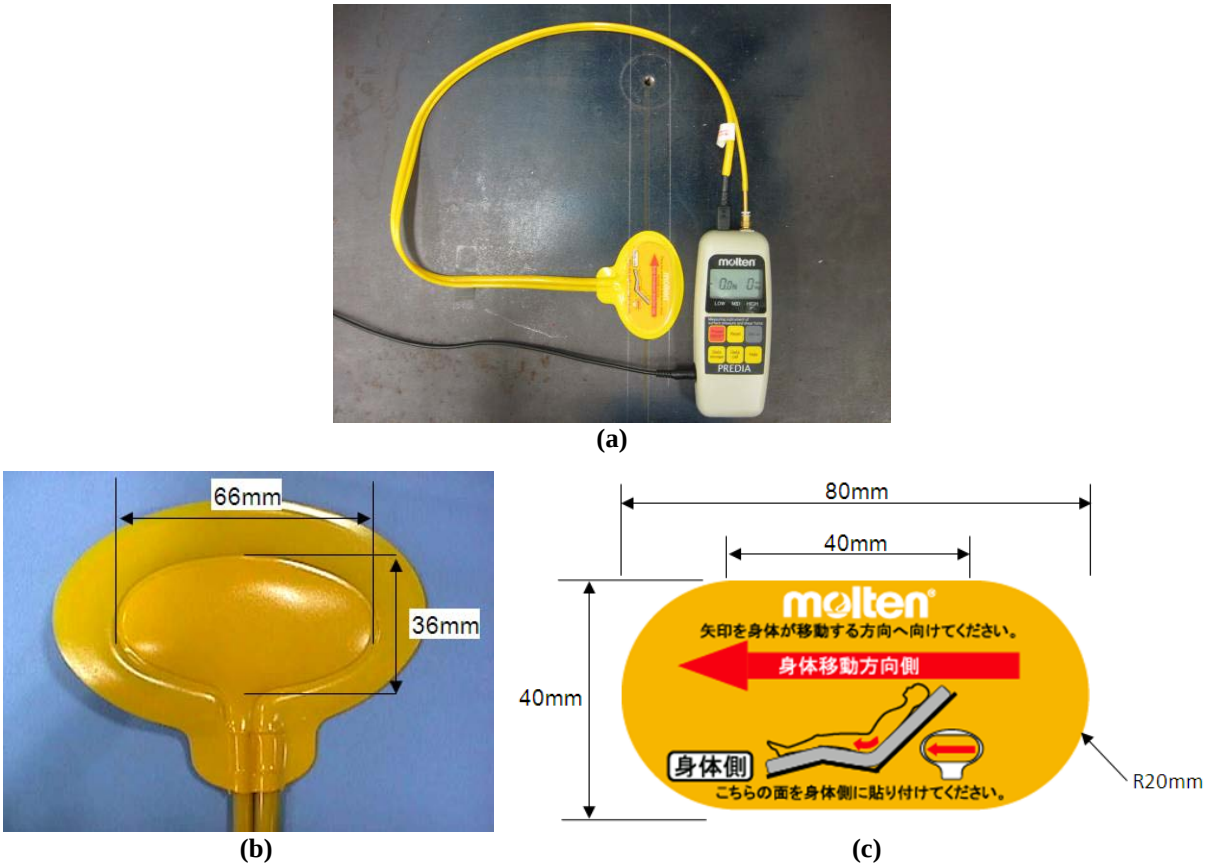

Figure 3: Predia pressure and shear force sensor shown (a) assembled, (b) dimensions for pressure sensing area and (c) dimensions for shear sensing area

The sensor has an analog-output for data collection and internal memory for storing up to five data values of pressure and shear. As the primary means of data collection, the analog-output cable (the black cable shown in Figure 3a) carries two voltages representing pressure and shear force measurements. The sensor is able to measure pressures ranging from 0 – 200 mmHg, which yields data from 0.0 – 2.0 volts; and the sensor is able to measure shear forces ranging from 0 – 50 N, which yields 1.0 – 2.0 volts. The data acquisition system and data storage function of the sensor were used to compare the two raw voltages to the values displayed on the sensor LCD. Pressure and shear forces were evaluated separately.

3.1.2 Calibration

A calibration procedure was performed pre- and post-test to test the accuracy and repeatability of the sensor. Development of a new calibration apparatus and procedure was required because a calibration method written by the Shear Force Initiative [43] was unable to test the full range of shear force and did not evaluate pressure.

3.1.2.1 Calibration Apparatus and Instrumentation

The calibration apparatus (Figure 4) consisted of the sensor, aluminum block, weights, Alliance RF/100 (MTS) and data acquisition system. The sensor was adhered to the MTS platform, perpendicular to the MTS crosshead and in-line with the load cell. Pressure and shear force were transmitted to the sensor via the aluminum block (0.2 kg) with a 32 RMS finish on the side in contact with the sensor. This surface finish provides a smooth, clean surface to transmit the loads directly to the sensor. A string attached the aluminum block to the load cell of the MTS via a pulley. The string was attached to the MTS and extended vertically from the MTS and horizontal to the aluminum block to ensure the measurement by the load cell was the load applied to the sensor. Weights were used to apply pressure and displacement of the MTS crosshead was used to apply shear force to the sensor. The calibration apparatus was capable of separately applying pressure and shear to the sensor to determine the accuracy of the output from the sensor.

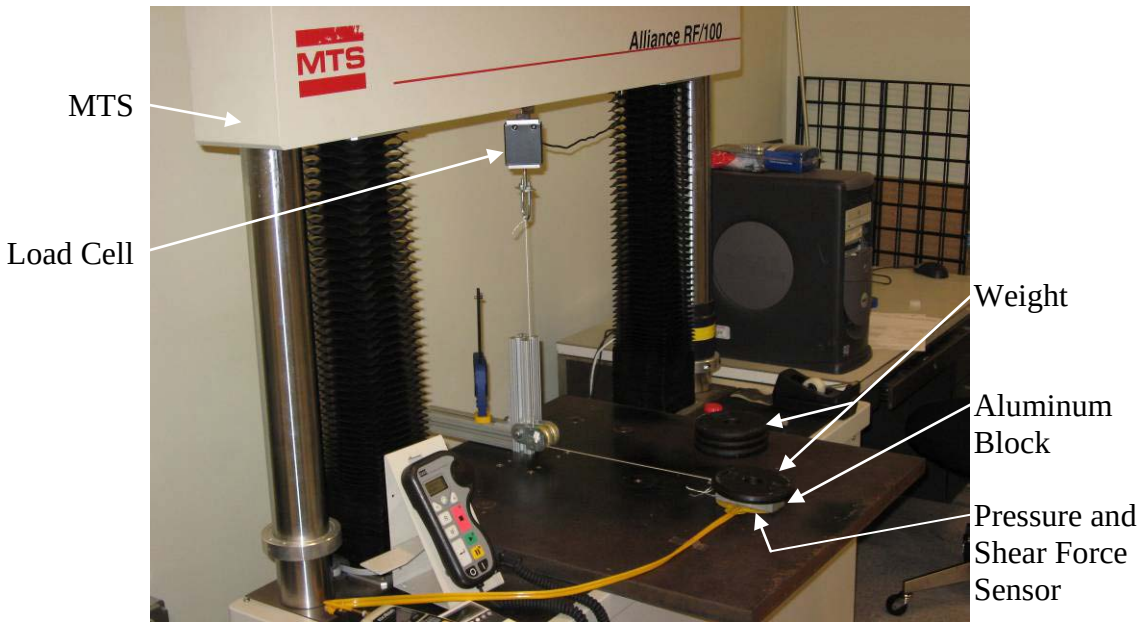

Figure 4: Calibration apparatus and instrumentation

3.1.2.2 Calibration Procedure

By following the calibration procedure, pre- and post-test accuracy and repeatability of the pressure and shear force sensor was obtained. Pressure was tested by incrementally applying 'dead weight' to the sensor and recording the sensor output after three seconds. Applied (true) average pressure was calculated by dividing the mass of the aluminum block and each weight by the contact area of the sensor (1865 mm^2). True pressures were: 8.1; 43.0; 86.0; 129.0 and 172.0 mmHg and a total of three trials were conducted at each pressure. Shear force was tested by applying incremental horizontal displacements to the aluminum block via the MTS. The sensor was adhered to the platform of the MTS and weighted to achieve an average pressure of 172 mmHg. Horizontal displacements (5, 10, 15 and 20 mm) were applied to the aluminum block and the sensor output was recorded after three seconds. The three second duration was arbitrarily selected and the calibration procedure is detailed below.

1. Preconditioning
    a. The calibration apparatus must be preconditioned for 24 hours at 23°C±2 and 50% ±5% relative humidity.
    b. Use a clean cloth or tissue and lightly wipe the test surfaces of the sensor and aluminum block to remove any loose fibers or debris which may be present. Care must be taken to insure the test surface is not disrupted.
2. Pressure
    a. Apply aluminum block atop the sensor and record a measurement after 3 seconds
    b. Apply (1) 2-1/2 lbs. weight to aluminum block and record a measurement after 3 seconds
    c. Apply an additional 2-1/2 lbs. weight atop the other weight(s) and record a measurement after 3 seconds
    d. Repeat (c) twice
    e. Remove weights and aluminum block
    f. Repeat (a) – (e) twice for a total of three trials
3. Shear
    a. Apply aluminum block atop the sensor
    b. Apply (4) 2-1/2 lbs. weights atop the aluminum block and record a measurement after 3 seconds
    c. Apply a horizontal displacement of 5 mm and record a measurement after 3 seconds
    d. Apply an additional 5 mm horizontal displacement (total of 10 mm) and record a measurement after 3 seconds

e. Apply an additional 5 mm horizontal displacement (total of 15 mm) and record a measurement after 3 seconds
f. Apply an additional 5 mm horizontal displacement (total of 20 mm) and record a measurement after 3 seconds
g. Remove applied displacement, weights and aluminum block
h. Repeat (a) – (g) twice for a total of three trials

3.1.3 Shear Characteristics

The methodology chosen for this study was a deviation from the horizontal and lateral stiffness test in Annex C of ISO 16840-2 [3]. The deviations included multiple horizontal displacements and a sampling frequency of 10 Hz. The original standard tested one horizontal displacement (10mm) and recorded one data point after 60s. The engineering definition of stiffness is the slope of a force-displacement curve. To have a curve, a minimum of two points must be collected and preferably three or more data points are needed to ensure the force-displacement relationship is linear.

Cushions from each HCPCS category (Table 1) were evaluated to identify category specific shear characteristics. The cushions chosen for testing were from manufacturers with a large market share to represent as many users as possible. The ROHO Group, Sunrise Medical and The Comfort Company have at least one cushion in each HCPCS category and Supracor has at least one cushion in each nonadjustable category. Supracor was chosen specifically because it does not offer adjustable cushions. A shear reducing cushion cover was chosen for each cushion when available.

Table 1: Wheelchair seat cushions listed by HCPCS category

HCPCS Code	Product Name	Cushion Cover	Manufacturer	Model Number	Material(s) of Construction
E2601	Mosaic	Standard two way stretch	ROHO	MOS1616C	Segmented Air Cell
	Jay Basic	Incontience-Resistant	Sunrise Medical	305-MJ	Contoured Elastic Foam
	Curve	Comfort-Tek	Comfort Company	463G-1616-B	Contoured Elastic Foam
	Stimulite Silver	Polyester	Supracor	SI1616	Honeycomb
K0734	High Profile Single Compartment	Standard two way stretch	ROHO	IR99C	Segmented Air Cell
	Adjuster	Comfort-Tek	Comfort Company	AJ-F-1616	Independent Air Cell
	Jay J2 Deep Contour	Ballistic stretch	Sunrise Medical	2466	Viscous fluid / Contoured Elastic Foam
E2603	Triumph	Standard two way stretch	ROHO	TS1616C	Viscoelastic Foam
	Ascent	Comfort-Tek	Comfort Company	HY-GF-1616	Contoured Elastic Foam
	Jay Xtreme	LoShear™	Sunrise Medical	966LS	Viscous fluid / Contoured Elastic Foam
	Stimulite Classic	Polyester	Supracor	CL1616 / SP1616	Honeycomb
E2605	Airlite	Standard two way stretch	ROHO	AL1616	Elastic Foam and Segmented Air Cell
	Ridge	Comfort-Tek	Comfort Company	RD-F-1616	Viscoelastic and Elastic Foam
	Jay Soft Combi P	Incontience-Resistant	Sunrise Medical	B2205 (15.5x16)	Contoured Elastic Foam
K0736	Quadtro Select High Profile	Standard two way stretch	ROHO	QS99C	Segmented Air Cell
	Vector	Comfort-Tek	Comfort Company	VT-F-1616	Independent Air Cell
	Jay J2 Deep Contour P	Ballistic stretch	Sunrise Medical	2466P	Viscous fluid / Contoured Elastic Foam
E2607	Harmony	Standard two way stretch	ROHO	H1616C	Segmented Air Cell
	Maxx	Comfort-Tek	Comfort Company	MAXFF-1616	Gel and Elastic Foam
	Jay Easy	Incontience-Resistant	Sunrise Medical	JE1616C	Viscous Fluid / Contoured Elastic Foam
	Stimulite Contoured	Polyester	Supracor	CD1616	Honeycomb

3.1.3.1 Shear Characteristics Apparatus and Instrumentation

The following equipment was used to capture the shear characteristics of the commercial cushions: loading rig; RCLI; pressure and shear force sensor; MTS; load cell; and digital indicator.

ISO 16840-2 specified the loading rig must be capable of applying a vertical load up to 830 N, measuring displacements to ±1mm and support a wheelchair seat cushion on a rigid horizontal surface without flexing under loading cushions. Additionally, the RCLI must be manufactured from a rigid material such as wood or fiberglass and have the dimensions specified in Annex A of the standard. Horizontal RCLI displacement, interface pressure, interface shear

force and horizontal force were recorded at 10 Hz. Vertical RCLI displacement was recorded at 60 and 120 seconds. Horizontal RCLI displacement was the horizontal displacement of the RCLI measured with a digital indicator with analog output (Swiss Precision Instruments, Inc., USA), interface pressure and interface shear force were the mechanical forces at the RCLI-cushion interface measured with a pressure and shear force sensor placed under the left IT of the RCLI (Predia, Molten Corp., Japan), and horizontal force was the force resulting from the applied horizontal displacements measured with a load cell (MTS Systems Corp., USA). Vertical RCLI displacement was the distance of RCLI immersion into the cushion. Interface shear stress was calculated by dividing the interface shear force by the sensing area (28.14 cm^2). Figure 5 shows a photograph of the apparatus and instrumentation.

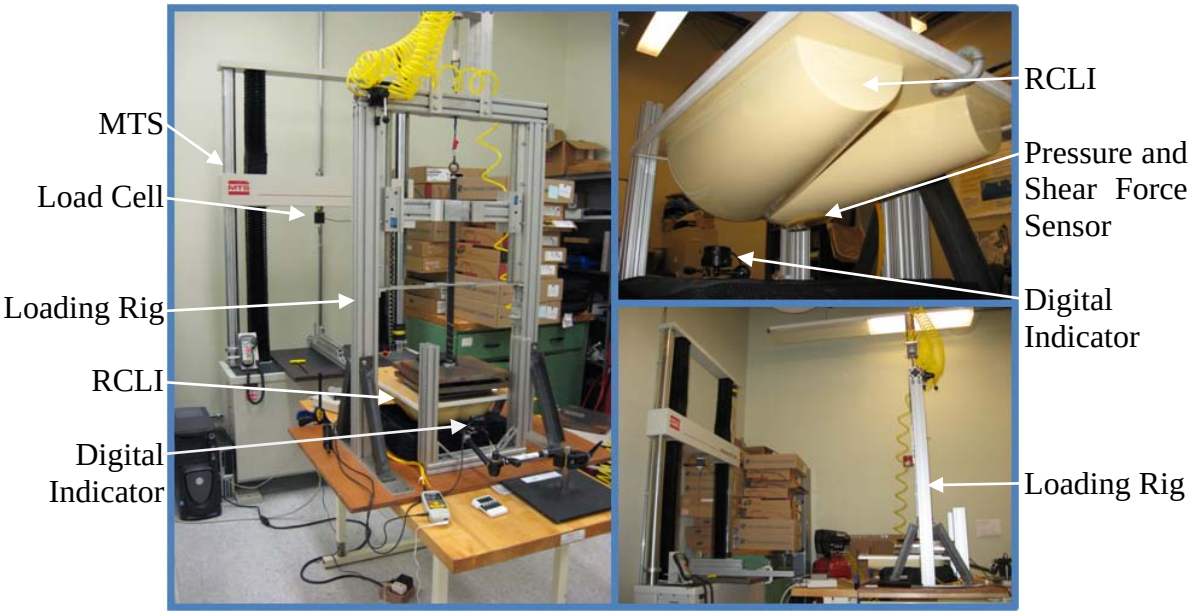

Figure 5: Shear characteristics test apparatus and instrumentation

3.1.3.2 Shear Characteristics Procedure

Shear characteristics of the cushions were obtained using the preconditioning, setup and test methodologies described below.

1. Precondition the cushion
    a. Acclimate the cushion to the test environment (23ºC ± 2ºC and 50% ± 5% relative humidity) for 12 hours
    b. Adjust the cushion to accommodate 830 N ± 10 N (84.7 ± 1.0 kg) load, if applicable
    c. Apply 830 N ± 10 N using the RCLI for 150 seconds
    d. Unload and reload within 120 seconds
    e. Remove load after 150 seconds
    f. Allow cushion to recover for a minimum of 5 minutes and a maximum of 60 minutes
2. Setup
    a. Adjust the cushion to accommodate 500 N ± 10 N (51.0 ± 1.0 kg) load, if applicable
    b. Reset the cushion material by flattening, if applicable
3. Test Method
    a. Place the RCLI in the loading jig
    b. Position the cushion under the RCLI such that the ITs of the indenter are 125 mm ± 25 mm forward of the back edge of the cushion or are aligned with the analogous part of the cushion

c. Apply a vertical load of 500 N ± 10 N to the RCLI and record immersion
d. Within 60 seconds ± 5 second, apply a horizontal RCLI displacement of 10 mm at a rate of 2 mm/s ± 1 mm/s for 120 seconds
e. Record pressure and shear force at 10 Hz
f. Record horizontal RCLI displacement at 10 Hz
g. Record vertical RCLI displacement at 60 and 120 seconds
h. Unload vertical and horizontal loads (reload within 120 seconds)
i. Reset cushion material by flattening, if applicable
j. Repeat c-i 4 times, a total of 5 trials
k. Repeat c-i for 15, 20 and 0 mm of horizontal RCLI displacement

3.1.4 Immersion

Immersion is the displacement of the user into the cushion. Good immersion ideally allows contact of the seat with the greater trochanter of the femur. Involving the greater trochanter in the seating system removes a portion of the load from the IT, reducing the risk of pressure ulcers.

Immersion was calculated by taking the difference of the initial and loaded cushion thicknesses. Initial cushion thickness was measured using the loaded contour depth procedure in the ISO 16840-2 standard [3]. Cushions were preconditioned and placed on a flat horizontal surface. The cushion thickness was measured at a location 127mm ± 25mm from the rear border of the cushion while applying 1.5 N ± 0.5N using the seat cushion thickness measurement rig as shown in Figure 6. Contoured cushions were measured at the lateral edge and flat cushions were measured at the midline. The mean of three trials was used as initial cushion thickness.

Figure 6: Cushion thickness test apparatus

Loaded cushion thickness was measured during shear characterization testing. After the loaded RCLI was applied to the cushion, the distance from the rigid horizontal surface to the IT of the RCLI was recorded. Immersion was calculated using the difference of the initial and loaded cushion thicknesses.

3.1.5 Statistical Analysis

3.1.5.1 Pressure and Shear Force Sensor

Incorporation of the sensor into the data acquisition system required processing of the analog output voltages using an algorithm. Analog-output voltages were plotted against the respective values displayed on the sensor in scatterplots. A regression analysis was performed from the respective data used for the scatterplots and the resulting slope, y-intercept and r-squared values were recorded. A criterion of the R^2 value above 0.70 was used to indicate a good fit. Upon good

fit, the respective slope and y-intercept were used in the data acquisition software to convert the raw voltages to the values displayed on the sensor LCD.

3.1.5.2 Calibration

Sensor repeatability and accuracy were determined using repeated measures ANOVA and one sample t-tests, respectively (α=.05). Repeatability was evaluated first to determine whether differences in sensor output occurred pre- and post-test. Repeated measures ANOVA compared pre- and post-test calibration data, i.e. repeatability of the sensor.

Accuracy was evaluated using one sample t-tests to compare true and measured forces. T-tests were performed on all data, both pre- and post-test, if the sensor was repeatable (no significant differences between pre- and post-test); and t-tests were performed individually on pre- and post-test data if the sensor was not repeatable (significant difference between pre- and post-test). No significant difference from the t-test would indicate the sensor accurately measured pressure/shear and a significant difference would indicate error was included the pressure/shear measurement.

3.1.5.3 Shear Characteristics

Statistical analyses for interface stresses and horizontal stiffness are described separately.

Interface Pressure and Shear Stress

Interface pressure and shear stress values were recorded at 60 and 120 seconds for each horizontal displacement. A repeated measures ANOVA was used to determine if differences existed between the two time points. Least significant difference (LSD) post-hoc analyses were performed to determine if a HCPCS category exhibited significantly greater or lower interface

stresses. Bonferroni correction was used to guard against Type I errors resulting in alpha equal to 0.008 for post-hoc analyses.

Horizontal Stiffness

Mean horizontal force and interface shear stress measurements were used with RCLI displacements (0, 10, 15 and 20 mm) to construct force-displacement and shear-force-displacement curves, respectively. A regression analysis of the force-displacement and shear-force-displacement curves resulted in overall horizontal stiffness and local horizontal stiffness, respectively. Correlation coefficients were calculated to determine if relationships exist between:

- mean horizontal force and overall horizontal stiffness
- mean horizontal force and local horizontal stiffness
- mean interface shear stress and overall horizontal stiffness
- mean interface shear stress and local horizontal stiffness
- overall horizontal stiffness and local horizontal stiffness
- overall horizontal stiffness and ISO 16840-2 stiffness
- local horizontal stiffness and ISO 16840-2 stiffness

ISO 16840-2 stiffness was calculated per the standard as the mean horizontal force measured at 10mm displacement after 60 seconds.

3.1.5.4 Immersion

Correlation coefficients were calculated to determine whether a relationship existed between immersion and interface pressure; immersion and shear stress; and immersion and horizontal force.

3.2 RESULTS

3.2.1 Pressure and Shear Force Sensor

Pressure ranged between 0 – 140 mmHg corresponding to a voltage range of 0.3 – 1.7 V and shear force ranged between -1.7 – 24.5 N corresponding to a voltage range of 1.3 – 1.8 V. The regression analysis for pressure and shear force resulted in highly linear relationships as noted by the r-squared values nearly equal, or equal to 1.0. Slope and y-intercept of the pressure line equation were 101.33 and -32.287, respectively; and slope and y-intercept of the shear force line equation were 50.169 and -64.984, respectively. Scatterplots of the analog-output voltages versus values displayed on the sensor are shown in Figure 7. The slope and y-intercepts of the pressure and shear force values were used in the data acquisition software to calculate the actual measurements from the analog-output of the sensor. Though the complete range of pressure and shear force were not tested, it can be assumed the higher range of each measurement could be accurately extrapolated due to the highly linear relationship.

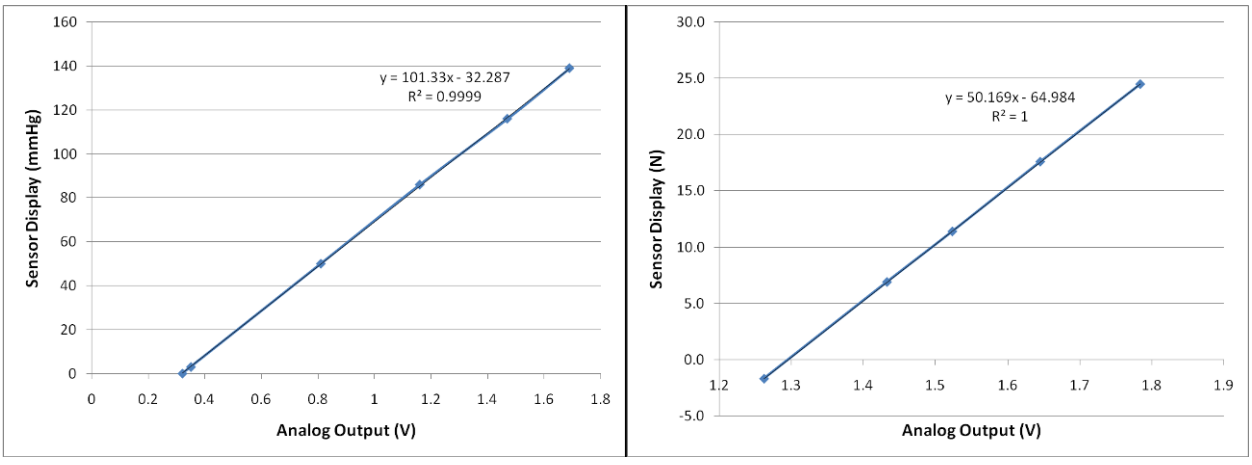

(a) **(b)**

Figure 7: Sensor analog output versus sensor display for (a) pressure and (b) shear

3.2.2 Calibration

The repeated measures ANOVA resulted in no significant differences for pressure pre- and post-test (p=.759) with a small effect size (partial η^2 =.010) as shown in Figure 8. The time*load interaction was not significant (p=.159) with a moderate effect size (partial η^2 =.454). As expected, pressure increased as load increased and was significantly different (p<.001).

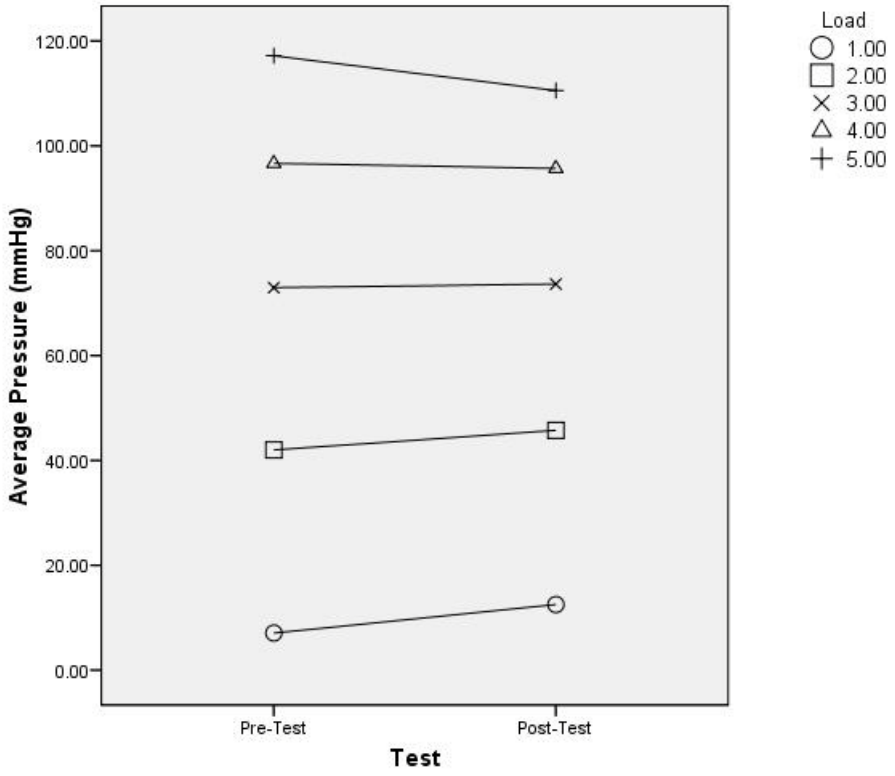

Figure 8: Pre- and post-test interface pressure calibration data

The repeated measures ANOVA resulted in a significant difference in shear force (p<.001) with a large effect size (partial η^2 =.984) as shown in Figure 9. The time*load interaction was significant (p<.001) with a large effect size (partial η^2 =.981). Measured shear force increased as applied shear force increased and was significantly different (p<.001).

Negligible change occurred pre- and post-test for loads 1 and 2; however, a sharp decline in shear force measurement occurred for loads 3, 4 and 5 as shown in Figure 9.

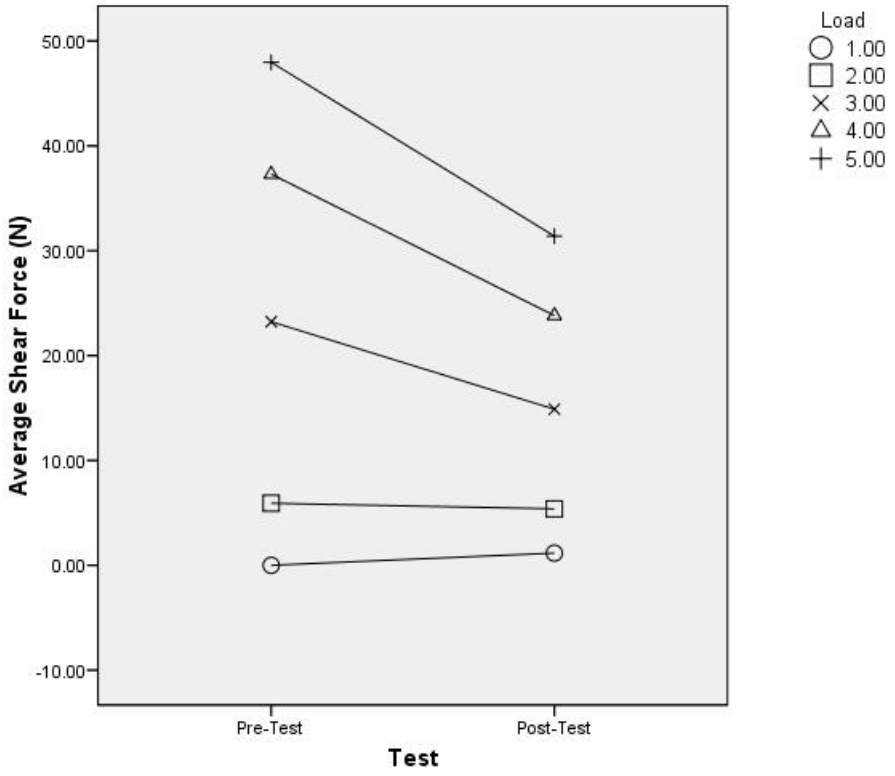

Figure 9: Pre- and post-test shear force calibration data

Because no significant difference was found between pre- and post-test pressure calibration measurements and the applied pressure was the same (dead weights), all measured pressure values were compared with the respective true pressures using t-tests. The pre- and post-test pressure calibration data (Figure 10) tested a pressure range of 0 – 172.0 mmHg and the pressure sensor measured a range of 0 – 113.9 mmHg. No significant difference indicates that the sensor accurately measured pressure and a significant difference indicates error was included in the pressure measurement. The results of the t-test for pressure and shear force are tabulated in

Table 2. At loads 1 (8.1 mmHg, p=.325) and 2 (43.0 mmHg, p=.453) the sensor accurately measured the applied pressure; however, at loads 3 (86.0 mmHg, p=.000), 4 (129.0 mmHg, p=.000) and 5 (172.0 mmHg, p<.001) error was included in the sensor measurement. The pre- and post-test pressure calibration results are illustrated in Figure 10 with the ideal pressure that should be measured.

Table 2: Pressure and shear force calibration data for sensor accuracy

Load	Measured			Applied			p	
	Mean		Std	Mean		Std		
Pre- and Post-Test Pressure Calibration (mmHg)								
1	9.79	±	4.02	8.09	±	0.00	0.325	
2	43.86	±	2.70	43.00	±	0.00	0.453	
3	73.29	±	2.68	86.01	±	0.00	0.000	*
4	96.18	±	2.95	129.01	±	0.00	0.000	*
5	113.87	±	5.84	172.02	±	0.00	0.000	*
Pre-Test Shear Force Calibration (N)								
1	-0.01	±	0.58	0.00	±	0.00	0.985	
2	5.91	±	1.29	10.00	±	0.00	0.005	*
3	23.23	±	0.60	21.30	±	0.00	0.005	*
4	37.30	±	1.16	30.90	±	0.00	0.001	*
5	47.97	±	0.56	39.20	±	0.00	0.000	*
Post-Test Shear Force Calibration (N)								
1	1.16	±	0.73	0.00	±	0.00	0.052	
2	5.39	±	0.06	10.03	±	0.00	0.000	*
3	14.89	±	0.20	17.02	±	0.00	0.000	*
4	23.82	±	0.39	23.50	±	0.00	0.232	
5	31.39	±	0.46	29.29	±	0.00	0.001	*

* p < .005

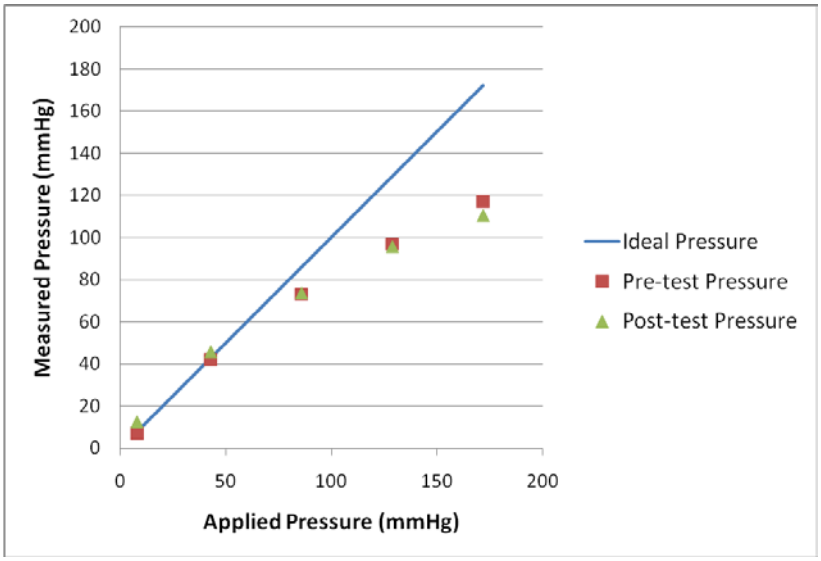

Figure 10: Pre- and post-test pressure calibration plot

The significant difference between the pre- and post-test shear calibration measurements required separate t-test to be conducted when compared to the true shear force. The pre-test shear calibration data (Figure 11a) tested a shear force range of 0 – 39.2 N and the shear force sensor measured a range of 0 – 48.0 N. The post-test shear calibration data (Figure 11b) tested a shear force range of 0 – 29.3 N and the shear force sensor measured a range of 1.1 – 31.4 N. No significant difference indicates that the sensor accurately measured shear and a significant difference indicates error was included the shear measurement. The sensor accurately measured the applied shear force at load 1 (0 mm, p=.052) both pre- and post-test and at load 4 (15 mm, p=.232) post-test. However, error was included in the sensor measurement at loads 2 (5 mm, p=.000), 3 (10 mm, p.000) and 5 (20 mm, p=.001) both pre- and post-test. Shear force t-test results are tabulated in Table 2. Pre- and post-test shear force calibration results are illustrated in Figure 11 with ideal shear force.

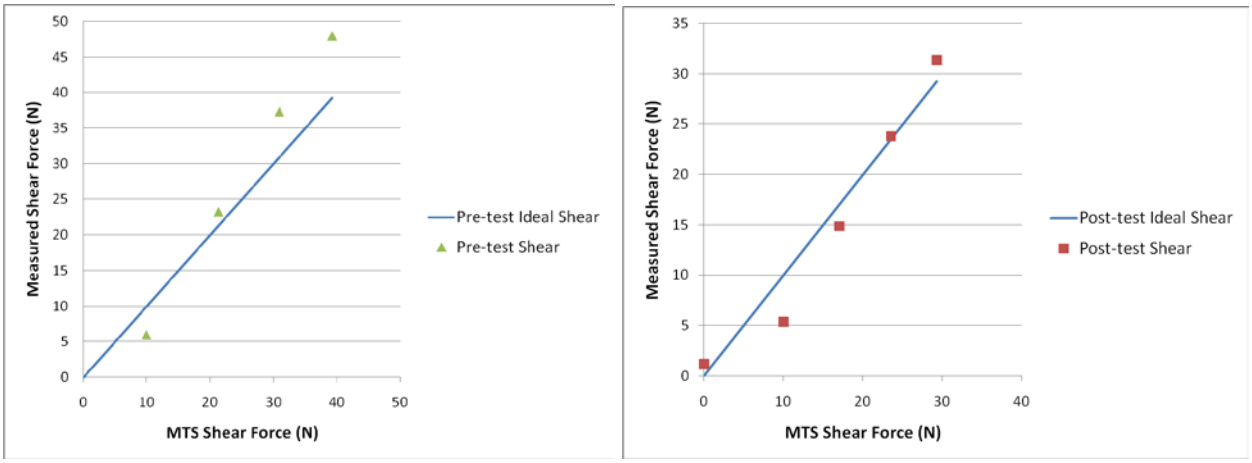

(a) **(b)**

Figure 11: Shear force calibration plots for (a) pre-test and (b) post-test

3.2.3 Shear Characteristics Test

3.2.3.1 Interface Pressure and Shear Stress

The repeated measures ANOVA on interface pressure resulted with no significant effect in time ($p=.089$) and the only significant interaction was time*category*displacement ($p=.036$). Both time and the time*category*displacement interaction had small effect sizes (partial $\eta^2=.008$ and partial $\eta^2=.070$, respectively) indicating the interaction terms would provide little contribution in the amount of variance accounted for by the model. Interface pressure was significantly different across categories ($p\leq.001$) with a moderate effect size (partial $\eta^2=.420$) and displacement was marginally significanct ($p=.054$) with a small effect size (partial $\eta^2=.021$). Interface pressure for the category*displacement ($p=.999$) interaction was not significantly different. An LSD post-hoc analysis resulted in the nonadjustable skin protection category (E2603) with significantly greater interface pressure than all categories ($p\leq.001$) except the general use category (E2601) ($p\leq.001$)

with mean differences as shown in Table 2; and interface pressure for the adjustable combination skin protection and positioning category (K0736) was significantly less than all other categories ($p \leq .001$) with mean differences as shown in Table 2.

Table 3: Mean differences between categories with the greatest and least interface pressure

Category	Category	Mean Difference		p
E2603	E2601	1.725		0.300
	K0734	16.491	*	0.000
	E2605	7.375	*	0.000
	K0736	22.420	*	0.000
	E2607	6.609	*	0.000
K0736	E2601	-20.695	*	0.000
	K0734	-5.928	*	0.001
	E2603	-22.420	*	0.000
	E2605	-15.045	*	0.000
	E2607	-15.810	*	0.000

* $p \leq .001$

Figure 12 illustrates differences in interface pressure across displacement by cushion category. The rank of category for interface pressures from least to greatest were: adjustable combination skin protection and positioning (K0736); adjustable skin protection (K0734); positioning (E2605); nonadjustable combination skin protection and positioning (E2507); general use (E2601) and nonadjustable skin protection (E2603) with no change in the rank of categories across displacements. Interface pressure peaked at 10mm displacement for all categories, except the adjustable combination skin protection and positioning category (K0736), which peaked at 20mm displacement. The adjustable combination skin protection and positioning category (K0736) was the only category that consistently increased as displacement

increased. The nonadjustable combination skin protection and positioning category (E2607) also increased from 15 to 20mm.

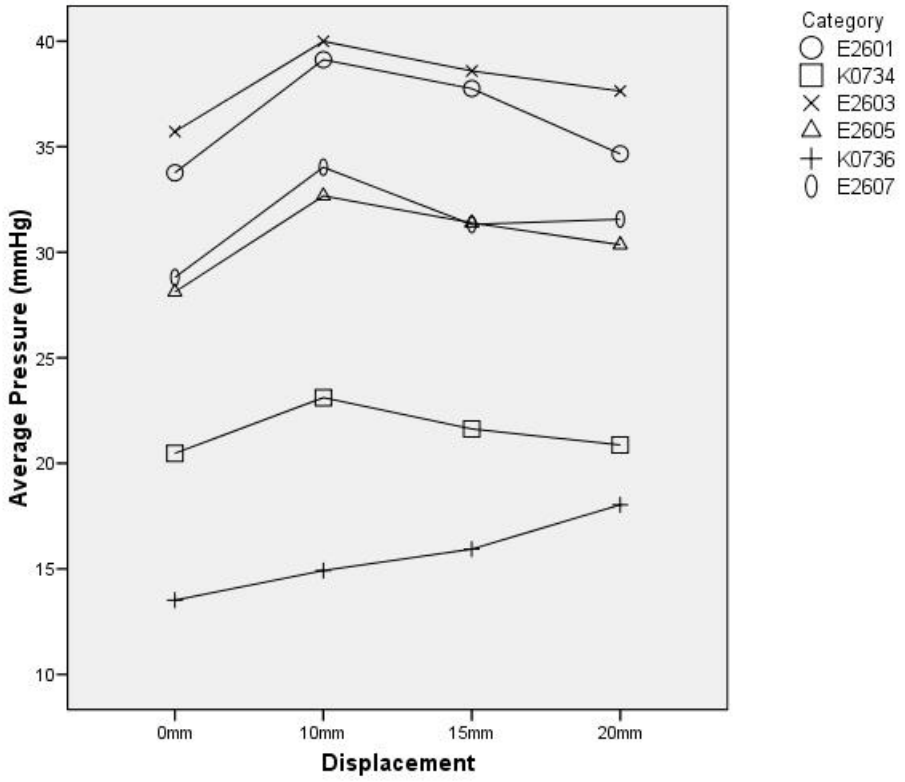

Figure 12: Mean interface pressure vs. displacement for each category at 60s

Interface pressure results were organized by materials of construction to determine the performance of the various cushion materials as shown in Figure 13. Cushions were combined into six material categories and four pressure ranges. The six material categories were: 1) air cell (segmented and independent); 2) viscous fluid; 3) elastic foam; 4) viscoelastic foam; 5) honeycomb; and 6) gel. The four pressure ranges were: I) 10 – 24.9 mmHg; II) 25 – 39.9 mmHg; III) 40+ mmHg; and IV) Not Tested. Cushions constructed using air cell and viscous fluid materials resulted in lowest interface pressure ranges. Five of seven of the air cell and two of

three viscous fluid cushions were in pressure range I and the remaining in pressure range II. The elastic foam resulted with two cushions in pressure range II, one in pressure range I, and two cushions not tested due to shear sensor saturation. Both viscoelastic cushions were in pressure range II, all three honeycomb cushions were in pressure range III, and the single gel cushion was in pressure range II.

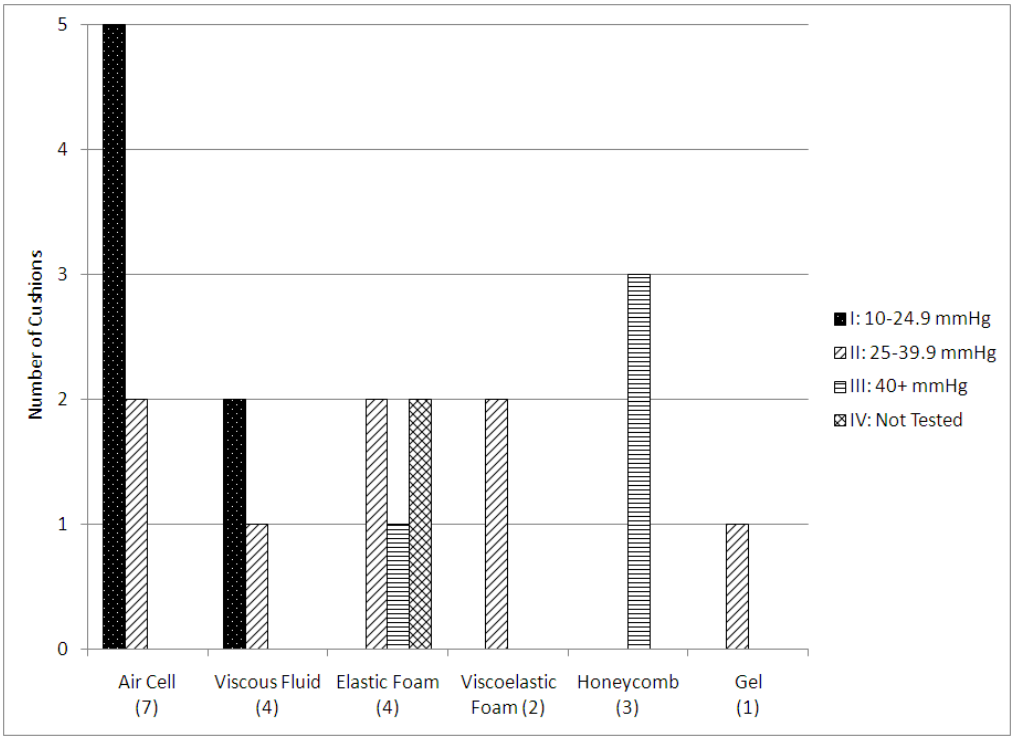

Figure 13: Mean interface pressure by materials of construction

(the number of cushions in each category shown in parentheses)

The repeated measures ANOVA on interface shear stress resulted with significant effect in time ($p \leq .001$) and all interactions: time*category ($p \leq .001$); time*displacement ($p \leq .001$) and time*category*displacement ($p = .049$). Effect size for time (partial $\eta^2 = .611$) was large, time*category (partial $\eta^2 = .148$) was small, time*displacement (partial $\eta^2 = .381$) was moderate

and time*category*displacement (partial η^2=.067) was small. Interface shear stress was significantly different across category ($p \leq .001$), displacement ($p \leq .001$) and the category*displacement interaction ($p \leq .001$) with effect sizes as small (partial η^2=.181), moderate (partial η^2=.386) and small (partial η^2=.111), respectively. An LSD post-hoc analysis resulted in the general use category (E2601) with significantly greater shear stress than all other categories ($p \leq .001$) and the adjustable skin protection category (K0734) with significantly less shear stress than all other categories ($p \leq .001$). Mean differences between categories with the greatest and least interface shear stress are shown in Table 4.

Table 4: Mean differences between categories with the greatest and least interface shear stress

Category	Category	Mean Difference	
E2601	K0734	3.575	*
	E2603	1.493	*
	E2605	1.588	*
	K0736	2.138	*
	E2607	2.157	*
K0734	E2601	-3.575	*
	E2603	-2.082	*
	E2605	-1.987	*
	K0736	-1.437	*
	E2607	-1.418	*

* $p \leq .001$

Figures 14 and 15 illustrate interface shear stress differences across displacements by cushion category for measurements recorded at 60 and 120s, respectively. Both figures were provided because a significant difference was found across time ($p \leq .001$). A change in the rank of category changed at each displacement except from 15 to and 20mm. From least to greatest

interface shear stress, the rank changes from E2605, E2607, E2603, E2601, K0736, and K0734 to K0734, K0726, E2607, E2603, E2605, and E2601. Interface shear stress increased as displacement increased.

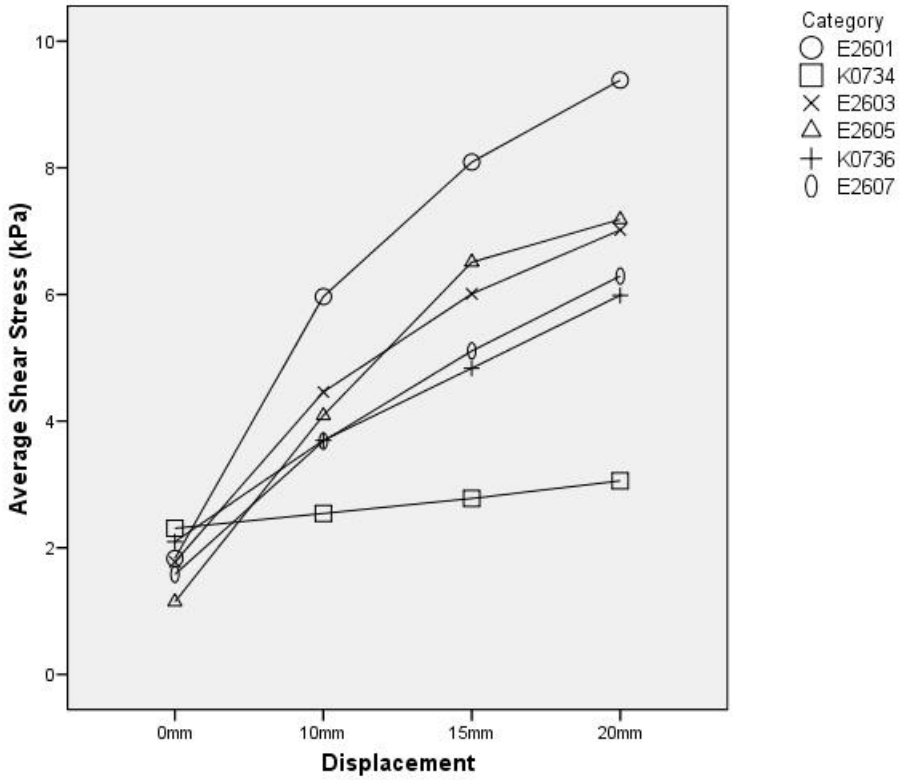

Figure 14: Mean interface shear stress vs. displacement at 60s

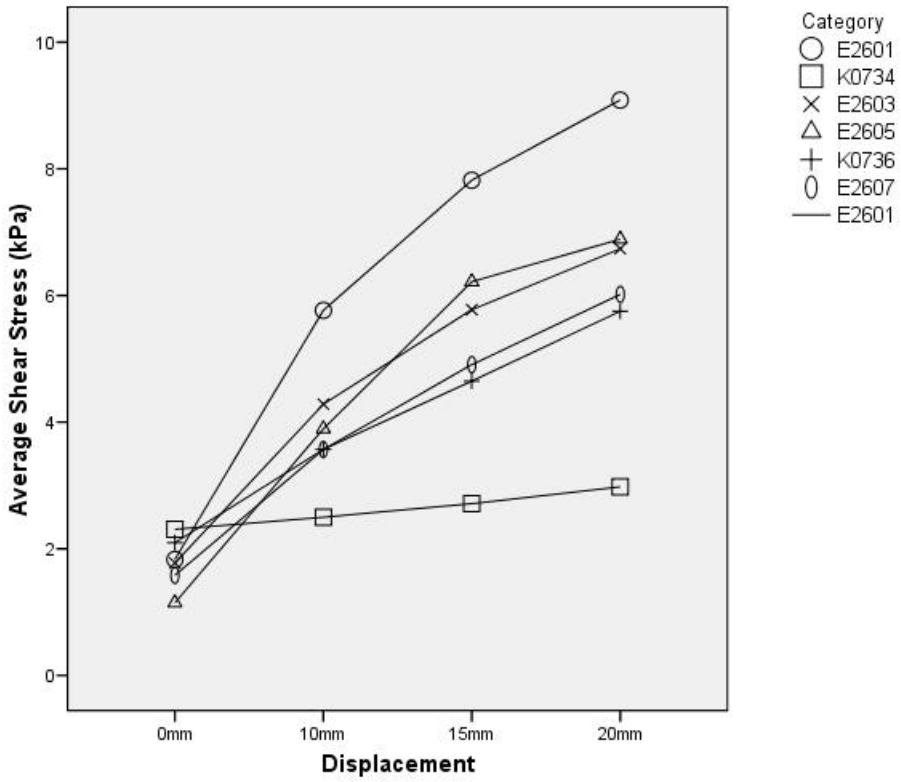

Figure 15: Mean interface shear stress vs. displacement at 120s

Interface shear stress results were organized by materials of construction to determine the performance of the cushion materials as shown in Figure 16. Cushions were combined into the same material categories and into four shear stress ranges: I) 0 – 4.9 kPa; II) 5 – 9.9 kPa; III) 10+ kPa; and IV) not tested. All four viscous fluid cushions and the single gel cushion were in shear stress range I. Four of the seven air cell cushions were in shear stress range I with the remaining in shear stress range II. The elastic foam material resulted with two cushions in shear stress range II and two not tested due to shear sensor saturation. One of the viscoelastic cushions were in shear stress range II and the other was in shear stress range III. All three honeycomb cushions were in shear stress range III.

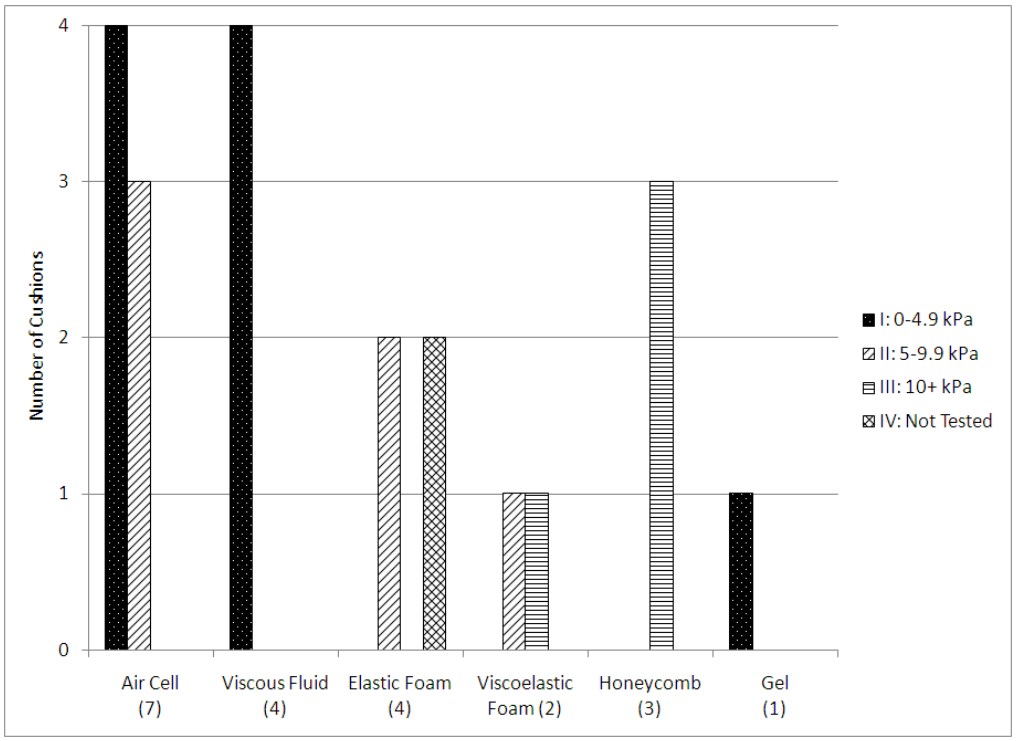

Figure 16: Mean interface shear stress by materials of construction

(the number of cushions in each category shown in parentheses)

Interface pressure and shear stress results are tabulated in Table 5 by cushion. Data was not tabulated for the Jay Basic and Jay Soft Combi P cushions because sensor saturation occurred during testing. Table 5 shows that the interface pressure and shear stress measurements of cushions within HCPCS categories were not similar, the adjustable skin protection category (K0734) being an exception. Interface shear stress values for all cushions in the adjustable skin protection category (K0734) were less than 5kPa.

Table 5: Interface pressure and shear stress by cushion

HCPCS Code	Product Name	Disp. (mm)	Pressure (mmHg)				Shear Stress (kPa)			
			60s		120s		60s		120s	
E2601	Mosaic	0	16.1 ± 0.3		16.1 ± 0.3		2.81 ± 0.04		2.81 ± 0.04	
		10	19.5 ± 0.5		19.6 ± 0.5		4.60 ± 0.16		4.43 ± 0.20	
		15	19.5 ± 0.5		19.5 ± 0.5		6.27 ± 0.37		6.02 ± 0.38	
		20	19.4 ± 0.4		19.5 ± 0.5		8.13 ± 0.24		7.80 ± 0.26	
	Curve	0	29.4 ± 0.8		29.4 ± 0.8		1.64 ± 0.07		1.64 ± 0.07	
		10	34.3 ± 0.5		34.3 ± 0.5		3.31 ± 0.07		3.21 ± 0.10	
		15	32.4 ± 0.5		32.4 ± 0.5		4.53 ± 0.06		4.37 ± 0.05	
		20	30.6 ± 0.8		30.8 ± 1.0		5.66 ± 0.18		5.41 ± 0.17	
	Stimulite Silver	0	55.8 ± 1.5		55.8 ± 1.5		1.05 ± 0.18		1.05 ± 0.18	
		10	63.7 ± 3.0		63.5 ± 3.1		9.99 ± 0.72		9.66 ± 0.91	
		15	61.2 ± 1.3		61.3 ± 1.3		13.47 ± 0.30		13.07 ± 0.35	
		20	53.4 ± 0.8		53.6 ± 1.1		14.37 ± 0.49		14.05 ± 0.51	
K0734	High Profile Single	0	9.1 ± 0.2		9.1 ± 0.2		2.60 ± 0.07		2.60 ± 0.07	
		10	12.8 ± 0.4		12.8 ± 0.4		3.17 ± 0.06		3.08 ± 0.04	
		15	13.0 ± 0.0		13.0 ± 0.0		3.89 ± 0.21		3.73 ± 0.19	
		20	13.6 ± 0.5		14.0 ± 1.0		4.47 ± 0.10		4.27 ± 0.10	
	Adjuster	0	28.9 ± 0.8		28.9 ± 0.8		2.19 ± 0.16		2.19 ± 0.16	
		10	32.9 ± 1.6		32.9 ± 1.6		2.21 ± 0.15		2.20 ± 0.13	
		15	29.2 ± 0.7		29.2 ± 0.7		2.39 ± 0.08		2.36 ± 0.07	
		20	27.9 ± 3.2		27.9 ± 3.7		2.61 ± 0.28		2.58 ± 0.29	
	Jay J2 Deep Contour	0	23.4 ± 0.5		23.4 ± 0.5		2.14 ± 0.04		2.14 ± 0.04	
		10	23.9 ± 0.4		23.7 ± 0.0		2.25 ± 0.08		2.22 ± 0.09	
		15	23.3 ± 0.5		22.7 ± 0.7		2.06 ± 0.14		2.04 ± 0.12	
		20	20.8 ± 0.0		20.8 ± 0.0		2.09 ± 0.07		2.09 ± 0.06	
E2603	Triumph	0	32.5 ± 1.0		32.5 ± 1.0		1.40 ± 0.10		1.40 ± 0.10	
		10	36.1 ± 1.4		36.2 ± 1.4		3.80 ± 0.27		3.63 ± 0.24	
		15	33.5 ± 1.2		33.7 ± 1.5		5.74 ± 0.11		5.40 ± 0.08	
		20	32.1 ± 0.5		32.1 ± 0.5		7.09 ± 0.18		6.70 ± 0.15	
	Ascent	0	27.6 ± 0.4		27.6 ± 0.4		1.50 ± 0.05		1.50 ± 0.05	
		10	33.6 ± 1.3		33.6 ± 1.2		4.48 ± 0.24		4.33 ± 0.24	
		15	33.8 ± 0.9		34.1 ± 0.7		5.37 ± 0.10		5.20 ± 0.10	
		20	35.6 ± 0.8		35.4 ± 0.8		6.31 ± 0.15		6.07 ± 0.16	
	Jay Xtreme	0	38.7 ± 1.0		38.7 ± 1.0		1.77 ± 0.06		1.77 ± 0.06	
		10	43.8 ± 1.8		42.8 ± 2.2		2.01 ± 0.17		2.01 ± 0.14	
		15	42.6 ± 1.3		42.4 ± 1.6		2.11 ± 0.09		2.10 ± 0.09	
		20	41.7 ± 0.6		41.5 ± 0.8		2.31 ± 0.07		2.25 ± 0.08	
	Stimulite Classic	0	44.1 ± 0.7		44.1 ± 0.7		2.44 ± 0.11		2.44 ± 0.11	
		10	47.5 ± 0.9		47.3 ± 0.6		7.54 ± 0.15		7.18 ± 0.13	
		15	44.5 ± 0.8		44.3 ± 0.5		10.82 ± 0.10		10.41 ± 0.10	
		20	41.5 ± 0.9		41.5 ± 0.9		12.36 ± 0.43		11.93 ± 0.42	

Table 5 (continued)

HCPCS Code	Product Name	Disp. (mm)	Pressure (mmHg)				Shear Stress (kPa)			
			60s		120s		60s		120s	
E2605	Airlite	0	24.1 ± 0.6		24.1 ± 0.6		0.98 ± 0.05		0.98 ± 0.05	
		10	29.8 ± 0.8		29.6 ± 0.7		2.94 ± 0.05		2.87 ± 0.04	
		15	28.3 ± 0.5		28.3 ± 0.5		3.33 ± 0.08		3.25 ± 0.05	
		20	27.5 ± 0.4		27.4 ± 0.5		3.53 ± 0.08		3.42 ± 0.06	
	Ridge	0	32.1 ± 0.5		32.1 ± 0.5		1.31 ± 0.10		1.31 ± 0.10	
		10	35.6 ± 0.5		35.7 ± 0.7		5.24 ± 0.10		4.92 ± 0.11	
		15	34.5 ± 0.5		34.4 ± 0.5		9.69 ± 0.46		9.19 ± 0.45	
		20	33.5 ± 0.5		33.3 ± 0.8		10.84 ± 0.17		10.36 ± 0.15	
K0736	Quadtro Select High Profile	0	8.7 ± 0.4		8.7 ± 0.4		2.75 ± 0.22		2.75 ± 0.22	
		10	11.1 ± 1.3		11.3 ± 1.1		5.46 ± 0.69		5.21 ± 0.65	
		15	12.8 ± 0.5		12.8 ± 0.5		7.85 ± 0.40		7.51 ± 0.35	
		20	14.5 ± 0.8		14.5 ± 0.8		10.43 ± 0.17		9.95 ± 0.17	
	Vector	0	13.5 ± 0.7		13.5 ± 0.7		1.10 ± 0.05		1.10 ± 0.05	
		10	18.5 ± 0.8		18.4 ± 0.5		3.34 ± 0.33		3.24 ± 0.30	
		15	17.5 ± 0.6		17.5 ± 0.7		4.09 ± 0.27		3.92 ± 0.28	
		20	17.6 ± 0.6		17.6 ± 0.6		4.85 ± 0.24		4.66 ± 0.18	
	Jay J2 Deep Contour P	0	18.4 ± 1.4		18.4 ± 1.4		2.44 ± 0.09		2.44 ± 0.09	
		10	15.4 ± 0.5		15.1 ± 0.4		2.29 ± 0.06		2.26 ± 0.03	
		15	17.5 ± 5.0		17.5 ± 4.9		2.57 ± 0.21		2.52 ± 0.22	
		20	22.0 ± 0.4		22.0 ± 0.4		2.68 ± 0.09		2.64 ± 0.10	
E2607	Harmony	0	11.7 ± 0.1		11.7 ± 0.1		1.50 ± 0.07		1.50 ± 0.07	
		10	14.0 ± 0.0		14.0 ± 0.0		5.13 ± 0.09		4.91 ± 0.11	
		15	14.2 ± 0.3		14.3 ± 0.3		6.05 ± 0.11		5.82 ± 0.12	
		20	14.3 ± 0.4		11.5 ± 6.4		6.42 ± 0.20		4.91 ± 2.75	
	Maxx	0	24.8 ± 0.7		24.8 ± 0.7		1.26 ± 0.08		1.26 ± 0.08	
		10	34.0 ± 0.5		34.4 ± 1.0		1.68 ± 0.07		1.67 ± 0.08	
		15	32.9 ± 0.8		33.0 ± 0.8		3.33 ± 0.07		3.19 ± 0.07	
		20	33.4 ± 1.0		33.4 ± 1.0		4.94 ± 0.20		4.67 ± 0.19	
	Jay Easy	0	34.3 ± 2.6		34.3 ± 2.6		1.73 ± 0.22		1.73 ± 0.22	
		10	40.7 ± 6.0		40.7 ± 6.0		2.14 ± 0.07		2.17 ± 0.08	
		15	35.1 ± 1.6		35.1 ± 1.5		3.08 ± 0.10		3.03 ± 0.11	
		20	33.5 ± 0.8		33.3 ± 0.5		3.63 ± 0.17		3.50 ± 0.16	
	Stimulite Contoured	0	44.4 ± 1.5		44.4 ± 1.5		1.84 ± 0.07		1.84 ± 0.07	
		10	46.9 ± 2.7		46.9 ± 2.7		5.78 ± 0.09		5.51 ± 0.07	
		15	43.0 ± 0.7		43.0 ± 0.7		7.97 ± 0.06		7.59 ± 0.10	
		20	41.8 ± 1.3		41.8 ± 1.3		10.20 ± 0.20		9.78 ± 0.21	

A comparison of cushion performance by material resulted in the air cell cushions with the 5 lowest interface pressures, and the viscous fluid and air cell cushions with the 5 lowest interface shear stresses.

3.2.3.2 Horizontal Stiffness

Overall and local horizontal stiffness values were determined using a regression analysis of the force-displacement and shear-force-displacement curves, respectively, as tabulated in Table 6 and illustrated in Appendix A. Relationships between: mean horizontal force and overall horizontal stiffness; mean horizontal force and local horizontal stiffness; mean interface shear stress and overall horizontal stiffness; and mean interface shear stress and local horizontal stiffness are tabulated in Table 7. Relationships between: overall horizontal stiffness and local horizontal stiffness; overall horizontal stiffness and 16840-2 stiffness; and local horizontal stiffness and 16840-2 stiffness are tabulated in Table 8.

Table 6: Overall and local horizontal stiffness values by cushion

(- represents data not collected due to sensor saturation)

HCPCS Code	Product Name	Overall Horizontal Stiffness				Local Horizontal Stiffness			
		60s		120s		60s		120s	
		(N/mm)	R^2	(N/mm)	R^2	(N/mm)	R^2	(N/mm)	R^2
E2601	Roho Mosaic	8.09	0.92	7.97	0.92	0.74	0.96	0.69	0.95
	Jay Basic	-	-	-	-	-	-	-	-
	TTC Curve	15.63	0.94	15.47	0.94	0.57	0.98	0.54	0.98
	Stimulite Silver	14.11	0.83	13.80	0.82	1.92	0.95	1.86	0.95
K0734	Roho High Profile Single	6.59	0.91	6.44	0.92	0.26	0.94	0.24	0.93
	TTC Adjuster	10.23	0.97	9.91	0.97	0.06	0.42	0.05	0.38
	Jay J2 Deep Contour	5.81	0.92	5.67	0.92	-0.01	0.06	-0.01	0.09
E2603	Roho Triumph	8.34	0.91	8.11	0.91	0.81	0.98	0.75	0.98
	TTC Ascent	9.33	0.58	9.29	0.60	0.66	0.97	0.63	0.97
	Jay Xtreme	8.05	0.94	7.92	0.95	0.07	0.79	0.06	0.80
E2605	Stimulite Classic	10.65	0.89	10.56	0.90	1.43	0.99	1.36	0.99
	Roho Airlite	15.01	0.90	14.82	0.97	0.36	0.90	0.35	0.90
	TTC Ridge	24.99	0.88	23.75	0.87	1.41	0.96	1.31	0.96
	Jay Soft Combi P	-	-	-	-	-	-	-	-
K0736	Roho Quadtro	11.27	0.97	11.14	0.97	1.06	0.96	0.99	0.95
	TTC Vector	14.23	0.97	13.87	0.97	0.51	0.96	0.48	0.96
	Jay J2 Deep Contour P	5.45	0.89	5.32	0.89	0.03	0.24	0.03	0.17
E2607	Roho Harmony	10.86	0.83	10.75	0.83	0.72	0.94	0.68	0.94
	TTC Maxx	23.60	0.92	22.99	0.92	0.51	0.83	0.47	0.83
	Jay Easy	8.30	0.95	8.18	0.95	0.27	0.89	0.25	0.90
	Stimulite Contoured	12.10	0.91	11.93	0.91	1.17	1.00	1.10	1.00

With applied displacement, positive relationships resulted between interface shear stresses and local horizontal stiffness values ($r \geq 0.905$) and between horizontal forces and overall horizontal stiffness values ($r \geq 0.944$) at 60 and 120 s. These two results were expected because the respective force is a linear combination of the stiffness variable. No significant correlations were found between interface shear stress and overall horizontal stiffness ($0.081 \leq r \leq 0.349$). However, significant positive relationships ($p \leq 0.05$) were found between horizontal force and local horizontal stiffness ($0.486 \leq r \leq 0.512$). At zero displacement, there was a

significant negative correlation between interface shear stress and overall horizontal stiffness (r = -0.578) and a negative correlation between interface shear stress and local horizontal stiffness (r = -0.193). Positive correlations were found between horizontal force and both overall horizontal stiffness (r = 0.184) and local horizontal stiffness (r = 0.405) at zero displacement.

Table 7: Correlation coefficients (r) for forces and horizontal stiffness values

RCLI Displacement (mm)	Overall Horizontal Stiffness	Local Horizontal Stiffness
Interface Shear Stress (60s / 120s)		
0	-0.578**	-0.193
10	0.086 / 0.081	0.907** / 0.905**
15	0.334 / 0.327	0.968** / 0.966**
20	0.349 / 0.341	0.980** / 0.979**
Horizontal Force (60s / 120s)		
0	0.184	0.405
10	0.945** / 0.944**	0.509* / 0.512*
15	0.988** / 0.988**	0.486* / 0.490*
20	0.984** / 0.984**	0.432 / 0.430

** Correlation significant at the 0.01 level

* Correlation significant at the 0.05 level

Table 8: Correlation coefficients for horizontal stiffness values

	Overall Horizontal Stiffness	Local Horizontal Stiffness	16840-2 Stiffness
Overall Horizontal Stiffness	1	0.428	.945**
Local Horizontal Stiffness	-	1	.509*
16840-2 Stiffness	-	-	1

** Correlation significant at the 0.01 level

* Correlation significant at the 0.05 level

A positive correlation resulted between overall horizontal stiffness and local horizontal stiffness and significant positive correlations resulted between overall and local stiffness values and ISO 16840-2 stiffness ($r = 0.945$ & $r = 0.509$, respectively).

3.2.4 Immersion

A weak negative correlation resulted between immersion and interface shear stress at each displacement and no correlation was found between immersion and horizontal force as shown in Table 9.

Table 9: Immersion correlation coefficients

RCLI Displacement (mm)	Interface Shear Stress	Horizontal Force
10	-0.232	0.136
15	-0.294	0.131
20	-0.223	0.124

3.3 DISCUSSION

Pressure, shear, heat, and humidity are extrinsic risk factors known to increase the risk of pressure ulcers [2]. Pressure mapping has allowed quantification of interface pressure and a visual representation of real-time pressure redistribution. Clinicians have incorporated the pressure mapping tool to aid in the decision making process of prescribing cushions. This was the first study to quantify interface shear stress of commercial cushions and provides clinicians additional information about a cushions effect on a patient's tissue integrity.

3.3.1 Calibration

The pressure and shear force sensor used in this study was used in previous studies [44-48] and the shear force measurement error was established as ± 1 N [44, 47, 48] and 2.7 N [45]. The largest range of shear force in previous studies ranged between 0 – 11.7 N [44] as compared to 0 – 40.4 N (0 – 14.4 kPa) in this study. The deviation between true and measured shear force ranged between 0.01 – 8.77 N. The greater shear force deviation in this study as compared to the previous studies could be due to sensor orientation during testing. Previously, the sensor was adhered to a flat, rigid surface and different wound dressings were evaluated by applying a horizontal displacement across the static sensor [44, 46]. This study also adhered the sensor to a flat, rigid surface; however, this surface was moved with respect a static cushion.

During calibration testing, constant pressure was applied using dead weights and shear force was applied using displacements of the MTS crosshead. The same displacements were used pre- and post-test; however, the range of shear force applied to the sensor pre-test was 0 – 39.2 N pre-test and 0 – 29.3 N post-test. This difference provides an explanation for the significant difference between shear force calibration measurements pre- and post-test. The different range of shear forces applied to the sensor can be explained in part by fluctuations in relative humidity. A relative humidity of 50 ± 5% was specified in the protocol; however, the relative humidity of the lab fluctuated with the relative humidity outside. Unfortunately, the temperature and relative humidity were not recorded during calibration testing. Measurement variation could also be minimized with the addition of a preconditioning procedure [49].

No significant difference between pre- and post-test pressure calibration measurements indicates that the sensor repeatedly measured pressure inaccurately. Repeatable results are satisfactory because a correction factor can be applied to obtain accurate measurements. In this

study, a Box-Cox Transformation could be performed on the pressure data and the resulting power equation could provide accurate pressure measurements [50].

3.3.2 Interface Pressure and Shear Stress

Interface pressure of cushions have been evaluated previously [41, 42]. Foam, air, gel, and powered alternating cushions resulted in mean interface pressures ranging between 46 – 157 mmHg and peak interface pressures saturating the sensor at 200 mmHg. In this study, mean interface pressure ranged between 9 – 64 mmHg. The discrepancy between the previous studies and this study was due to the method of force application, the sensor's ability to accurately measure pressure, and sensor placement. Forces were applied to cushions using humans in the previous studies and a RCLI was used in this study. Variations between humans and the RCLI include rigidity, size and shape. The sensor was able to repeatedly measure pressure; however, the measurement was inaccurate as shown in Figure 10. The sensor placement was just anterior to the left IT of the RCLI and provided a flat, rigid surface. Placement of the sensor on the IT would result in erroneous interface pressures, pilot data indicated that sensor bending resulted in erroneous pressure and shear force measurements.

Bennett et al. and Goossens et al. previously measured interface shear stress of rigid plastic (0.9 – 2.6 kPa) [19, 20], wood (4.6 – 9.6 kPa) [22], foam (6.5 – 6.8 kPa) [21], gel (4.4 – 6.4 kPa) [21, 22], and a LiquiCell (LiquiCell Technologies, Inc.) overlay (4.0 – 4.8 kPa) [21]. In this study, interface shear stress ranged between 1.0 – 14.4 kPa. The greater amount of interface shear stress measured in this study was most likely sensor specific. The difficulty in obtaining interface shear stress measurements has been simply to design a sensor capable of such. Bennett et al. noted that the sensor used in his study would register less than the true values of local shear

due to dissimilar materials in contact with the sensor and the location of the sensor was 2 – 3 cm lateral of the IT [16]. The sensor used by Goossens et al. was not completely validated [22]. However, the values obtained by all sensors were on the same order of magnitude and the sensor used in this study was commercially available.

Interface shear stress varied significantly from 60 to 120 seconds ($p = .000$, partial $\eta^2 = .611$) and generally reduced with time. The large effect size indicates that time largely contributed to the amount of variance accounted for by the model. A reduction in stress over time with constant strain is defined as stress relaxation. In this study, constant strain was synonymous with constant displacements. Multiple displacements were applied in the study; however, the reduction in stress with respect to time was individually measured at each displacement. The stress reduction was small over the 60 second duration, but could become a significant reduction in interface shear stress over a longer period of time. Stress relaxation is a desired quality for cushions to reduce interface stresses and should be investigated further. A preconditioning procedure could also be included in future testing to minimize the variability in measurements [49].

Change in the categories rank of interface shear stress across displacements was most notable for adjustable skin protection category (K0734). Initially, K0734 resulted with the greatest initial interface shear stress, but the least at all displacements. The reduction in interface shear stress with displacement indicates that cushions in the K0734 were able to absorb the applied forces instead of shearing the tissue of patients.

The HCPCS Code Set separates cushion technologies into categories that are specific to wheelchair users' needs. The categories include general use (E2601), adjustable/nonadjustable skin protection (K0734/E2603), positioning (E2605), and adjustable/nonadjustable combination

skin protection and positioning cushions (K0736/E2607). The interface pressure and shear stress results of the cushions were organized by HCPCS category and materials of construction. Organized by HCPCS code, the adjustable combination skin protection and positioning cushions (K0736) resulted in the least amount of interface pressure followed by the adjustable skin protection cushions (K0734). The adjustable skin protection cushions (K0734) resulted in the least amount of interface shear stress followed by the adjustable combination skin protection and positioning cushions (K0736). Organization of results by materials of construction, the air cell and viscous fluid materials resulted in the least amount of interface pressure and the air cell, viscous fluid, and gel materials resulted in the least amount of interface shear stress. The materials of construction that made up both the adjustable skin protection (K0734) and the adjustable combination skin protection and positioning (K0736) cushions were one viscous fluid cushion and two air cell cushions. These results quantitatively showed that air cell and viscous fluid materials reduce interface pressure and shear stress and suggest that the rationale for the improved performance was the adjustable technology required of cushions in the adjustable skin protection (K0734) and the adjustable combination skin protection and positioning (K0736) categories.

The nonadjustable skin protection cushions (E2603) resulted in the greatest amount of interface pressure followed by the general use cushions (E2601) and the general use cushions (E2601) resulted in the greatest amount of interface shear stress. Organized by materials of construction, the elastic foam and honeycomb materials resulted in the greatest amount of interface pressure and the elastic, viscoelastic, and honeycomb materials resulted in the greatest interface shear stress. The materials of construction for the nonadjustable skin protection cushions (E2603) were a viscoelastic foam, elastic foam, viscous fluid, and honeycomb cushion.

The materials of construction for the general use cushions (E2601) were one air cell, one honeycomb, and two elastic foam cushions. Several materials of construction were present in each of the nonadjustable skin protection (E2603) and general use (E2601) categories which does not provide evidence that a single material of construction was responsible for the increased interface pressure and shear stress. However, organization of the results by materials of construction showed that all cushions using honeycomb as the material of construction resulted in the largest interface pressure and shear stress ranges.

The positioning category (E2605) resulted with the second largest amount of interface shear stress, but was in the middle with respect to interface pressure. The materials of construction in the positioning category were an air cell, a viscoelastic foam, and an elastic foam. These results suggest that the positioning cushions increased interface shear stress; however, the number of tested cushions was two. More cushions should be evaluated in this category before a conclusion could be made specific to the positioning category (E2605).

The HCPCS categories with adjustable technology (K0734 and K0736) resulted in the lowest interface pressure and shear stress and the greatest interface pressure and shear stress were from categories without the adjustable technology. This study quantitatively identified that the adjustable technology used in cushion design reduces interface pressure and shear stress.

3.3.3 Horizontal Stiffness

In a previous study, horizontal stiffness was collected for 21 wheelchair seat cushions using the Lateral and Forward Stiffness Test Protocol from Annex C of ISO 16840-2 [49]. The same protocol was used to determine horizontal stiffness as in this study except that only one displacement (10 mm) was used. The horizontal stiffness measurements ranged between 80 –

325 N as compared to 92 – 403 N in this study (recorded at 10 mm displacement). The reason for greater values measured in this study was the method of securing the cushion during testing. The cushion was adhered to a scale in the previous study [49] and to the base of the test apparatus in this study. The scale was designed with flexible plastic tabs at each corner to stabilize a platform as shown in Figure 17. The flexible plastic tabs absorbed a portion of the horizontal force, resulting in lower measurements.

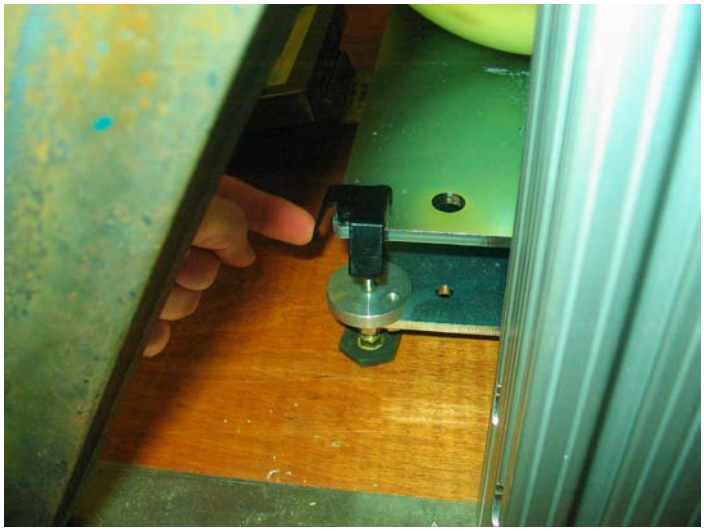

Figure 17: Plastic tabs on scale used in a previous study [49]

Large positive relationships resulted between interface shear stresses and local horizontal stiffness values ($r \geq 0.905$), and between horizontal forces and overall horizontal stiffness values ($r \geq 0.944$) at 60 and 120 seconds. This test was performed to verify the displacements applied during testing were consistent. Overall horizontal stiffness values were calculated by taking the slope of the mean force-displacement curve. Calculating correlation coefficients simply verified that each displacement was applied consistently throughout testing. Similarly, local horizontal stiffness was calculated using the mean shear-force-displacement curve.

A significant negative relationship was found between overall horizontal stiffness and interface shear stress at zero displacement. This indicates that a cushion with greater stiffness initially resulted in smaller interface shear stresses. However, interface shear stress for the adjustable skin protection category (K0734) was greatest at zero displacement and least for 10, 15, and 20 mm displacements.

No significant relationship between interface shear stress and overall horizontal stiffness ($0.081 \leq r \leq 0.349$) indicates that testing the overall horizontal stiffness of a cushion does not provide information about the cushion's ability to reduce interface shear stress at the IT.

A high correlation between ISO 16840-2 stiffness and overall horizontal stiffness ($r = .945$), and a moderate correlation between ISO 16840-2 stiffness and local horizontal stiffness ($r = .509$) was found in this study. The single displacement used to calculate ISO 16840-2 stiffness compared to a baseline and three displacements used to calculate the horizontal stiffness values in this study required less testing, data processing, and data analysis. Furthermore, local horizontal stiffness and interface shear stress were directly correlated ($.905 \leq r \leq .979$). Therefore, this study has provided evidence that the current test methodology (ISO 16840-2) provides sufficient information. However, a pressure and shear force sensor in a clinical setting could provide information analogous to pressure mapping technology by allowing real-time comparisons of cushions for specific users.

3.3.4 Immersion

The weak negative correlation between immersion and interface shear stress suggests that interface shear stress may be reduced by increasing immersion. In fact, this technique is currently used by the seat cushion industry to reduce interface pressure at the ITs. Increased immersion

allows the load to be transferred to the greater trochanter of the femur and distributed over a larger area.

4.0 PROTOTYPE CUSHION DESIGN ELEMENT

Results from the evaluation of commercial wheelchair seat cushions provided evidence of materials and technologies that reduce the risk of pressure ulcers. The air cell and viscous fluid cushions resulted in the lowest interface pressure and shear, and the honeycomb cushions resulted in the greatest interface pressure and shear. These results drove the prototype cushion designs.

The novel cushion technology incorporated into all prototypes was a closed-loop control system. The closed-loop control system monitored interface stress amplitude to modulate cushion properties. Methods of monitoring shear included an interface shear sensor and strain gauges. An interface shear sensor with analog output was placed on the surface of the cushion inferior to the left IT. Strain gauges were placed on rigid cushion components and indirectly measured shear from applied bending moments. A computer monitored shear measurements and activated necessary elements to reduce potentially hazardous interface conditions. Three prototype cushions developed were a magnetorheological fluid (MRF) cushion, segmented cushion, and air exchange cushion.

4.1 MAGNETORHEOLOGICAL FLUID CUSHION

The magnetorheological fluid (MRF) cushion design consisted of a closed-cell polyurethane base and a MRF filled insert secured to the base as shown in Figure 18. MRF is a smart fluid capable of variable viscosity controlled with external magnetic fields. The MRF viscosity was controlled using an electromagnet array inserted into a closed-cell polyurethane base. The *off* state of MRF is highly viscous, increasing immersion into the cushion to provide even pressure distribution and reduced shear with minimal stability. Transitioning to the *on* state, MRF exhibits low viscosity increasing cushion stiffness/stability while maintaining the initial immersion for even pressure distribution and shear reduction. The dynamic ability to transition between *off* and *on* provides an adjustable contour for any posture or activity such as propulsion. The prototype algorithm controls the electromagnetic flux densities of individual electromagnets transferring undesirable pressure and shear forces at bony prominences to areas with higher tolerance to loading.

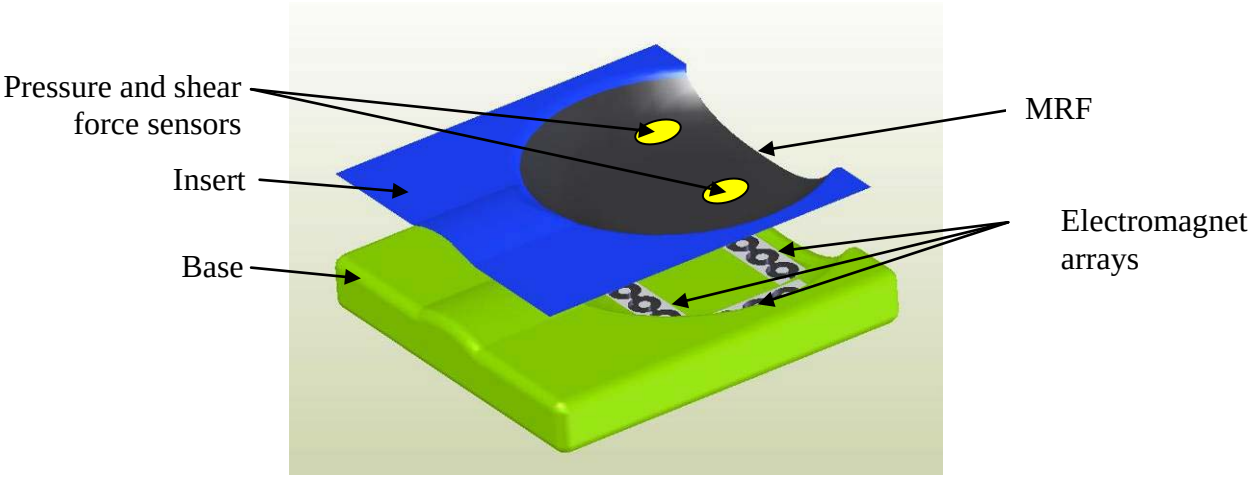

Figure 18: MRF cushion using electromagnet arrays

A small scale prototype was developed using commercial MRF and electromagnets. Unfortunately, the magnetic flux density required to activate MRF to exhibit the desired viscosity was unobtainable. An electromagnet capable of such flux densities would be too large, require too much power, and produce too much heat to be incorporated into a cushion design.

4.2 SEGMENTED CUSHION

The segmented cushion design divided the cushion surface into multiple segments to provide a cushion with variable horizontal stiffness as shown in Figure 19. Actuators control individual segments of the cushion using a ball and socket joint design. A ball and socket joint provided relief in anterior-posterior and medial-lateral directions and was controlled with a pneumatic system. Pressure applied to pistons controlled the amount of force against the ball. Low force allowed segmental movement and high force provided stability to the seating surface. Interface pressure and shear stress were indirectly measured with strain gauges placed on the shaft connecting the ball and platform. A computer program monitored the strain gauges and triggered the pneumatic control system to regulate platform rotation.

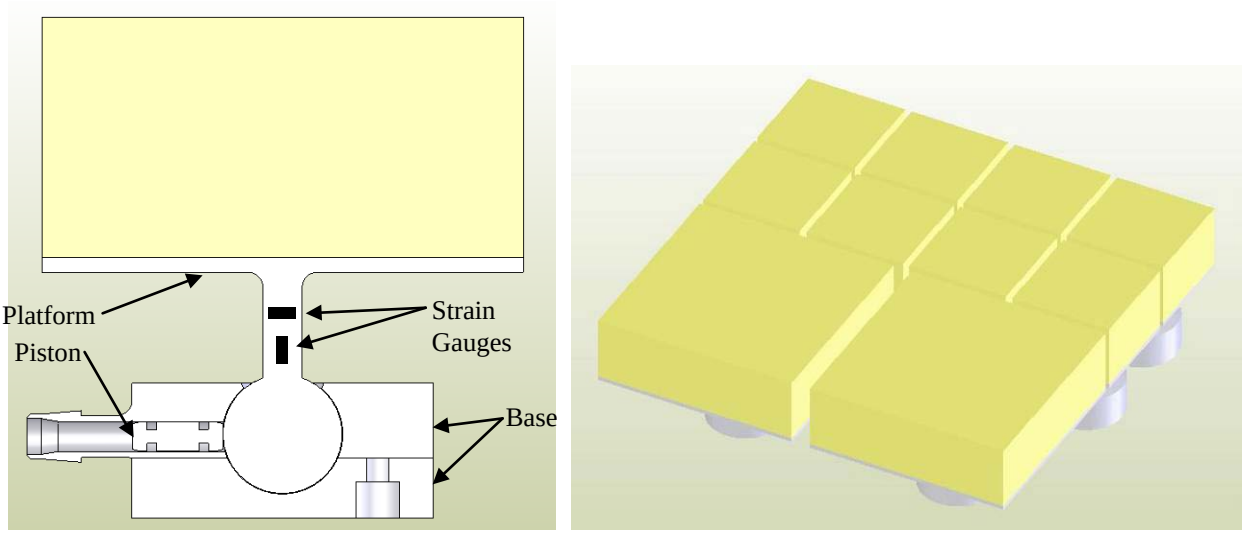

Figure 19: Segmented cushion design (a) design component and

(b) complete cushion using array of design components

A single actuator was manufactured using stereolithography, a rapid prototyping technology. Axial force and bending moments were measured using strain gauges and a data acquisition system. The force applied by the piston to the ball of the ball and socket joint was not sufficient to overcome the force generated by the platform. A rubber disk was adhered to the end the pistons improved actuator performance; however, the small cross-sectional area of the pistons did not generate adequate force. An actuator redesign was not performed because the increased diameter of the pistons would increase the overall height of the design resulting in a nonfunctional cushion.

4.3 AIR EXCHANGE CUSHION

The air exchange cushion design transformed a static commercial product into an automated shear reducing cushion. The Roho Quadtro Select® and Single Compartment cushions were

tested in this study and resulted in similar interface pressures (14.5 & 13.6 mmHg, respectively), but different interface shear stresses (10.43 & 4.47 kPa, respectively). The Quadtro was designed with ISOFLO® Memory Control that offers “on-demand adjustment to maximize function” as shown in Figure 20. A valve controls pressure redistribution and provides additional stability. An open valve allows pressure redistribution throughout the cushion and a closed valve isolates pressure into quadrants. This study has shown that increased stability provided by closing the valve and isolating the quadrants was at the price of increased interface shear stress.

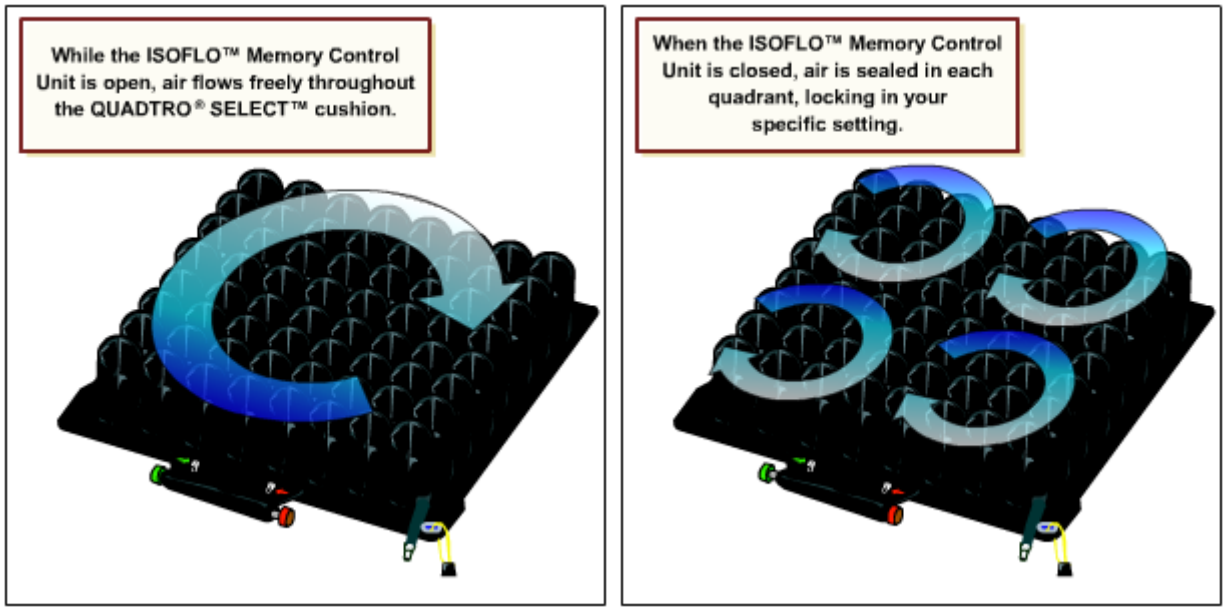

Figure 20: ROHO Quadtro Select® cushion with ISOFLO® memory control

(images from www.therohogroup.com)

The air exchange cushion was tested using a modification of the shear characteristic procedures from Chapter 3. The valve of the air exchange cushion started in the open position and the rigid cushion loading indenter (RCLI) was applied to the cushion, then the valve was manually closed. Displacements were applied using the same methodology; however, the valve

was manually opened after 40 seconds and manually closed after 70 seconds to determine to effect of switching the valve. Evaluation of the air exchange cushion resulted in minimal changes in horizontal force and no change of interface pressure or shear stress. Because no decrease was found when the valve was operated manually an automated valve was not designed.

Air from each of the cushion quadrants was ported directly into the valve and valve position either restricted (closed) or allowed (open) air flow between quadrants. The flow path to the valve and the orifice within the valve restricted flow capacity between quadrants. The limited flow rate was noticed when the cushion was loaded with the RCLI. Increased cross-sectional area of the flow path and orifice would increase flow rate and improve the volume and rate of air exchange.

5.0 SUBCUTANEOUS BUTTOCK SOFT TISSUE

Prediction of subcutaneous stress and strain distribution is necessary in the absence of a noninvasive methodology. Previous researchers have used finite element models to investigate the subcutaneous tissue response to mechanical loading [4-13]; however, this study improved upon image collection methodology, model construction, and validation techniques. A limitation of the most recent FE models developed by Linder-Ganz et al. [7, 8] and Makhsous et al. [9] was the lack of a cushion model. Subjects were supported by a 2 cm flat, semi-rigid foam cushion [7, 8] and an air bladder [9], yet neither model included a support surface in the FE model simulation. Another limitation of the Makhsous et al. study was the application of a uniform load to the inferior portion of the buttock. An air bladder was used to apply a uniform load to the buttock surface; however, the load would not distribute uniformly across the buttock due to local effects of bony prominences. Quantification of subcutaneous tissue stresses and strains provides information on the ability of a wheelchair seat cushion to reduce pressure ulcer development. The purpose of this study was to quantify subcutaneous tissue stresses and strains using a finite element (FE) model.

5.1 METHODS

5.1.1 Subject

One healthy, 35 year old male was the single subject in this study. The individual was selected among laboratory personal and had complete motor and sensory function. All procedures were approved by the institutional review board and written informed consent was obtained prior to screening and experimental procedures.

5.1.2 Instrumentation

MR images of the subject were collected in an Upright^{TM} MRI (FONAR Corp., Melville, NY, USA) as shown in Figure 21. The Upright^{TM} MRI is capable of collecting MR images of patients in recumbent, seated, and standing postures. Magnet orientation is horizontal allowing a platform to be placed in between the two magnets. The platform has three degrees of freedom, two translational and one rotational, to place the subject's anatomy of interest at the magnet isocenter.

Figure 21: Upright™ MRI from FONAR Corp. (image from www.fonar.com)

An interface pressure sensor array (FSA, Vista Medical, Winnipeg, Manitoba, Canada) was used to measure interface pressure at the cushion interface and a pressure and shear force sensor (Predia, Molten Corp., Japan) was used to measure interface shear stress at the cushion interface.

5.1.3 Image Collection

Sagittal MR images of the left buttock were collected in three seated postures: non-loaded; upright; and reclined as shown in Figure 22. The non-loaded seated posture orientated the subject into a supine position while maintaining a seated posture. This orientation transferred the load from the buttock to the torso and provided images of buttock soft tissues without compression. The upright seated posture orientated the subject into a seated position with a trunk angle of 90° with respect to the thigh. The reclined seated posture orientated the subject into a seated postured with a trunk angle of 120° with respect to the thigh. The reclined seated posture provided a shear induced posture to identify the effects of shear on subcutaneous tissues. The subject sat on an

HR45 open-cell polyurethane foam cushion (16”x16”x3”) for all postures. The protocol below was used for image collection:

1) The subject was positioned into a non-loaded seated posture (Figure 22a).
    a. Sagittal MR images were collected in the buttock region.
2) The subject was positioned into a loaded upright seated posture, 90° from the horizontal (Figure 22b).
    a. Sagittal MR images were collected in the buttock region.
3) The subject was positioned into a reclined seated posture, 60° from the horizontal (Figure 22c).
    a. Sagittal MR images were collected in the buttock region.

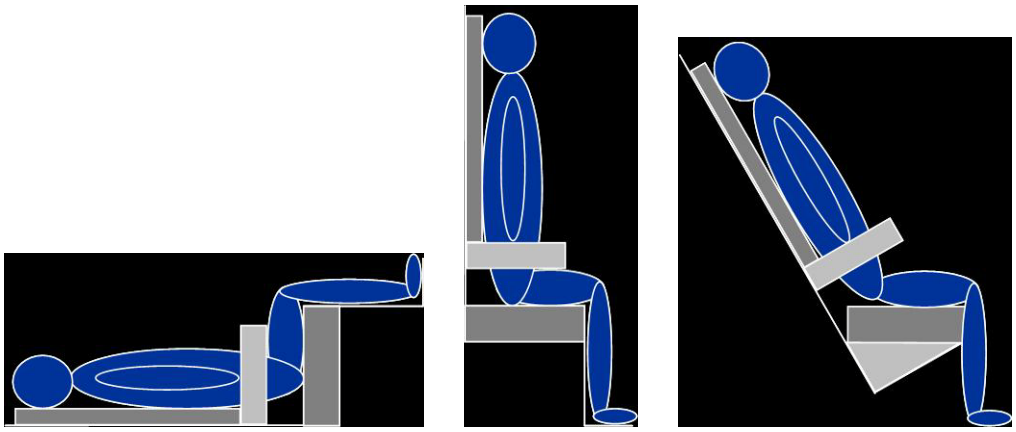

(a) (b) (c)

Figure 22: Sitting postures for MRI data collection (a) non-loaded seated posture (b) upright seated posture (c) reclined seated posture

4) The interface pressure sensor array was placed in between the subject and cushion, and the interface pressure and shear force sensor was placed inferior to the left IT by palpation.
    a. The subject was positioned into each posture as shown in Figure 22 and measurements were recorded after 60 seconds.

Image collection required unique placement of a lumbar coil. A lumbar coil is typically placed anterior to the lumbar spine of a patient; however, in this study the lumbar coil was placed beneath the cushion, inferior to the subject's left buttock. The MRI parameters were a 3-D gradient echo sequence, 0.6 T, 256 x 256 matrix, 30 cm x 30 cm field of view, 2 mm slice thickness, and zero gap thickness. Matrix dimensions and slice thickness were improved to 512 x 512 matrix and 1mm slice thickness using a post-processing technique.

5.1.4 Model Construction

The 3-D FE model was constructed using geometry from MR images. The non-loaded, upright, and reclined slices that corresponded with maximal compression of soft tissue between the IT and cushion were chosen for model construction. The corresponding images were digitized and extruded 4mm to obtain the 3-D model. Model construction methodology was based on previous research [7, 8].

The subject's anatomy was segmented into anatomical structures using Mimics (Materialise, Leuven, Belgium). The segments were: 1) pelvis; 2) skin and inferior adipose tissue; 3) superior adipose tissue; 4) posterior muscle group; and 5) anterior muscle group. Posterior muscle group included gluteus maximus, medius, and minimus. Anterior muscle group

included obturator internus, obturator externus, adductor longus, adductor brevis, adductor magnus, piriformis, vastus lateralis, vastus intermedius, vastus medialis, and rectus femoris. Polylines were created for each segmented group and exported as IGES files. The polylines were imported into Solidworks (Concord, MA, USA) and a spline function outlined the polylines to create 3-D models of each segment. The 3-D models of each segment were imported into ANSYS Workbench (ANSYS 11.0, ANSYS Inc., Canonsburg, PA) and meshed using 4mm sized elements. The models are shown in Figure 23.

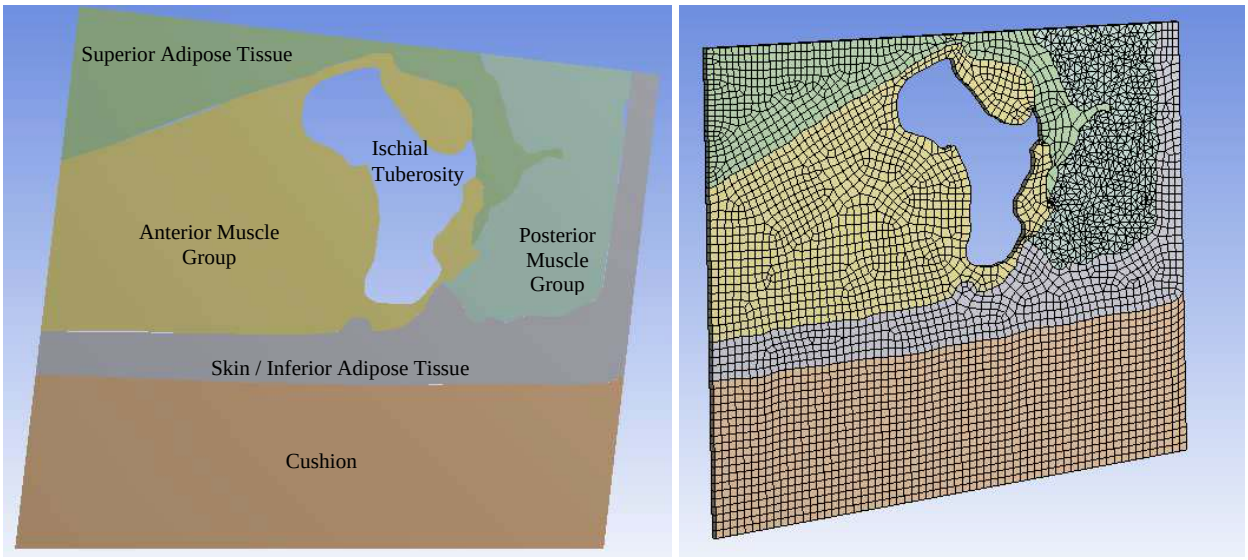

(a) **(b)**

Figure 23: 3-D FE Model with (a) segments labeled and (b) 4mm mesh elements

5.1.4.1 Material Models

Bone tissue was assumed rigid and soft tissues were assumed incompressible, non-linear materials which undergo stress relaxation. The incompressible, non-linear behavior of the soft tissues was described by a Neo-Hookean hyperelastic constitutive model based on the strain energy function:

$$W = \frac{\mu}{2}(\bar{I}_1 - 3) + \frac{1}{d}(J-1)^2 \quad (1)$$

where I_1 = first deviatoric strain invariant = $\lambda_1^2 + \lambda_2^2 + \lambda_3^2$

λ_p = principal stretch ratios of the left Cauchy-Green tensor

J = determinant of the elastic deformation gradient

μ = initial shear modulus

d = material incompressibility parameter

The polyurethane cushion was described using a first-order Ogden hyperelastic constitutive model based on the strain energy function:

$$W = \sum_{i=1}^{N} \frac{\mu_i}{\alpha_i}\left(\bar{\lambda}_1^{\alpha_i} + \bar{\lambda}_2^{\alpha_i} + \bar{\lambda}_3^{\alpha_i} - 3\right) \quad (2)$$

where $\bar{\lambda}_p$ (p=1,2,3) = deviatoric principal stretches, defined as $\bar{\lambda}_p = J^{-1/3}\lambda_p$

N = 1 (first order)

μ_p, α_p = material parameters

Hyperelastic and viscoelastic material parameters were determined based on values in the literature [4, 7, 51, 52]. The initial shear modulus (μ) was 8.5 kPa [52] for muscle tissue and 31.9 kPa [40] for adipose tissue. The material incompressibility parameter was calculated using the formula from Dabnichki et al [4]. Cushion material parameters μ_p and α_p were 0.016 MPa and

10, respectively [10]. The stress relaxation behavior (viscoelasticity) of the soft tissues was described by the Prony series expansion [51]

$$S(t) = (1-\delta)\frac{\partial W}{\partial E} + \int_0^t \delta \frac{\partial W}{\partial E} e^{\frac{t-\xi}{\tau}} d\xi \tag{3}$$

where S = second Piola Kirchhoff stress

E = Green Langrange strain

δ and τ = viscoelastic material parameters

Only the transient tissue response was included in this study because Palevski et al. [52] has shown that most stress relaxation in porcine gluteal muscle tissue occurs within approximately 20 seconds. Pressure ulcers and deep tissue injuries develop over time periods on the order of minutes to hours, therefore, equation (2) reduces to

$$S \cong (1-\delta)\frac{\partial W}{\partial E} \tag{4}$$

The viscoelastic material parameter δ was set equal to 0.5 and was within the range measured in previous studies [51-53]. Cauchy stresses were calculated from the second Piola Kirchhoff stresses using

$$\sigma_{jr} = F_{ij} S_{ik} J^{-1} F_{rk} \tag{5}$$

where F is the mapping tensor

A Coulomb friction model was applied at the contact surface between the skin/inferior adipose tissue layer and cushion. A coefficient of friction of 0.5 was chosen for the model because the value was previously used by Oomens et al [10].

5.1.4.2 Boundary Conditions

Boundary conditions were used to constrain the model and apply IT displacement and pelvic rotation. A fixed support was applied to the inferior surface of the cushion and the distal surfaces of the skin/inferior adipose tissue and anterior muscle group. All other surfaces were free to move in superior-inferior and anterior-posterior planes, but constrained in the sagittal plane. The non-loaded seated posture provided the anatomical geometry used as the initial condition, and the upright and reclined seated postures provided displacement/rotational boundary conditions. Ischial tuberosity displacement was measured as the vertical displacement of the IT from non-loaded and upright seated postures. Only vertical displacement was measured as horizontal displacement of the IT was assumed zero. Pelvic rotation in the sagittal plane (i.e. pelvic tilt) was measured as the rotation of the IT from upright and reclined seated postures. Pelvic rotation was assumed to occur about the center of the femoral head.

Ischial tuberosity displacement and pelvic rotation were applied in two load steps: 1) IT displacement was applied to IT surfaces; 2) pelvic rotation was applied about the center of the femoral head. The FE model was solved using ANSYS (ANSYS 11.0, ANSYS Inc., Canonsburg, PA) and the solutions provided stress and strain distributions for each load step. Large displacements were accounted for in the models.

5.1.5 Model Validation

The FE model solutions were validated using interface pressure measurements, interface shear stress measurements, and comparison of soft tissue displacements. Interface pressure and shear stress measurements were recorded using an interface pressure sensor array and shear force sensor, respectively. Model validation criterion was established as a difference less than 10% between measured and predicted interface stresses and soft tissue displacements. A validation criterion of 10% was arbitrarily chosen because no criterion was established by previous researchers. Upon model validation, subcutaneous tissue stresses and strains could be assumed a realistic estimate.

5.1.5.1 Interface Stresses

The interface pressure sensor array provided measurements along the entire interface. The location of the ITs was identified as the areas of greatest pressure on the upright pressure map. The location of the left IT was identified, along with the anterior and posterior pressure measurements as shown in Figure 24a. The anterior/posterior position of the left IT was assumed to be constant between the upright and reclined pressure maps because the overall footprint of pressure distribution was similar. The medial/lateral position of the buttock, however, was shifted and the appropriate interface pressure measurements were identified as shown in Figure 24b. The interface pressure measurements used for validation of the FE model were collected at a sampling frequency of 10 Hz and averaged over a 5 second duration, 60 seconds after the subject was seated in the respective postures. Interface pressure measurements were compared to predicted principal compressive stresses along the cushion surface of the FE model as shown in Figure 26.

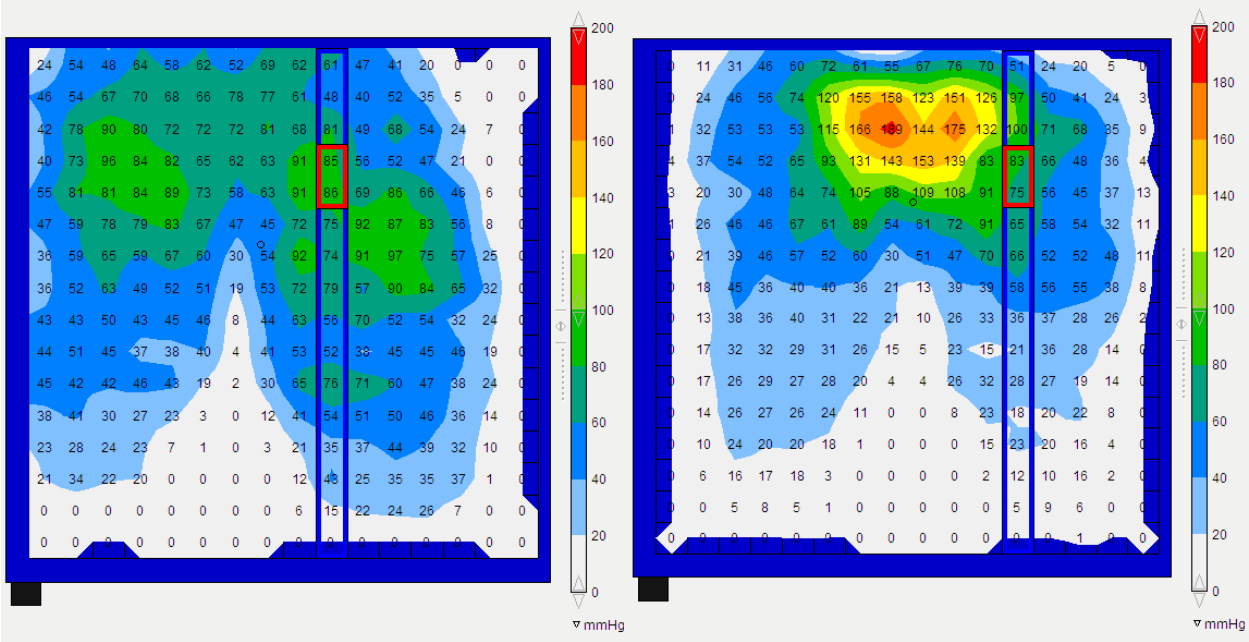

(a) **(b)**

Figure 24: Pressure map of (a) upright and (b) reclined seated postures. The location of the IT is outlined in red and the values used in the validation of the FE model are outlined in blue.

5.1.5.2 Soft Tissue Displacements

Predicted soft tissue displacements from the FE model were compared to the MR images using a method described by Makhsous et al [9]. Five regions of interest (ROI) were selected along the interface between the skin/adipose tissue and cushion. Five vectors originated at the center of the femoral head (CoFH) and extended towards the cushion at angles of -15, 0, 15, 30, and 45° with respect to the vertical axis as shown in Figure 25. The location of the ROIs was defined as the intersection of vector with the cushion interface. Distance was calculated from the CoFH to each ROI in the FE model (upright and reclined load steps) and MR images. The difference between the measured and predicted soft tissue displacements were calculated for the upright and reclined seated postures.

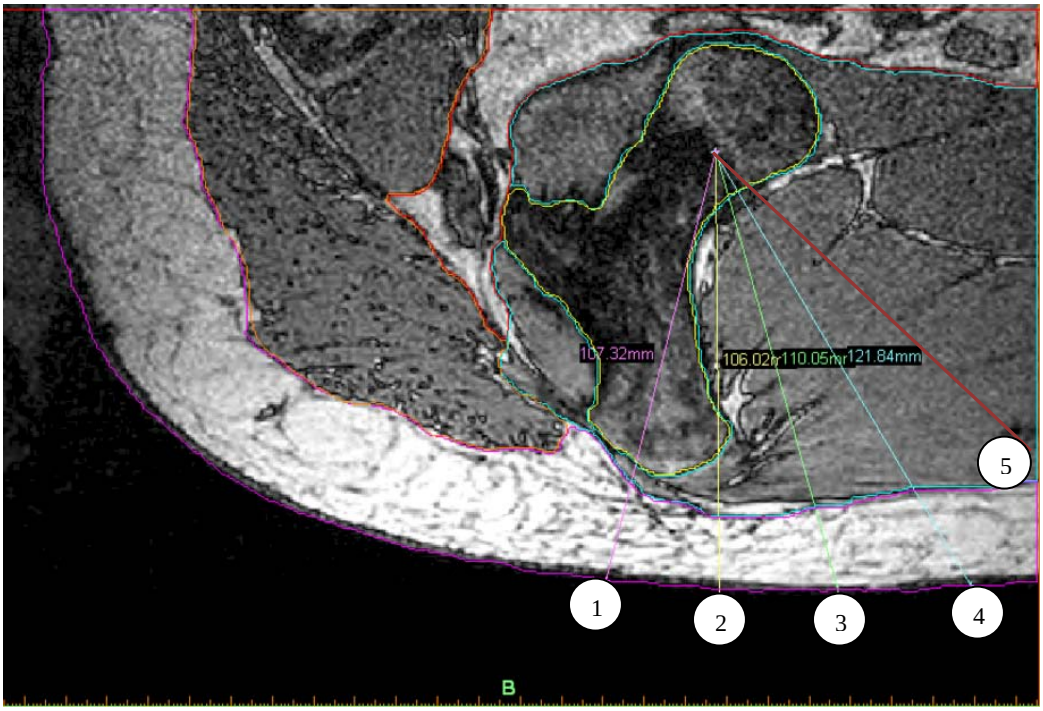

Figure 25: MR image of the upright seated posture with ROIs measured

5.1.6 Parametric Analysis

A parametric analysis was performed on material parameters of the upright seated posture to increase the agreement between the measured and predicted interface stresses and soft tissue displacements. The material parameters used in previous studies were 'fine tuned' or not stated making material parameter selection and adjustment difficult [7-9]. The initial shear modulus (μ) and material incompressibility parameter (d) from the Neo-Hookean hyperelastic constitutive model of the muscle and adipose tissues was adjusted. The material incompressibility parameter was decreased and increased by an order of magnitude, and the initial shear modulus was increased by 50%. Additionally, the initial shear modulus (μ) and the parameter α from the

Ogden hyperelastic constitutive model of the foam cushion were adjusted. Both parameters were increased and decreased by 50%. The material parameters are summarized in Table 10.

Table 10: Material properties used in parametric analysis

	Neo-Hookean Constitutive Model				Ogden Constitutive Model	
	Muscle Tissue		Adipose Tissue		Foam Cushion	
Model	μ (kPa)	d (-)	μ (kPa)	d (-)	μ (kPa)	α (-)
Reference	8.50	6.00E-05	31.90	6.00E-05	16.00	10
Rev 2	8.50	**6.00E-04**	31.90	**6.00E-04**	16.00	10
Rev 3	8.50	**6.00E-06**	31.90	**6.00E-06**	16.00	10
Rev 4	**12.75**	6.00E-05	**47.85**	6.00E-05	16.00	10
Rev 5	8.50	6.00E-05	31.90	6.00E-05	**8.00**	10
Rev 6	8.50	6.00E-05	31.90	6.00E-05	**32.00**	10
Rev 7	8.50	6.00E-05	31.90	6.00E-05	16.00	**5**
Rev 8	8.50	6.00E-05	31.90	6.00E-05	16.00	**15**

* Bold indicates parameter adjusted

5.1.7 Subcutaneous Stresses and Strains

Principal compressive stresses and strains were evaluated along a vertical path from the inferior tip of the IT to the cushion surface as shown in Figure 26. The path was attached to the nodes located at the IT and cushion. The resulting stresses and strains were calculated along the path, which included the anterior muscle and skin/inferior adipose tissue.

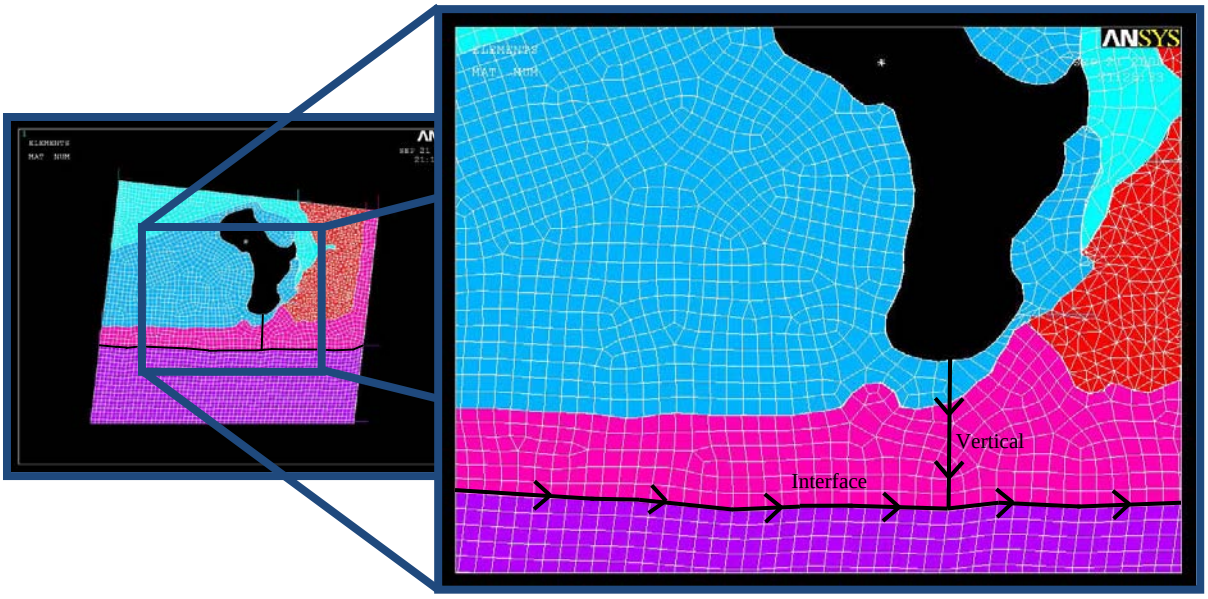

Figure 26: Interface and vertical paths used to report interface and subcutaneous stresses and strains

5.2 RESULTS

5.2.1 Model Validation

Validation criteria required a difference less than 10% between measured and predicted interface stresses and soft tissue displacements. Validated subcutaneous tissues stresses and strains provide information of the effects of various mechanical loading.

5.2.1.1 Interface Stress

Interface pressure was measured and predicted along the cushion interface as shown in Figure 27. Principal compressive stress was used to predict interface pressure. For the upright seated posture, measured and predicted interface pressures at the IT were 86.5 and 58.6 mmHg, respectively. For the reclined seated posture, measured and predicted interface pressures at the IT

were 75.2 and 78.1 mmHg, respectively. The measured interface pressure for the upright seated posture resulted in an even distribution across the cushion; however, the predicted interface pressure was not evenly distributed. The measured and predicted interface pressures for the reclined seated posture resulted in asymmetrical distributions. The measured interface pressure distribution was shifted posterior and the predicted was shifted anterior to the IT.

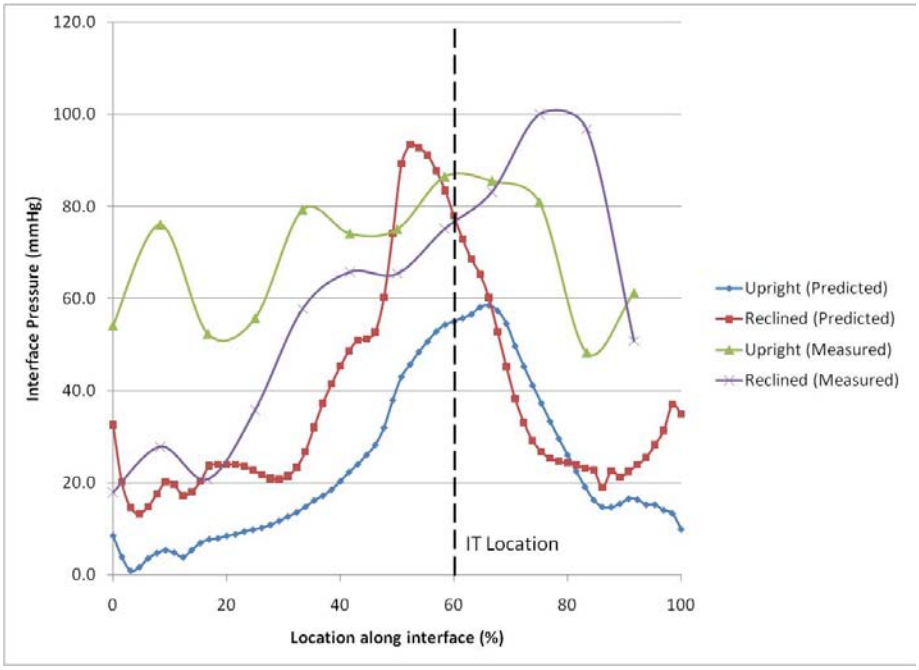

Figure 27: Measured and predicted interface pressure along cushion

Interface shear stress was measured inferior to the left IT and predicted along the cushion interface as shown in Figure 28. Shear stress was calculated in the x-y plane with positive x defined posterior. In the upright seated posture, the predicted interface shear stress was 0.3 kPa compared to 1.8 kPa measured. In the reclined posture, the predicted interface shear stress was 2.6 kPa compared to 0.7 kPa measured. The model predicted greater interface shear stress in the reclined posture, but greater interface shear stress was measured in the upright seated posture. In

the upright seated posture, predicted interface shear stress changed from positive to negative at the IT location which is consistent with the incompressible nature of biological tissues. In the reclined seated posture, a similar interface shear stress distribution was predicted; however, the interface shear stress remained positive along the cushion interface.

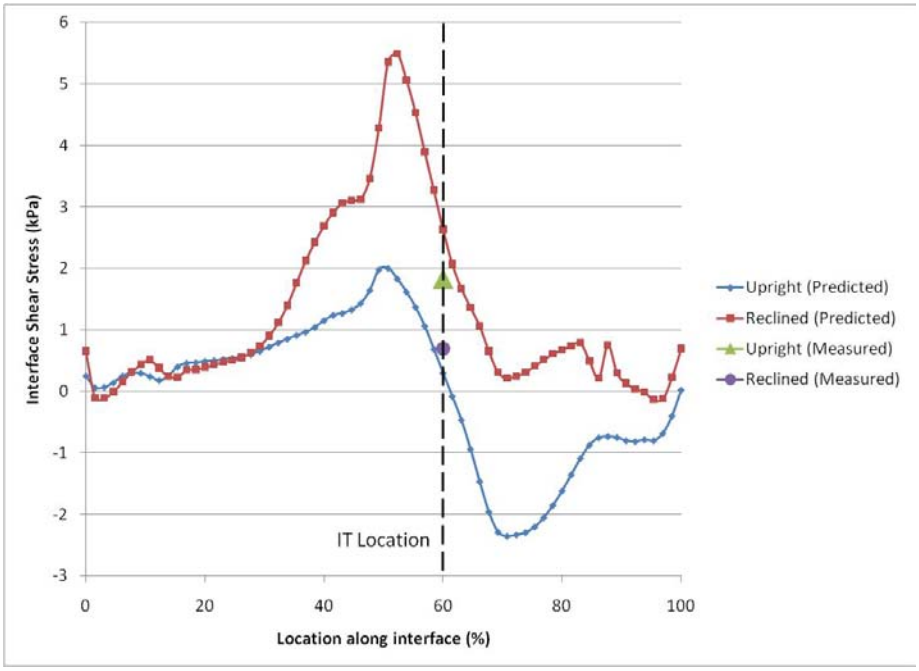

Figure 28: Measured and predicted interface shear stress along cushion

5.2.1.2 Soft Tissue Displacement

Five ROIs were used to determine differences between soft tissue displacements measured on the MR images and predicted by the model as shown in Table 11. Agreement between measured and predicted soft tissue displacement was greater for the upright seated posture as compared to the reclined seated postured. The least amount of discrepancy between the measured and predicted displacements occurred just posterior to the IT and increased with anterior RIOs.

Table 11: Comparison of measured and predicted soft tissue displacement

	Upright			Reclined		
ROI	Measured (mm)	Predicted (mm)	Difference (mm)	Measured (mm)	Predicted (mm)	Difference (mm)
1	107.3	101.7	5.6	116.2	101.5	14.7
2	106.0	98.3	7.7	114.7	99.9	14.8
3	110.0	101.1	8.9	120.5	102.9	17.6
4	121.8	110.3	11.5	133.0	111.5	21.5
5	-	131.7	-	159.5	132.2	27.3

5.2.2 Parametric Analysis

Predicted interface stresses and soft tissue displacement were not similar to the measured values. Material parameters were adjusted to increase interface pressure and decrease the difference between measured and predicted soft tissue displacements. Adjustments to the initial shear modulus changed the reference interface pressure from 55.0 mmHg to 45.5 and 64.1 mmHg, and adjustments in the material incompressibility parameter changed the interface pressure to 31.1 and 85.0 mmHg as shown in Figure 29. Adjustments to the initial shear modulus resulted in a proportional change of interface pressure and adjustments to the material incompressibility parameter resulted in an inverse relationship. The decreased material incompressibility parameter, Rev 3, increased the predicted interface pressure measurement at the IT to a value similar to the measured interface pressure. Agreement between the predicted and measured interface pressures located anterior and posterior to the IT did not improve.

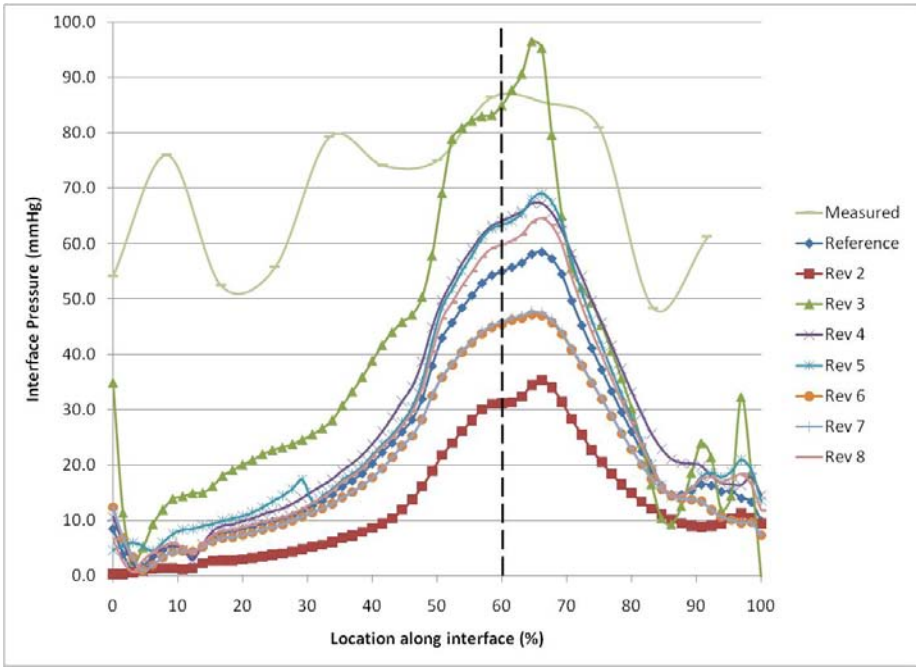

Figure 29: Interface pressure for upright seated posture with adjusted material parameters

Similar relationships were found between parametric adjustments and interface shear stress as shown in Figure 30. Interface shear stress varied proportionally with initial shear modulus and inversely with the material incompressibility parameter. Unfortunately, the parametric analysis resulted in little variation of interface shear stress at the IT as shown in Figure 31. All models except Rev 3 converged to a value near zero just posterior to the IT. Interface stresses were not evaluated for the reclined seated posture because soft tissue displacements were greater than 10% for all ROIs.

The parametric analysis resulted in minor variations in soft tissue displacement. Error increased from ROI 1 to 5, which was the same trend as the Reference Model. For the upright seated posture, Rev 3 resulted in the smallest variation for ROIs 1-3 and both Rev 6 and 7 resulted in the smallest variation at ROI 4. Rev 6 and 7 resulted in nearly identical soft tissue displacements and interface stresses for the upright seated posture. The initial shear modulus of

the foam cushion was increased by 50% in Rev 6 and the alpha parameter of the foam cushion was decreased by 50% in Rev 7. However, the opposite adjustment (Rev 5 and 8) for the same parameters did not result in nearly identical soft tissue displacements and interface stresses.

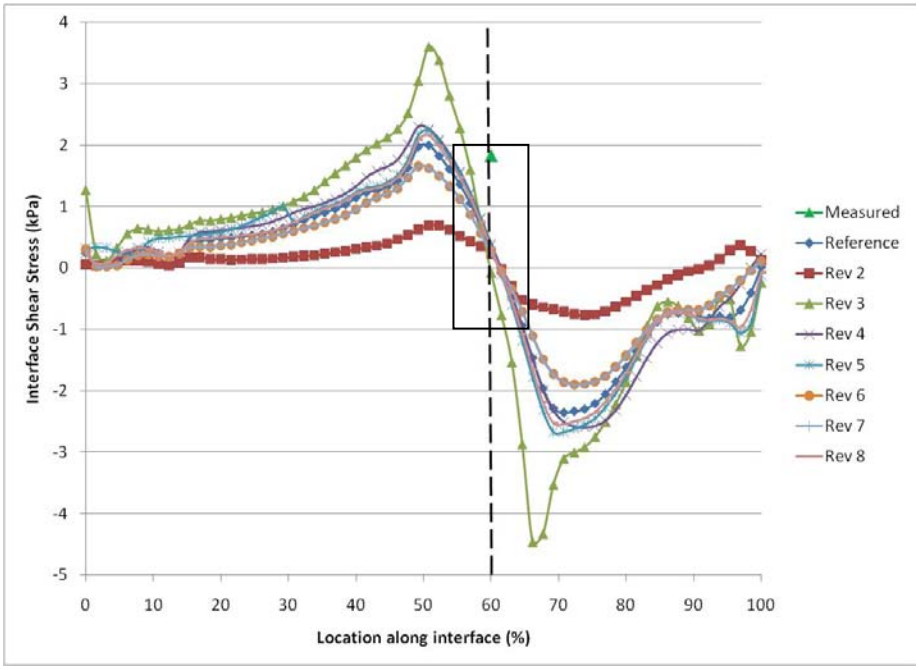

Figure 30: Interface shear stress for upright seated posture with adjusted material parameters

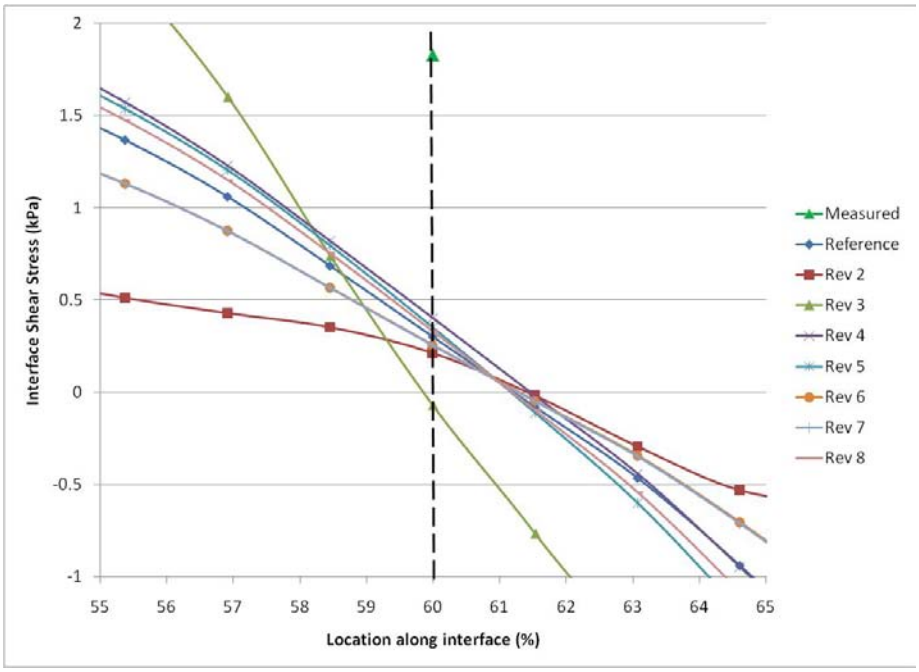

Figure 31: Interface shear stresses for upright seated posture with adjusted material parameters – a magnified view

Table 12: Percent difference between measured and predicted soft tissue displacement

	ROI	Measured (mm)	Reference	Rev 2	Rev 3	Rev 4	Rev 5	Rev 6	Rev 7	Rev 8
Upright	1	107.3	5.2%	6.4%	4.5%	5.1%	6.4%	4.6%	4.6%	6.1%
	2	106.0	7.3%	8.1%	6.3%	6.8%	8.1%	6.4%	6.4%	7.8%
	3	110.0	8.1%	8.7%	7.4%	7.8%	8.6%	7.4%	7.5%	8.4%
	4	121.8	9.5%	9.9%	9.4%	9.3%	9.8%	9.0%	9.0%	9.6%
	5	-	-	-	-	-	-	-	-	-
Reclined	1	116.2	12.7%	13.1%	11.7%	12.0%	13.4%	11.6%	11.6%	13.1%
	2	114.7	12.9%	13.8%	11.7%	12.2%	14.0%	11.8%	11.8%	13.5%
	3	120.5	14.6%	15.3%	13.4%	13.8%	15.3%	13.6%	13.6%	14.9%
	4	133.0	16.2%	16.8%	15.2%	15.7%	16.8%	15.4%	15.5%	16.6%
	5	159.5	17.1%	17.2%	17.3%	17.0%	18.0%	17.4%	17.4%	17.3%

For the Rev 3 Model, measured and predicted interface pressure at the IT and soft tissue displacements for the upright seated posture differed by less than 10%; therefore, the upright

seated posture was partially validated because interface shear stress values differed greater than 10%. Agreement between the measured and predicted values for the reclined seated posture was greater than 10% and was not validated.

5.2.3 Subcutaneous Tissue Stresses and Strains

Results for the Reference Model and Rev 3 Model were reported. The Reference Model was not validated and the results are reported for informational purpose only. The Rev 3 Model results were partially validated (upright seated posture) and should be interpreted as estimated subcutaneous tissue stresses and strains.

5.2.3.1 Reference Model

Principal compressive stress distributions for the upright and reclined seated postures are illustrated in Figures 32 and 33, respectively. Principal compressive stresses were mapped to the vertical path from the inferior tip of the IT to the cushion surface and are shown in Figure 34. Because the path was attached to nodes at the IT and cushion, the path varied between upright and relined seated postures. Peak principal compressive stress occurred in the muscle tissue just inferior to the IT in both upright and reclined seated postures. Peak principal compressive stress for the upright seated posture was 11.7 kPa. A small decrease in stress was present through the muscle tissue followed by a larger decrease through the adipose tissue to a value of 7.3 kPa. Peak principal stress for the reclined seated posture was 25.7 kPa. A sharp decrease in stress was present through the muscle tissue followed by a minimal increase, then decrease through the adipose tissue to a value of 10.4 kPa.

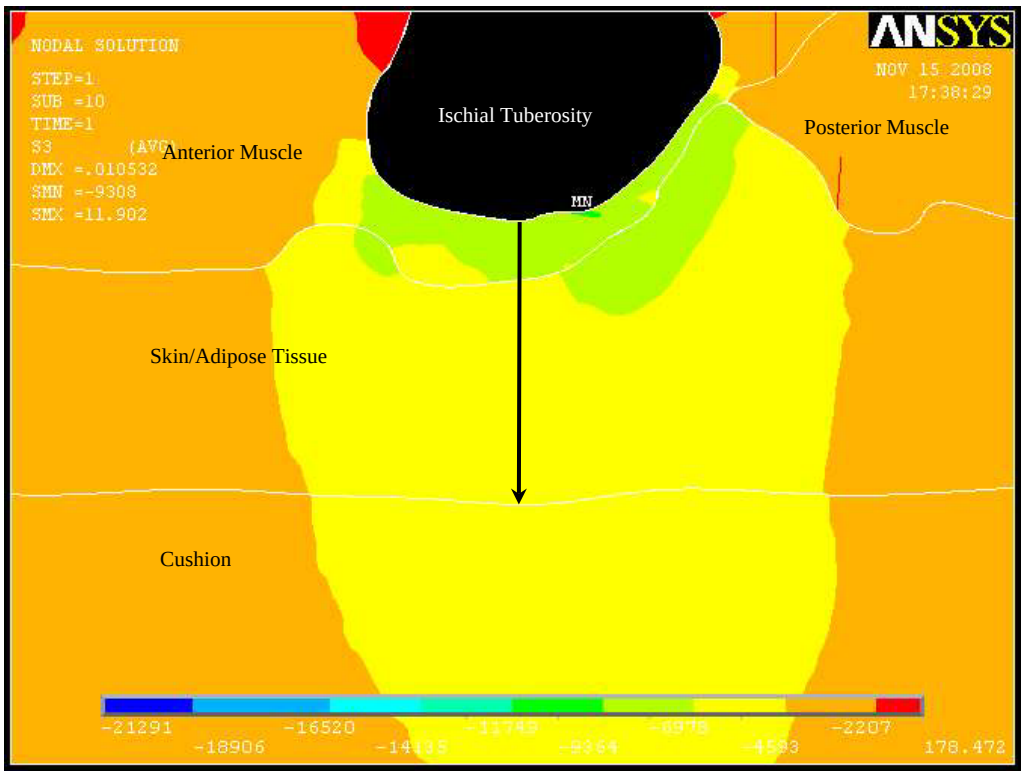

Figure 32: Typical principal compressive stress distribution for the upright seated posture

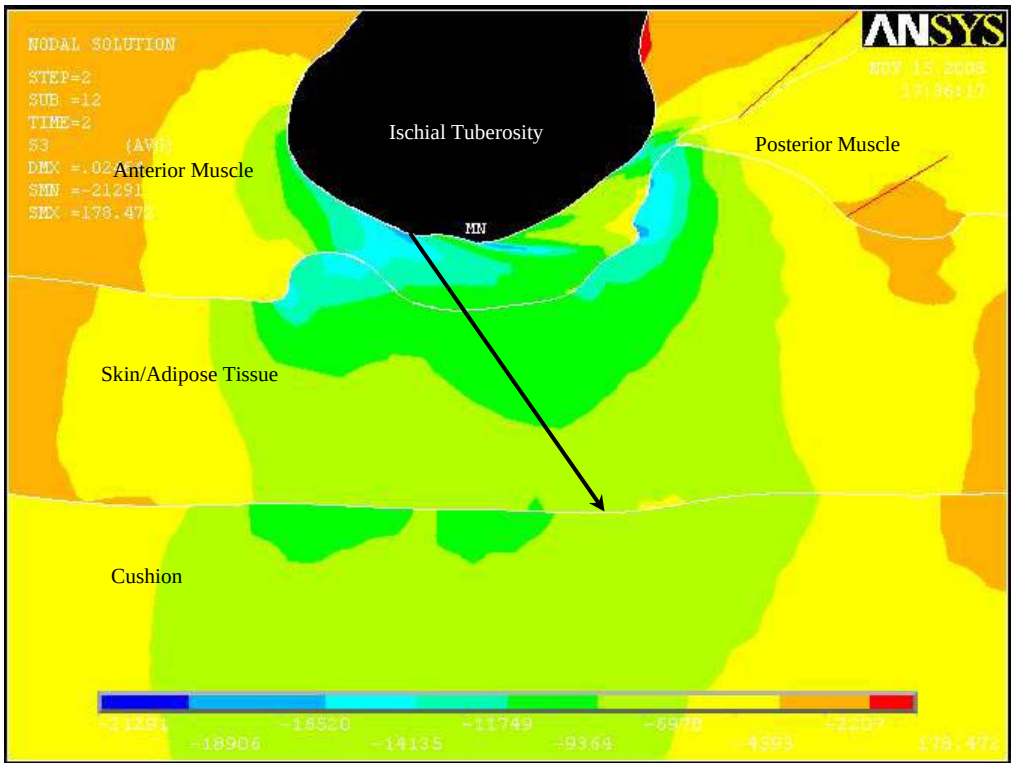

Figure 33: Typical principal compressive stress distribution for reclined seated posture

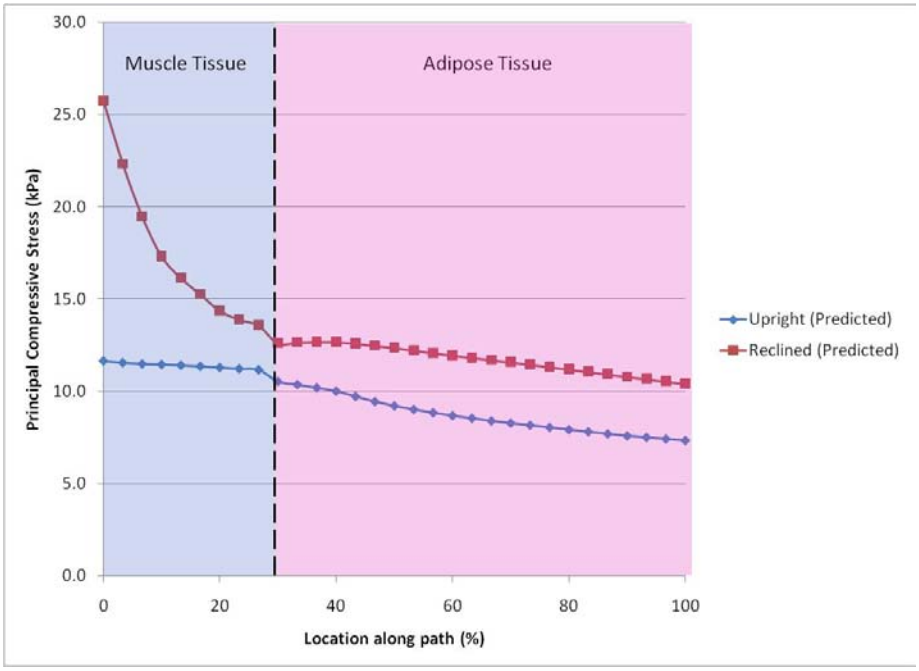

Figure 34: Principal compressive stress along vertical path for upright and reclined seated postures of the Reference model

Principal compressive strain distributions for the upright and reclined are illustrated in Figures 35 and 36, respectively. Principal compressive strains were mapped to the vertical path from the inferior tip of the IT to the cushion surface and are shown in Figure 37. For the upright seated posture, principal compressive strain increased through the muscle tissue and peaked near the adipose tissue. A sharp decrease in strain occurred at muscle-adipose tissue border followed by a small decrease through the adipose tissue. Peak compressive strain for the upright seated posture was 0.42 and peak principal compressive strain for the reclined seated posture was 1.12. A positive compressive strain indicates that a tensile strain occurred at the inferior tip of the IT. For the reclined seated posture, a large decrease in strain was present through the muscle tissue followed by a sharp decrease at the muscle-adipose tissue border. Similar to the principal

compressive stress, a minimal increase in strain resulted through the adipose tissue and was followed by a decrease to a value of 0.21.

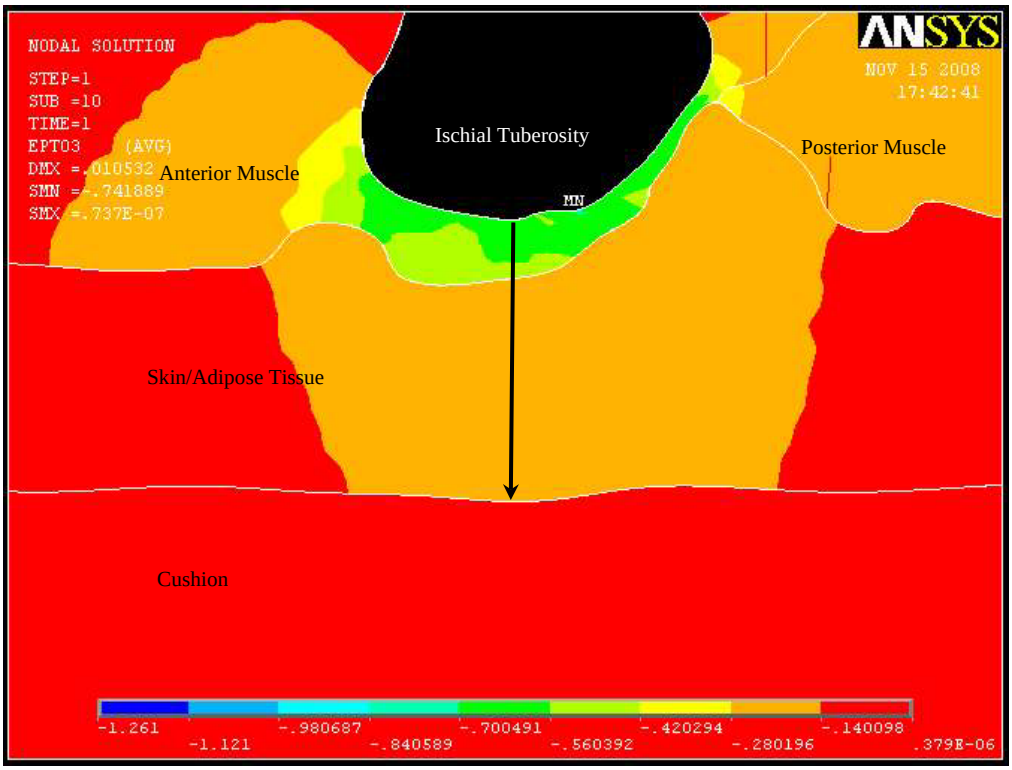

Figure 35: Typical principal compressive strain distribution for the upright seated posture

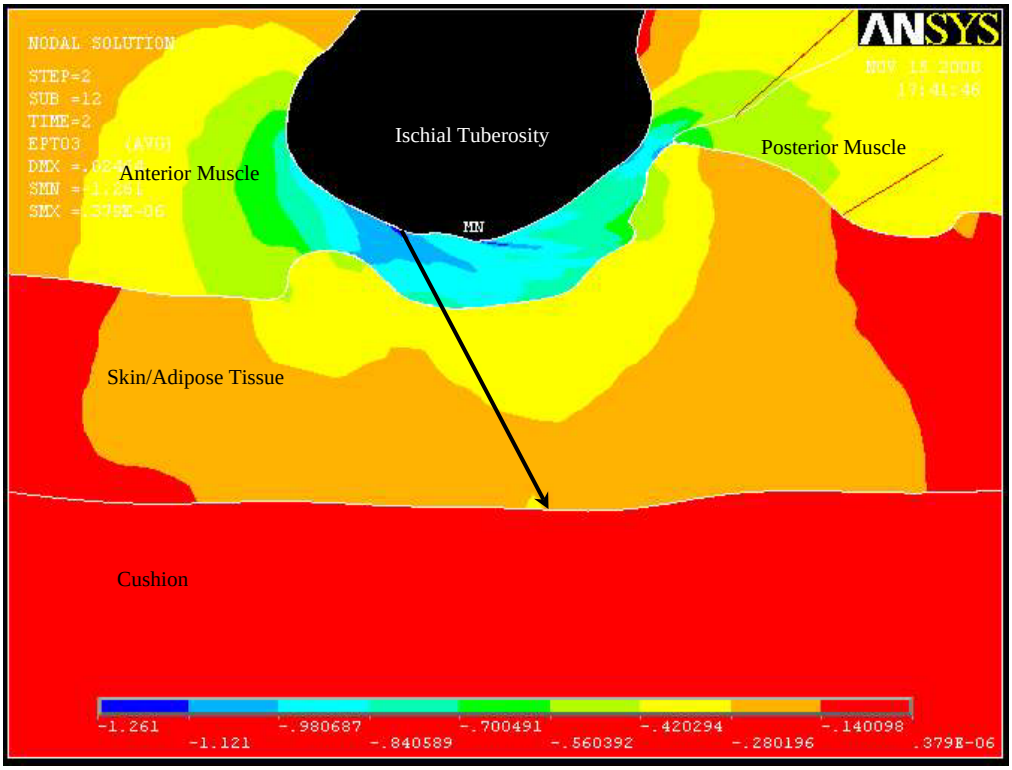

Figure 36: Typical principal compressive strain distribution for the reclined seated posture

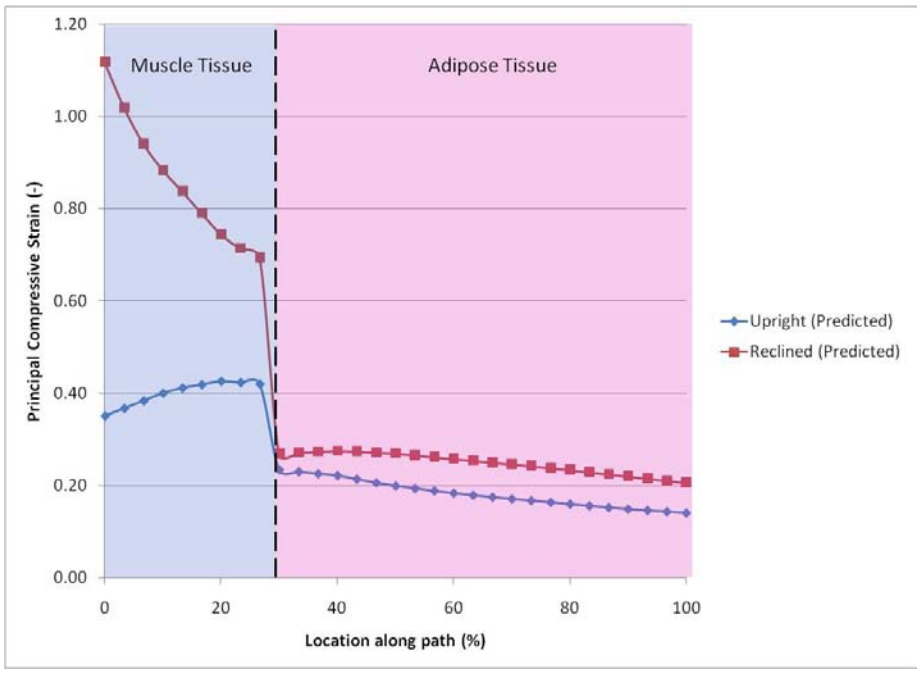

Figure 37: Principal compressive strain along vertical path for the reclined seated posture

5.2.3.2 Rev 3 Model

Principal compressive stresses from the inferior tip of the IT to the cushion surface for the Reference and Rev 3 Upright Models are shown in Figure 38. Peak principal compressive stress for both models occurred just inferior to the tip of the IT for both models. Decreasing the material incompressibility parameter resulted in an increase in peak compressive stress from 11.7 to 17.8 kPa and a greater decrease in compressive stress through the adipose tissue to a value of 11.3 kPa.

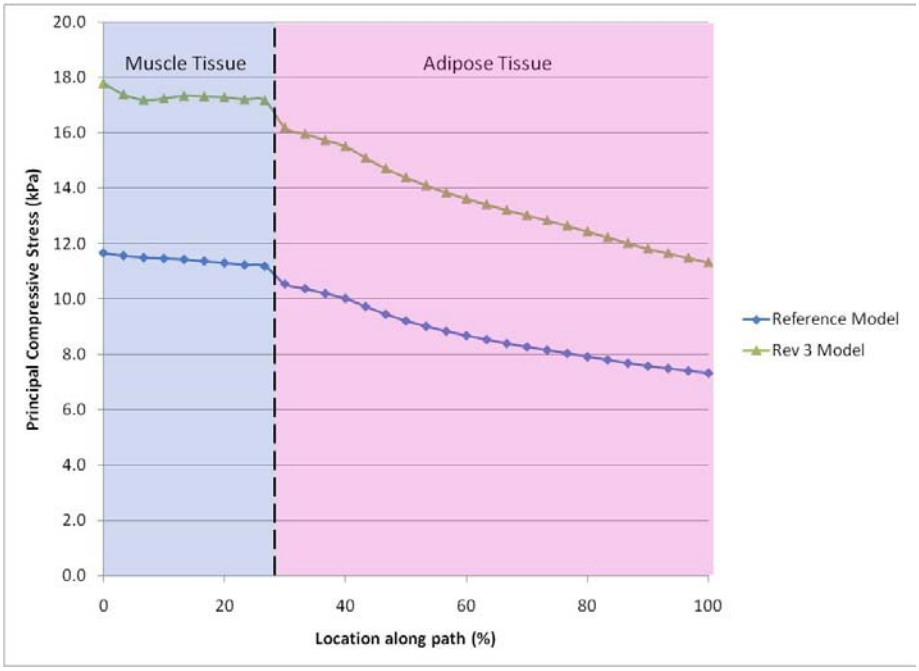

Figure 38: Principal compressive stress along vertical path for the Reference and Rev 3 Upright Models

A large difference in the compressive strain at the IT was present between the Reference and Rev 3 Upright Models as shown in Figure 39. Through the muscle tissue, Rev 3 increased at a greater rate, but the peak compressive strain (0.36) was less than the Reference Model (0.43).

Rev 3 also resulted in a greater rate of change through the adipose tissue, crossing the Reference Model at approximately 60%.

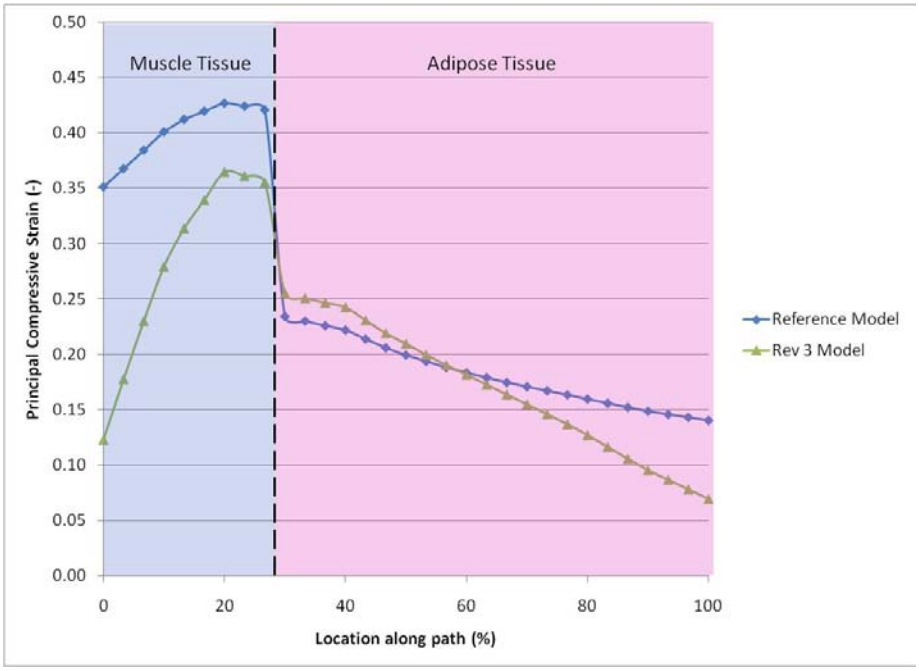

Figure 39: Principal compressive strain along vertical path for the Reference and Rev 3 Upright Models

5.3 DISCUSSION

The purpose of this study was to quantify subcutaneous tissue stresses and strains using an FE model. The non-linear FE model was developed using anatomical buttock geometry and non-linear material properties. The upright seated posture was partially validated using interface pressure and soft tissue displacements. This was the first study to analyze a reclined posture and to incorporate an interface shear force sensor for model validation.

Previous authors only compared measured and predicted interface pressures at the IT [7-9]. Similar interface pressures at a single point were obtained in this study; however, the

predicted interface pressure distribution was not similar to the measured distribution. A possible explanation of the difference in measured and predicted interface pressure distribution was tissue mass. Tissue masses were not included in the model and the addition of tissue masses could increase the agreement between measured and predicted interface pressure distribution. Only interface pressures from Linder-Ganz et al. [7, 8] were available for comparison because the Makhsous et al. model used a constant interface pressure as a loading condition [9]. For healthy subjects, the range of measured interface pressure was 6 – 24 kPa and predicted was 5 – 23 kPa [7, 8]. This study resulted in a measured interface pressure of 11.5 kPa and a predicted (Rev 3) of 11.3 kPa. Interface pressures from this study corresponded well with the data reported by Linder-Ganz et al [7, 8].

Table 13 shows a comparison of peak compressive stresses and strains. The stresses and strains in the muscle tissue of this study were consistent with the adipose tissue of Linder-Ganz et al., and the stresses and strains in the adipose tissue were less than the values reported by Linder-Ganz et al. A possible explanation for lower subcutaneous stresses and strain from this study was due to the cushion model. The support surface modeled in this study provided a 'soft' surface to distribute the loads as opposed to a rigid, fixed support used by Linder-Ganz et al.[7, 8]

Table 13: Comparison of subcutaneous stresses and strains

Author	Tissue	Peak Compressive Stress (kPa)	Peak Compressive Strain (-)
Linder-Ganz [7, 8]	Muscle	24-50	.62 - .84
	Adipose	14-24	.36 - .55
Akins	Muscle	17.8	0.36
	Adipose	16.2	0.26

The reclined seated posture was not validated for this study because soft tissue displacements were outside the validation criteria and the interface pressure distribution was incorrect. The reclined posture resulted in the sacrum supporting a majority of the subject's mass instead of the IT as shown in Figure 24(b). The reclined seated posture of the FE model did not account for a portion of the load shifting to the sacrum as the pelvis rotated. Therefore, the peak interface pressure was anterior to the IT instead of posterior. An additional displacement boundary condition could be incorporated into the model to simulate a reduced load due to the sacrum.

The reclined seated posture was selected to induce a shear force in an attempt to determine the effects of the additional shear force. Predicted interface shear stress increased as expected; however, the measured interface shear stress decreased from the upright to the reclined seated posture. The decrease in the measured interface shear stress was possibly due to the rotation of the IT in the anterior direction. The interface shear force sensor was placed inferior to the IT by palpation in the upright seated posture. Theoretically, shear force is proportional to the normal force and a reduction in the normal force would result in a reduction in shear force. Relocating the sensor by palpation of the IT in the reclined seated posture is a better method of measuring interface shear stress in the reclined seated posture.

Vertical displacement (inferior-superior), horizontal displacement (anterior-posterior) and rotation in the sagittal plane are the three displacement boundary conditions available to model the movement of the pelvis. Movement of the pelvis was identified by comparing the non-loaded MR images to the upright and reclined images. However, assumptions of the displacements and rotation used in the model were required because an image marker was not used during image collection. An image marker would provide a known location from image to image. The location

of the pelvis with respect to the marker would provide the information to quantify the movement. Without quantified movement, vertical displacement of the IT was assumed for the upright seated posture and pelvic rotation about the center of the femoral head (CoFH) was assumed for the reclined seated posture. The assumption of vertical displacement of the IT to simulate the upright seated posture is an appropriate assumption because the subject was in the same posture as the unloaded condition. Horizontal displacement of the IT was possible, but determination of the direction and magnitude was not possible. The reclined seated posture could be modeled by two scenarios: 1) pelvic rotation about the CoFH and 2) pelvic rotation about the IT. Pelvic rotation about the CoFH requires the assumption that both femurs were fixed and the pelvis pivoted about the femoral head. Pelvic rotation about the IT requires the assumption that the pelvis rotated about the IT and both femurs translated anterior. Pelvic rotation is likely a combination of rotation about both the CoFH and the IT, but without the known location across all images an assumption was required. The author chose the assumption of pelvic rotation about the CoFH because, as discussed previously, the IT most likely shifted anterior to the interface shear force sensor which resulted in a decreased measurement in the reclined seated posture. Consequently, the strain distribution superior to the IT would be exaggerated as compared to the pelvic rotation about the IT.

Makhsous et al. evaluated measured and predicted soft tissue displacement by comparing multiple regions of interest [9]. The model was half of a buttock and contained four main regions: proximal medial, proximal lateral, distal medial, and distal lateral. The posterior medial region, location of the IT, resulted in the largest measured displacements (36.9 ± 9.0 mm) and the largest average difference between the measured and predicted displacements (18.1 ± 5.8 mm) [9]. Therefore, the percent difference between the measured and predicted displacement in

the posterior medial region was nearly 50%. The validation criteria chosen for this study was a percent difference of less than 10%.

A limitation of this and previous studies [7-9] was the use of a single MR image to construct the subject specific FE model. The reliability of using MR images to obtain accurate soft tissue geometry is unknown and requires further investigation. Additionally, errors in soft tissue geometry are possibly specific to the MRI device and sequence used to collect images.

6.0 CONCLUSIONS AND RECOMMENDATION

The purpose of this study was to quantify interface shear stresses of commercial wheelchair seat cushions, develop a prototype wheelchair seat cushion, and model subcutaneous tissues stresses and strains.

6.1 SHEAR CHARACTERISTICS OF WHEELCHAIR SEAT CUSHIONS

Combining cushions into HCPCS categories may seem logical because cushions were placed in these categories to meet specific needs of patient populations. Grouping the cushions into 6 categories also allowed statistical analyses to be performed with greater power as compared to 19 groups. However, large variations in interface pressure, interface shear stress, and horizontal stiffness within each category made this a poor choice. Future studies should group cushions by materials of construction or a post-test grouping based upon performance.

The statistical correlation found between ISO 16840-2 stiffness, overall horizontal stiffness, and local horizontal stiffness provides evidence that the test methodology of ISO 16840-2 is sufficient to characterize the horizontal stiffness of wheelchair seat cushions. The ISO 16840-2 methodology requires less data collection and processing to obtain similar results. A limitation to the ISO 16840-2 methodology is instrumentation. A shear force sensor is not used

and quantification of interface shear stress can provide a clinician additional information during the cushion prescription process.

A Randomized Clinical Trial on Preventing Pressure Ulcers with Seat Cushion used viscous fluid, air bladder (cell), and foam/gel cushions in long-term care facilities [54]. Pressure ulcers were reported by cushion and location. For participants that developed pressure ulcers, 8 of 42 (19%) used the viscous fluid, 1 of 22 (5%) used the air bladder, and 2 of 9 (22%) used the foam/gel cushions. The most frequent pressure ulcer was a stage 2 ulcer on the sacrum for 9 of 31 (29%). During the defense of her dissertation [54], Dr. Allegretti noted that initial data indicated that sacral ulcers were most common on viscous fluid cushions. Therefore, viscous fluid cushions were not prescribed to participants demonstrating posterior pelvic tilt. Interface shear stress and horizontal stiffness of wheelchair seat cushions provide the needed resistance against sliding to prevent users from sliding out of his/her wheelchair. However, animal and human studies have provided evidence that high levels of shear compromise tissue integrity. In this study, interface shear stress and horizontal stiffness were quantified and viscous fluid cushions resulted in the smallest values. The small interface shear stress and horizontal stiffness values from this study and high rate of sacral ulcers from the randomized clinical trial can be used to establish a threshold for cushion designers and clinicians. The threshold of interface shear stress and horizontal stiffness is proposed as 3.0 kPa and 6.0 N/m, respectively.

A limitation of this study was the inability to control relative humidity during testing. The tolerance was based on ISO 16840-2 and was especially important when measuring shear because fluctuations in relative humidity result in fluctuations in the coefficient of friction. The variation in the coefficient of friction due to relative humidity was not investigated in this study, but should be investigated in future studies. The lack of relative humidity control and

documentation during calibration resulted in a poor statistical agreement pre- and post-test. Future research should investigate cushion performance at different microclimates and stress relaxation properties of cushions.

6.2 PROTOTYPE CUSHION DESIGN ELEMENT

Three prototype cushion design elements were conceptualized, prototyped, and evaluated based on results from the cushion evaluation. Each design incorporated a closed-loop control system to monitor interface stresses and actively modulate cushion properties. Electromagnets in an appropriate size and power range were unable to provide the necessary magnetic flux density to the magnetorheological fluid (MRF) cushion, actuator size was unable to provide the necessary force to the segmented cushion, and the valve was unable to provide sufficient air flow to the air exchange cushion. Future directions of this project should focus on the air exchange cushion because the limitation was not size or power. A joint effort between the cushion manufacturer and the author has been established to produce an air exchange cushion that is capable of actively reducing interface stresses.

6.3 SUBCUTANEOUS BUTTOCK SOFT TISSUE STRESSES

A non-linear 3-D finite element model was developed and partially validated using anatomical geometry with hyperelastic and viscoelastic constitutive models. The upright seated posture was validated using interface pressure and soft tissue displacements. The subcutaneous buttock soft

tissue stresses predicted in this study were within the range reported by Linder-Ganz [7, 8]. The validated model will be used in future studies to evaluate the SCI population and to evaluate commercial and prototype wheelchair seat cushions.

Limitations of this study include model construction, boundary conditions, and image collection techniques. The FE model used in this study was only a 4mm extrusion based on a single MRI slice. While this limitation did not limit the model's ability to estimate interface and subcutaneous stresses in the upright seated posture, it did limit estimated stresses in the reclined seated posture. The incompressible nature of soft tissues results in tissue displacement in all directions; however, boundary conditions constrained tissue displacements to the sagittal plane. The boundary condition resulted in the model not accounting for medial-lateral tissue displacements. An image marker was not used during image collection. An image marker would have provided a known location in the images collected for the three postures. Because an image marker was not used, the author made the assumption of only vertical displacement of the IT for the upright seated posture and pelvic rotation about the center of the femoral head for the reclined seated posture. While the assumptions were logical and provided subcutaneous tissues stresses in the upright seated posture, the assumptions did not accurately describe pelvic movement. The parametric analysis of tissue material properties did not improve the agreement between measured and predicted interface shear stress. Future research should investigate if changes in the coefficient of friction can improve measured and predicted interface shear stresses. The reclined seated posture was not validated due to a lack of agreement between measured and predicted interface pressure, interface shear stress, and soft tissue displacement. The measured interface pressure revealed that a majority of pressure was shifted from the IT to the sacrum and this was not accounted for in the model. Future research must account for a shift

in pressure or include the sacrum in the model. A complete 3-D model of the buttock should be developed using the image collection methodology described in this thesis. The model would include the sacrum and provide appropriate modeling for the reclined seated posture. The procedure to obtain a 3-D model of the buttock is included in Appendix B.

APPENDIX A

HORIZONTAL FORCE DISPLACEMENT AND SHEAR FORCE DISPLACEMENT CURVES

Horizontal-Force-Displacement Curves

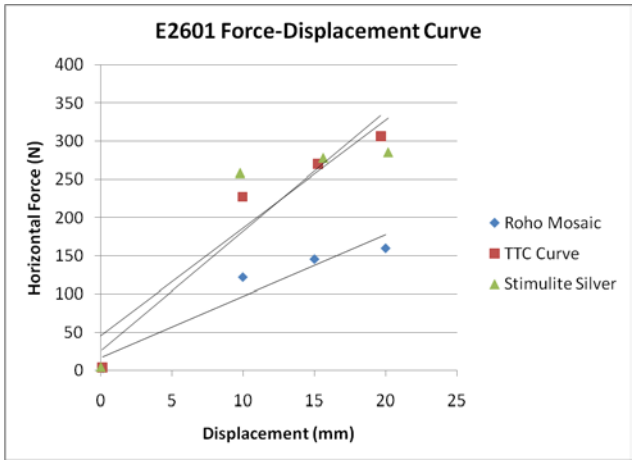

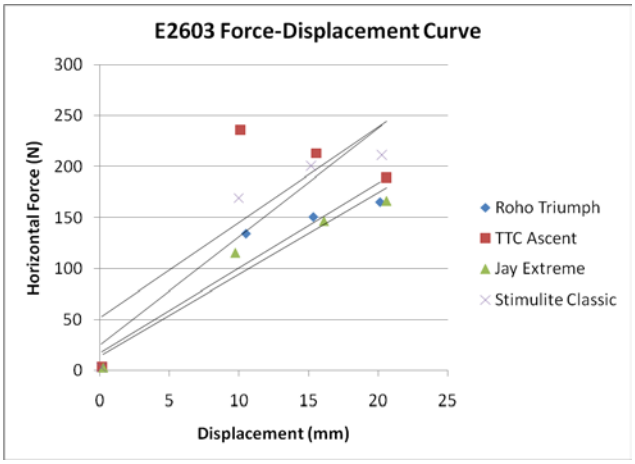

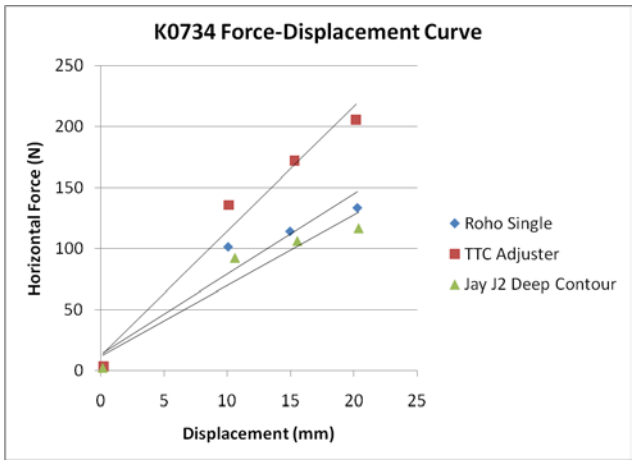

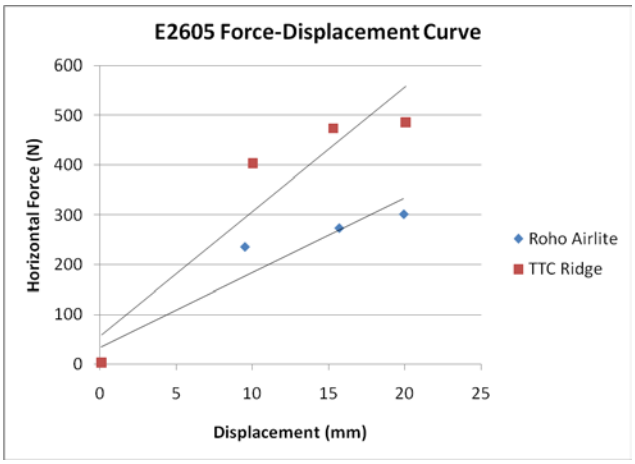

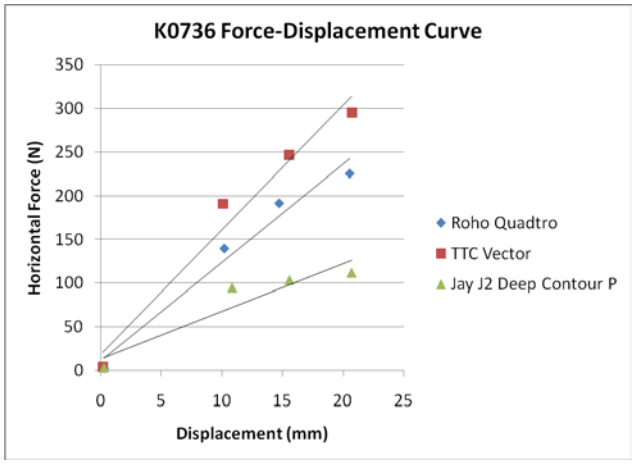

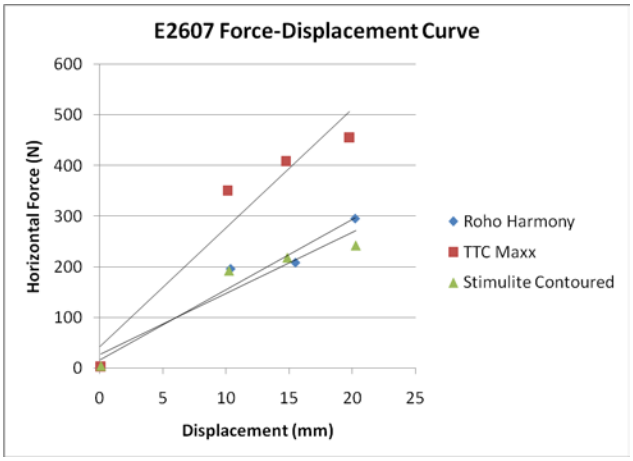

Shear-Force-Displacement Curves

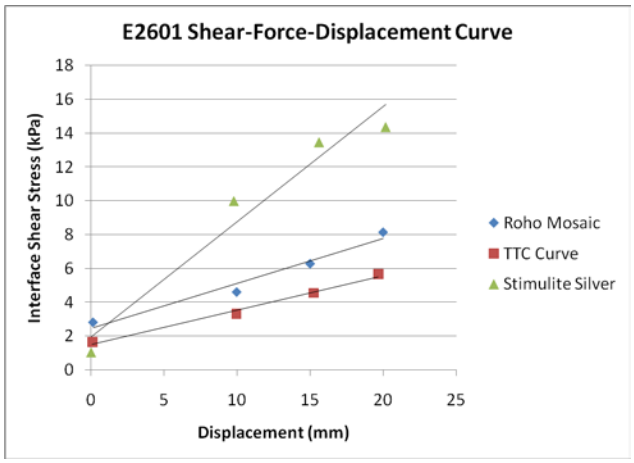

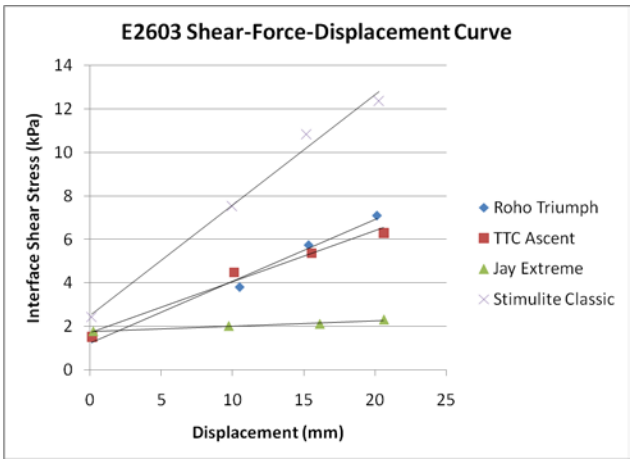

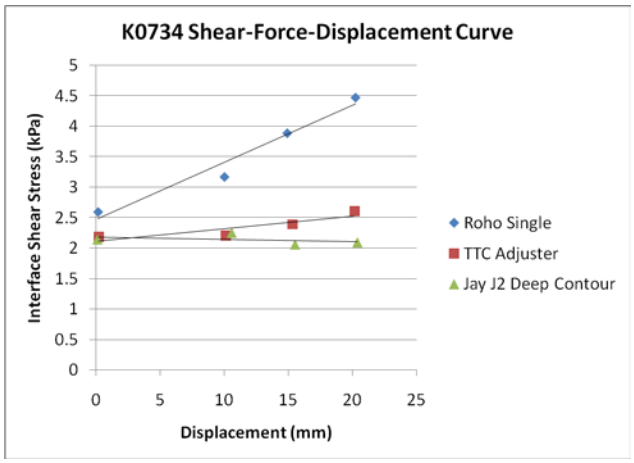

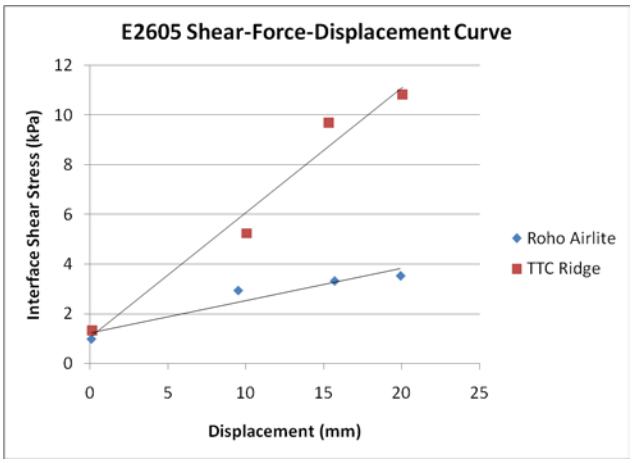

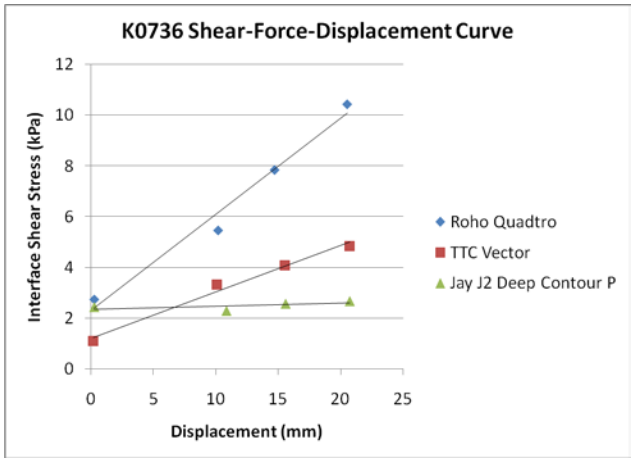
K0736 Shear-Force-Displacement Curve
Interface Shear Stress (kPa)
Displacement (mm)
0
2
4
6
8
10
12
0
5
10
15
20
25
Roho Quadtro
TTC Vector
Jay J2 Deep Contour P

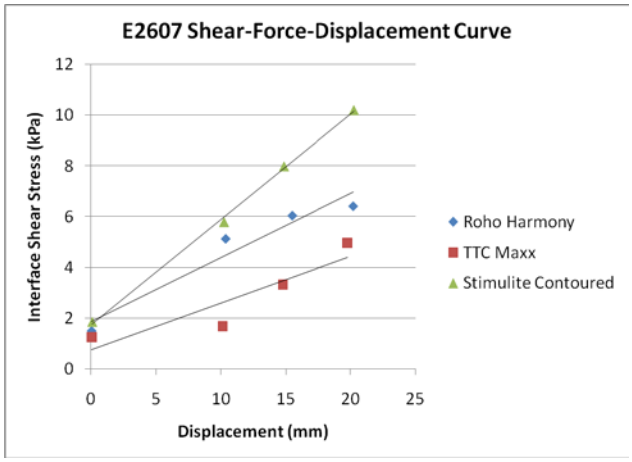
E2607 Shear-Force-Displacement Curve
Interface Shear Stress (kPa)
Displacement (mm)
0
2
4
6
8
10
12
0
5
10
15
20
25
Roho Harmony
TTC Maxx
Stimulite Contoured

APPENDIX B

PROCEDURE TO PROCESS MR IMAGES FOR FULL 3-D MODEL

1. Identify and segment anatomical structures using Mimics (Materialise, Leuven, Belgium)
2. Smooth segments and export as STL files using Magics 9.9 (Materialise, Leuven, Belgium)
3. Import STL files into Solidworks (Concord, MA, USA) using STL Import (Sycode, Goa, India)
4. Remove empty space between solids
5. Convert to parasolid files and export
6. Import parasolid files into ANSYS 11.0 (Canonsburg, PA, USA)
7. Mesh parts using tetrahedral elements and applied non-linear material properties
8. Apply boundary conditions and calculate stresses and strains

BIBLIOGRAPHY

1. Whittington, K.T. and R. Briones, *National Prevalence and Incidence Study: 6-year sequential acute care data.* Adv Skin Wound Care, 2004. **17**(9): p. 490-4.

2. Brienza, D.M. and M.J. Geyer, *Using support surfaces to manage tissue integrity.* Advances in Skin & Wound Care, 2005. **18**(3): p. 151-7.

3. International Organization for Standardization (ISO), 2007, *Wheelchair seating - Part 2: Determination of physical and mechanical characteristics of devices intended to manage tissue integrity - Seat Cushions*, ISO/FDIS 16840-2, Geneva, Switzerland.

4. Dabnichki, P.A., A.D. Crocombe, and S.C. Hughes, *Deformation and stress analysis of supported buttock contact.* Proceedings of the Institution of Mechanical Engineers. Part H, Journal of engineering in medicine, 1994. **208**(1): p. 9-17.

5. Gefen, A., et al., *In Vivo Muscle Stiffening Under Bone Compression Promotes Deep Pressure Sores.* Journal of Biomechanical Engineering, 2005. **127**: p. 512.

6. Lim, D., et al., *Evaluation of a new sitting concept designed for prevention of pressure ulcer on the buttock using finite element analysis.* Med Biol Eng Comput, 2007.

7. Linder-Ganz, E., et al., *Assessment of mechanical conditions in sub-dermal tissues during sitting: A combined experimental-MRI and finite element approach.* Journal of Biomechanics, 2007. **40**(7): p. 1443-1454.

8. Linder-Ganz, E., et al., *Strains and stresses in sub-dermal tissues of the buttocks are greater in paraplegics than in healthy during sitting.* Journal of Biomechanics, 2008. **41**(3): p. 567-580.

9. Makhsous, M., et al., *Finite Element Analysis for Evaluation of Pressure Ulcer on the Buttock: Development and Validation.* IEEE Transactions on Neural Systems and Rehabilitation Engineering, 2007. **15**(4): p. 517-525.

10. Oomens, C.W.J., et al., *Can Loaded Interface Characteristics Influence Strain Distributions in Muscle Adjacent to Bony Prominences?* Computer Methods in Biomechanics and Biomedical Engineering, 2003. **6**(3): p. 171-180.

11. Ragan, R., et al., *Seat-interface pressures on various thicknesses of foam wheelchair cushions: A finite modeling approach.* Archives of Physical Medicine and Rehabilitation, 2002. **83**(6): p. 872-875.

12. Sun, Q., et al., *Finite element modeling of human buttock thigh tissue in a seated posture.* 2005 Summer Bioengineering Conference, June, 2005: p. 22-26.

13. Todd, B.A. and J.G. Thacker, *Three-dimensional computer model of the human buttocks, in vivo.* J Rehabil Res Dev, 1994. **31**(2): p. 111-119.

14. Miller, H. and J. Delozier, *Cost implications of the pressure ulcer treatment guideline.* Columbia, MD: Center for Health Policy Studies; 1994, Contract No. 282-91-0070. Sponsored by the Agency for Health Care Policy and Research.

15. Russo, C. and A. Elixhauser. *Hospitalization Related to Pressure Sores, 2003. HCUP Statistical Brief #3*. 2006 [cited January 26, 2007]; Available from: http://www.hcup-us.ahrq.gov/reports/statbriefs/sb3.pdf.

16. Bennett, L., et al., *Shear vs pressure as causative factors in skin blood flow occlusion.* Archives of Physical Medicine & Rehabilitation, 1979. **60**(7): p. 309-14.

17. Reichel, S.M., *Shearing force as a factor in decubitus ulcers in paraplegics.* J Am Med Assoc, 1958. **166**(7): p. 762-3.

18. Thompson, D., *A critical review of the literature on pressure ulcer aetiology.* Journal of Wound Care, 2005. **14**(2): p. 87-90.

19. Bennett, L., et al., *Skin blood flow in seated geriatric patients.* Archives of Physical Medicine & Rehabilitation, 1981. **62**(8): p. 392-8.

20. Bennett, L., et al., *Skin stress and blood flow in sitting paraplegic patients.* Archives of Physical Medicine & Rehabilitation, 1984. **65**(4): p. 186-90.

21. Goossens, R.H., *Shear Stress measured on three different materials*. 2001, LiquiCell Technologies, Inc.

22. Goossens, R.H., et al., *Shear stress measured on beds and wheelchairs.* Scandinavian Journal of Rehabilitation Medicine, 1997. **29**(3): p. 131-6.

23. Goossens, R.H., et al., *Influence of shear on skin oxygen tension.* Clinical Physiology, 1994. **14**(1): p. 111-8.

24. Rose, E.H., L.M. Vistnes, and G.A. Ksander, *The panniculus carnosus in the domestic pig.* Plast Reconstr Surg, 1977. **59**(1): p. 94-7.

25. Dinsdale, S.M., *Decubitus ulcers: role of pressure and friction in causation.* Archives of Physical Medicine & Rehabilitation, 1974. **55**(4): p. 147-52.

26. Goldstein, B. and J. Sanders, *Skin response to repetitive mechanical stress: a new experimental model in pig.* Archives of Physical Medicine & Rehabilitation, 1998. **79**(3): p. 265-72.

27. Fitzgerald, S., et al., *Evaluating Wheelchair cushions*, in *Rehab Management*. 2001.

28. *Terms and definitions related to support surfaces* 2007 [cited 2008 March 13]; Available from: http://www.nmmra.org/resources/NHQI/96_886.pdf.

29. Brienza, D. and M. Geyer. *Support Surface Technology*. 2000 [cited 2008 March 13]; Available from: http://www.wheelchairnet.org/WCN_WCU/SlideLectures/DAB/SuptSurfTech5.pdf.

30. Yarkony, G.M., *Pressure ulcers: a review.* Arch Phys Med Rehabil, 1994. **75**(8): p. 908-17.

31. Sprigle, S., *The match game.* Team Rehab Report, 1992. **3**: p. 20-21.

32. *The four principles of dry floatation technology*. 2008 [cited 2008 March 13]; Available from: http://www.therohogroup.com/dryfloat.jsp.

33. *Supracor - Total Pressure Management*. 2008 [cited 2008 March 13]; Available from: http://www.supracor.com/medical/total_pressure_management.htm.

34. *HCPCS General Information*. [cited 2008 August 18]; Available from: http://www.cms.hhs.gov/MedHCPCSGenInfo/.

35. *KNOW THE CODE - For Wheelchair Seating*. 2008 May [cited 2008 June 13]; Available from: http://trgweb.rohoinc.com/Web%20Databases/PDFs/Web%20PDFs.nsf/0/D960048B9A155161862571DB006DAAC4/$File/Know+the+Code+for+Wheelchair+Seating+-+Update+May+2008.pdf.

36. Gilsdorf, P., R. Patterson, and N. Appel, *Sitting forces and wheelchair mechanics.* Journal of Rehabilitation Research and Development, 1990. **27**(3).

37. Fontaine, R., S. Risley, and R. Castellino, *A quantitative analysis of pressure and shear in the effectiveness of support surfaces.* Journal of Wound, Ostomy and Continence Nursing, 1998. **25**(5): p. 233-9.

38. Akins, J., P. Karg, and D. Brienza. *Measurement & Analysis of Wheelchair Seat Cushions' Shear Characteristics*. in *RESNA 2008 Annual Conference*. 2008. Washington, D.C.

39. Chow, W.W. and E.I. Odell, *Deformations and stresses in soft body tissues of a sitting person.* J Biomech Eng, 1978. **100**: p. 79-87.

40. Brosh, T. and M. Arcan, *Modeling the body/chair interaction–an integrative experimental–numerical approach.* Clinical Biomechanics, 2000. **15**(3): p. 217-219.

41. Brienza, D.M., et al., *The Relationship Between Pressure Ulcer Incidence and Buttock-Seat Cushion Interface Pressure in At-Risk Elderly Wheelchair Users.* Archives of Physical Medicine and Rehabilitation, 2001. **82**(4): p. 529-533.

42. Burns, S.P. and K.L. Betz, *Seating pressures with conventional and dynamic wheelchair cushions in tetraplegia.* Archives of Physical Medicine and Rehabilitation, 1999. **80**(5): p. 566-571.

43. Call, J. and E. Call, *Force Calibration Method by an Inclined Plane*. 2006, Shear Force Initiative.

44. Nakagami, G., et al., *Comparison of Two Pressure Ulcer Preventive Dressings for Reducing Shear Force on the Heel.* Journal of Wound, Ostomy and Continence Nursing, 2006. **33**(3): p. 267-272.

45. Oduncu, H. and J. Melhuish, *Evaluation of sensors for measuring shear forces associated with wound healing and formation,* in *Wounds UK 2007 Wound Care Conference Harrogate*. 2007: Harrogate, United Kingdom.

46. Ohura, T., M. Takahashi, and N. Ohura, *Influence of external forces (pressure and shear force) on superficial layer and subcutis of porcine skin and effects of dressing materials: Are dressing materials beneficial for reducing pressure and shear force in tissues?* Wound Repair and Regeneration, 2007(16): p. 102-107.

47. Okazaki, H., et al., *The developement and validity of a sensor for simultaneously measuring pressure and shear force [in Japanese]*. Jpn J Pressure Ulcers, 2002. **4**: p. 263.

48. Okubo, Y., M. Konagaya, and K. Ogawa, *The sliding effects on the supinated human body due to bed inclination [in Japanese]*. Jpn J Pressure Ulcers, 2000. **4**(1): p. 45-50.

49. Bafana, R., *Developement, evaluation and implementation of wheelchair seat cushion testing standards,* in *Bioengineering*. 2005, University of Pittsburgh: Pittsburgh.

50. Carroll, R.J. and D. Ruppert, *On prediction and the power transformation family.* Biometrika, 1981. **68**(3): p. 609-615.

51. Bosboom, E.M.H., et al., *Passive transverse mechanical properties of skeletal muscle under in vivo compression.* Journal of Biomechanics, 2001. **34**(10): p. 1365-1368.

52. Palevski, A., et al., *Stress Relaxation of Porcine Gluteus Muscle Subjected to Sudden Transverse Deformation as Related to Pressure Sore Modeling.* Journal of Biomechanical Engineering, 2006. **128**: p. 782.

53. Bosboom, E.M.H., et al., *Quantification and localisation of damage in rat muscles after controlled loading; a new approach to study the aetiology of pressure sores.* Medical Engineering and Physics, 2001. **23**(3): p. 195-200.

54. Allegretti, A.L.C., *Factors associated with clinical decisions and pressure ulcer development in long term care residents*, in *Department of Rehabilitation Science and Technology*. 2008, University of Pittsburgh: Pittsburgh.